

**Technical Memorandum
TM-UCB PRC-2000-1**

**TESTS TO EVALUATE THE STIFFNESS
AND
PERMANENT DEFORMATION CHARACTERISTICS
OF
ASPHALT/BINDER-AGGREGATE MIXES**

A CRITICAL DISCUSSION

C.L. Monismith, J.T. Harvey, F. Long, S. Weissman

June 2000

TABLE OF CONTENTS

LIST OF FIGURES	v
LIST OF TABLES	ix
EXECUTIVE SUMMARY	xi
1.0 INTRODUCTION	1
2.0 MECHANICS OF PERMANENT DEFORMATION AND ITS MEASUREMENT	3
2.1 Volume-Change versus Shape-Distortion	4
2.1.1 Laboratory Test Data	4
2.1.2 Finite Element Simulations of Pavement Response	8
2.1.2.1 AC Response	8
2.1.2.2 Loading and Temperature Considerations	11
2.1.2.3 Results	13
2.2 Laboratory Test Considerations	19
2.2.1 Finite Element Simulations of Test Specimens	21
2.2.2 Axial Deformations	23
2.2.3 Effective Stiffness Modulus	28
2.3 Non-linear Response Characteristics of Asphalt Aggregate Mixes	29
3.0 LABORATORY TESTS	41
3.1 Triaxial Test	41
3.2 Constant Height Simple Shear Test	45
4.0 CREEP VERSUS REPEATED LOADING	51
5.0 TEST SPECIMEN PREPARATION	55
6.0 MIX DESIGN, ANALYSIS, AND PERFORMANCE EVALUATION	65
6.1 Mix Design	65
6.2 Performance Analysis/Evaluation	70
6.2.1 San Francisco International Airport	70
6.2.2 WesTrack	73
6.3 Mix Stiffness Considerations	78
7.0 SUMMARY AND CONCLUSIONS	81
8.0 REFERENCES	83

LIST OF FIGURES

Figure 1a. Volume change.....	6
Figure 1b. Shape distortion.....	6
Figure 2. Average strain history for 15 different mixes (I).....	6
Figure 3. Normalized curves for average strain history for 15 mixes shown in Figure 2.	6
Figure 4. Variation of f'' with x , and its dependency on the temperature.....	12
Figure 5. Perspective view of the finite element mesh used to represent AC pavement structure	12
Figure 6a. Lateral (top) component.....	14
Figure 6b. Longitudinal shear component.....	14
Figure 6c. Tire-pavement contact stress.....	15
Figure 7. Vertical deformation in the AC layer first (500 mm from the symmetry plane); effect of variation in G while maintaining K constant, or vice-versa.....	17
Figure 8. Lateral deformation in the AC layer (first 500 mm from the symmetry plane); effect of variation in G while maintaining K constant, or vice-versa.....	18
Figure 9. Variation of the maximum vertical displacement in the AC later with changes in material properties.....	18
Figure 10. Variation of the distance between points located 50 mm below the tire edges(under the tire center in the longitudinal direction) as a function of the changes in material properties.....	19
Figure 11. Test data variability for three replicate specimens: repetitive simple shear tests at constant height.....	21
Figure 12. Example of the mesh for the Pleasanton aggregate mix, 640×640 elements, mesh dimensions are 150×150 mm: black = mastic, white = aggregate, locations of the virtual LVDT stations or axial tests are in the horizontal direction and all LVDTs are centered about the dashed line	22
Figure 13. Contours of axial displacements (y direction): Pleasanton aggregate, $E_{aggregate} = 100$ MPa and $E_{mastic} = 100$ MPa.....	25
Figure 14. Contours of axial displacements (y direction): Pleasanton aggregate, $E_{aggregate} = 100$ Mpa and $E_{mastic} = 1$ Mpa	25

Figure 15. Contours of axial strain (y direction): Pleasanton aggregate, $E_{aggregate} = 100$ Mpa and $E_{mastic} = 1$ Mpa	26
Figure 16. Effect of gage length on measured axial strain (x direction): Pleasanton aggregate, $E_{aggregate} = 100$ Mpa and $E_{mastic} = 100$ MPa	26
Figure 17. Effect of gage length on measured axial strain (x direction): $E_{aggregate} = 100$ Mpa and $E_{mastic} = 1$ Mpa.	27
Figure 18. Variation of effective stiffness E as a function of mastic property, plotted by orientation.....	29
Figure 19. Averaged results of the three replicate specimens for each strain and temperature ...	32
Figure 20. Complex shear modulus versus frequency at 20°C.....	34
Figure 21. Complex shear modulus versus frequency at 40°C.....	35
Figure 22. Complex shear modulus versus frequency at 57°C.....	36
Figure 23. Apparent Poisson's ratio versus frequency, low air void content mixes	38
Figure 24. Poisson's ratio versus frequency, low air void content mixes.....	38
Figure 25. Poisson's ratio versus frequency, high air void content mixes.....	39
Figure 26. Comparison of direct Poisson's ratio values and apparent Poisson's ratio values, Mix V0W0	39
Figure 27. Axial loading to measure deviatoric distortion	44
Figure 28. Proposed test configuration using two gyratory-compacted specimens	44
Figure 29. Ratio of measured G to actual G as a function of L/R or L/D (19).....	45
Figure 30. Simple shear test; traction represented by dotted arrows in not applied.....	47
Figure 31. Convergence of the measured of G with increased ratio of length-to-height	48
Figure 32. Engineering shear strain distribution for plane-strain simulation of a simple shear at constant height test: height = 75 mm, length = 225 mm.....	49
Figure 33. Vertical displacement distribution for plane-strain simulation of a simple shear at constant height test: height = 75 mm, length = 225 mm.....	50
Figure 34. Plane-strain simulations of a simple shear at constant height test: variation of measured effective G as a function of length-to-height ratio.....	50

Figure 35. Repetitions to a permanent shear strain of 5 percent versus binder content; tests performed at 50°C (122°F)	53
Figure 36a. Effect of compaction procedure stabilometer "S" value (26): crushed granite	56
Figure 36b. Effect of compaction procedure stabilometer "S" value (26): crushed quartzite	56
Figure 36c. Effect of compaction procedure stabilometer "S" value (26): crashed gravel	56
Figure 37. Comparison of stress at 2 percent strain for specimens prepared by static and kneading compaction; constant rate of strain triaxial compression tests at 60°C	57
Figure 38. Comparison of mechanical performance [LCPC (30)]	61
Figure 39a. Influence of compaction method on behavior of mixes in the RSST-CH at 40°C, 50°C, and 60°C; conventional dense-graded AC (33): 40°C	62
Figure 39b. Influence of compaction method on behavior of mixes in the RSST-CH at 40°C, 50°C, and 60°C; conventional dense-graded AC (33): 50°C	62
Figure 39c. Influence of compaction method on behavior of mixes in the RSST-CH at 40°C, 50°C, and 60°C; conventional dense-graded AC (33): 60°C	62
Figure 40a. Influence of compaction method on behavior of mixes in the RSST-CH at 40°C, 50°C, and 60°C; gap-graded asphalt-rubber hot mix: 40°C	63
Figure 40b. Influence of compaction method on behavior of mixes in the RSST-CH at 40°C, 50°C, and 60°C; gap-graded asphalt-rubber hot mix: 50°C	63
Figure 40c. Influence of compaction method on behavior of mixes in the RSST-CH at 40°C, 50°C, and 60°C; gap-graded asphalt-rubber hot mix: 60°C	63
Figure 41. Permanent deformation system	67
Figure 42. Permanent shear strain versus stress repetitions in RSST-CH at 50°C; PBA-6A mix, 4.7 percent binder control	68
Figure 43. Mix design example, gap-graded with crumb rubber modified binder	69
Figure 44. Aggregate gradations	71
Figure 45. Shear stress repetitions to 5 percent shear strain versus air-void content at 50°C— <i>High Stability</i> mixes	71
Figure 46. Shear stress repetitions to 5 percent shear strain versus air-void content at 50°C—mixes containing AR-4000 asphalt content	72
Figure 47. Shear stress repetitions to 5 percent shear strain versus air-void content at 50°C— <i>all mixes</i>	73

Figure 48. Mix target gradations	75
Figure 49. Figure 49. Downward rut depth versus γ_p at $N = 7000$ repetitions in RSST-CH at 50°C; coarse mixes, original test sections	76
Figure 50. Downward rut depth versus γ_p at $N = 7000$ repetitions in RSST-CH at 50°C; fine mixes, original test sections	77
Figure 51. Downward rut depth versus γ_p at $N = 7000$ repetitions in RSST-CH at 50°C; fine plus mixes, original test sections.....	77
Figure 52. Downward rut depth versus γ_p at $N = 2700$ repetitions in RSST-CH at 50°C; coarse mixes, replacement sections. (Note: test data from both $t=0$ cores and from cores obtained at the conclusion of traffic $t =$ post mortem are included.)	78
Figure 53. Mix stiffness measured in shear versus air-void content	80

LIST OF TABLES

Table 1.	Geometrical layouts of cross-sections.....	9
Table 2.	Temperature conditions.....	10
Table 3.	Material properties	10
Table 4.	Average values for complex shear modulus and phase angle base on three replicate specimens	31
Table 5.	Ratios of G^* at 0.05 and 0.1 percent strain to that measured at 0.01 percent strain ...	37
Table 6.	Stabilometer “S” values for mixes containing AR-8000 and PBA-6A binders.....	53
Table 7.	Comparison of permanent deformation response measured in RSST-CH for specimens compacted by gyratory, laboratory rolling wheel, and field vibratory compactors	60
Table 8.	Experiment designs WesTrack sections.....	75
Table 9.	Aggregate and binders used in WesTrack test sections	76
Table 10.	Mix stiffness for mixes considered for Interstate 710 project.....	80

EXECUTIVE SUMMARY

This technical memorandum provides a summary of investigations, made primarily at the Pavement Research Center, University of California, Berkeley, on the stiffness and permanent deformation characteristics of asphalt/binder-aggregate mixes. Material is presented on the Strategic Highway Research Program (SHRP)–developed simple shear test, results of which have led to its use to evaluate rutting performance of asphalt concrete (AC) mixes. While the discussion is concentrated on the simple shear test, information is also presented relative to the use of uniaxial and triaxial tests to define stiffness and permanent deformation response.

Included herein are: 1) a discussion of the mechanics of permanent deformation of asphalt mixes; 2) a set of factors to be considered in selecting tests to measure permanent deformation response including specimen preparation, specimen size relative to the representative volume element, non-linear response, and static versus dynamic loading; and 3) examples illustrating the use of the simple shear test performed in repeated loading maintaining the specimen at constant height (RSST-CH) for mix analysis and design.

Chapter 2 presents data suggesting that shape (shear) distortion as compared to volume change is the main contributor to permanent deformation at higher temperatures in the asphalt-bound layer. This is illustrated by test results from shear-creep and hydrostatic pressure tests at 50°C on 15 different mixes.

Three-dimensional finite element analyses of three different pavement structures were also conducted to ascertain the relative importance of the two deformation modes on pavement behavior at temperatures in the range 40°C to 60°C (104°F to 140°F). Using a nonlinear hyperelastic constitutive relationship for the AC, which accounted for difference in volumetric and shear responses as well as temperature dependence, it was demonstrated that the

accumulation of permanent deformation in the AC layer is very sensitive to the layer's resistance to shape distortion and relatively insensitive to volume change.

These two studies demonstrate the importance of selecting a test which measures primarily shape (shear) distortion rather than volume change for defining the permanent deformation response of an asphalt mix.

Chapter 2 also contains a discussion of the size of the specimen relative to the maximum size of the aggregate contained in the AC. Data and analyses are presented indicating that to measure permanent deformation response which is statistically meaningful, dimensions of individual test specimens must be at least as large as the *representative volume element* (RVE). This is defined as the smallest volume large enough so that the global characteristics of the material remain constant, regardless of the location of the RVE.

Information is presented in Chapter 2 showing that important contributors to the RVE dimensions are aggregate size, shape, and orientation. These dimensions also depend on temperature and time (rate) of loading. At low temperatures and fast rates of loading the mastic (asphalt and fine aggregate) and the larger aggregate exhibit about the same response; whereas at higher temperatures the aggregate may be orders of magnitude stiffer than the mastic. Thus for the former conditions the RVE will be smaller than for the latter.

It must be recognized, therefore, that the RVE is unique for each mix and construction method, and the three characteristic lengths for a test specimen may be different.

Chapter 2 concludes with a discussion of the non-linear response characteristics of AC as influenced by rate of loading, temperature, and strain level. It emphasizes that when comparisons of material response, e.g. stiffness, are made, these should be done at the same strain level. In addition the data emphasize that the use of Equation 3, i.e.,

$$G^* = \frac{E^*}{2(1+\nu)} \quad (3)$$

where

G^* = shear stiffness

E^* = axial stiffness

ν = Poisson's ratio

To deduce G^* from E^* , or vice versa, is reasonable only at low temperatures and high frequencies.

Chapter 3 discusses the characterization of permanent deformation response of AC with the axial/triaxial compression and simple shear tests.

For the axial/triaxial, test discussion is included of the importance of “frictionless” end conditions and the influence of bulk modulus, K , on measured values of E in compression.

To measure the deviatoric component of strain with an axial test, the test configuration shown in Figure 27 should be used. This requires a specimen with a height/diameter of at least 2 to 1 and axial tension and radial compression stresses to be applied. Moreover, strains in both the axial and radial directions should be measured to deduce the deviatoric component of strain.

For the simple shear test, the discussion includes an analysis of the influence of missing tractions on the vertical faces of the specimen using finite element simulations. These analyses demonstrate that the effects of this imperfection decrease as the length-to-height ratio of the specimen is increased reaching a relatively small influence when this ratio is 3 to 1.

Considerations of RVE and specimen shape are also included. One of the key suggestions resulting from the analysis is the use of a rectangular parallelepiped rather than a cylindrical (core) specimen.

Chapter 4 contains a discussion of the use of creep and repeated load tests to measure permanent deformation response. Based on the information presented it is concluded that it is important to use a “dynamic” (repeated load) rather than a static test to measure this response, particularly if modified binders are used in the mix.

The influence of the method used to compact specimens for permanent deformation testing is evaluated in Chapter 5. A review of some studies evaluating compaction influences on mix characteristics is presented. In addition results of a recent study of specimens prepared by the Superpave Gyrotory Compaction (SGC-Pine), laboratory rolling wheel compaction, and field compaction is presented. The data indicate a difference in mix response in the shear test (RSST-CH) for specimens prepared by the SGC as compared to field and laboratory rolling wheel compaction.

Chapter 6 describes some experiences gained with using the RSST-CH for mix design and performance evaluation/analyses. Mix designs are illustrated by RSST-CH test results for mixes containing a PBA-6A binder, an asphalt-rubber binder, and a conventional AR-8000 asphalt cement. The procedure follows that developed during the SHRP asphalt program.

A study of mix performance on taxiways at the San Francisco International Airport illustrates the use of the RSST-CH to develop performance criteria for mixes for use on taxiways subjected to turning and stop and go movements of fully loaded B747-400 aircraft.

Also reported in Chapter 6 are the results of RSST-CH tests on mixes used at WesTrack. In this example the test was used to evaluate the rutting performance of AC mixes subjected to up to 5.0×10^6 ESALs. Results are presented in the form of rut depth versus plastic strain measured in the RSST-CH test at 50°C from tests on field mixed field compacted cores obtained from the 26 original and 8 replacement sections just prior to trafficking. For each set of mixes,

four total, a reasonable relationship between rut depth and plastic strain at a predetermined number of stress repetitions was obtained.

Chapter 7 contains a summary of the information presented with conclusions. The results clearly indicate that shear deformation contributes a significantly greater proportion to total permanent deformation (rutting) than volume change as seen from: 1) the results of the laboratory tests; and 2) the results of a representative pavement section. These results are supported by observed rutting in in-service pavements as well. Moreover, the shear deformations leading to rutting are limited to the upper portion of the AC layer. This suggests that a laboratory test which measures primarily shear deformations is the most effective way to define the propensity of a mix for rutting. Moreover, to make this evaluation, a specimen representative of the upper 75-100 mm (3-4 in.) appears most appropriate; this suggests, in turn, a specimen reflecting the mix in this part of the pavement, in terms of both aggregate structure and degree of compaction.

For the triaxial test, if shear deformation response is the primary contributor to specimen performance, then a test with the form of loading shown in Figure 27 should be utilized. If this is the case, to satisfy RVE requirements for a mix containing 19 mm maximum size aggregate, a specimen 125 mm (5 in.) in diameter by at least 350 mm (10 in.) high should be used, since it will be necessary to glue the loading plates to the ends of the specimens. Similarly in shear, it is likely that a specimen 100 mm high by 300 mm long should be used based on the information contained herein. When it is not possible to use specimens of these dimensions, the implications described herein should be noted.

It has been shown that asphalt mixes are non-linear in terms of applied stress, particularly at higher temperatures and comparatively slow rates of loading. This non-linearity significantly

reduces the possibility of deducing shear response from an axial test unless a configuration for both specimen size and loading of the type noted above are used. Similarly it would be difficult to deduce axial response from a test which measures primarily shear response, for the same reason.

It should be noted that if perfectly smooth ends are not used for relatively short ($H/D \sim 1$) specimens, the effects of the bulk modulus, K , on the laboratory determined E modulus becomes significant especially at elevated temperatures since the bulk modulus is significantly larger than the E modulus under these conditions.

In addition to the above items pertaining to specimen size and shape to define the propensity of mixes to rutting, information has also been presented on the effects of mode of loading (creep versus dynamic/repeated) and aggregate structure as influenced by method of compaction. For mixes containing modified binders, available data indicate that it is important to use dynamic (repeated) loading rather than creep loading. In addition, available data suggest that to simulate aggregate structure resulting from field compaction, a form of rolling wheel compaction is necessary.

Finally, data are presented which illustrate the efficacy of the SHRP-developed simple shear test, performed in the repeated load, constant height mode, for mix design and performance evaluation. Moreover, the data suggest that this type of test better evaluates the permanent deformation response of mixes containing modified binder as compared to conventional tests such as the Hveem Stabilometer.

1.0 INTRODUCTION

The purpose of this technical memorandum is to provide a summary of work that has contributed to the development of the simple shear test as a tool to evaluate the performance of asphalt concrete (AC) mixes. It is based primarily on investigations at the Pavement Research Center, University of California, Berkeley, related to the definition of the stiffness and permanent deformation characteristics of AC mixes. While the discussion is concentrated on the SHRP-developed simple shear test, some information is presented on the uniaxial and triaxial modes of loading as well.

This discussion includes the following:

1. the mechanics of permanent deformation in AC;
2. factors to be considered in test selection including: representative volume element; non-linear response; test specimen preparation; and static versus dynamic loading.
3. use of the simple shear tests for mix evaluation including mix design

This memorandum has been prepared to provide information related to activities at the national level directed to the development of a performance test to be included as part of the Superpave mix design and analysis procedure.

2.0 MECHANICS OF PERMANENT DEFORMATION AND ITS MEASUREMENT

The material presented in this section is based primarily on material contained in Reference (1) prepared by Dr. S. Weissman of Symplectic Engineering for the Pavement Research Center (PRC). Its purpose was to provide a theoretical basis for the selection of laboratory tests to identify AC material properties critical to the characterization of permanent deformation in pavement structures.

An investigation of laboratory test data obtained during the SHRP asphalt research effort (2) together with 3-D finite element analyses of pavement structures¹ suggest the following:

- Shape distortion (shear) is the main contributor to permanent deformations in the asphalt-bound layer.
- Accumulation of permanent deformations in this layer is very sensitive to the layer's resistance to shape distortion, and is relatively insensitive to resistance to volume change.
- The nonlinear nature of asphalt-aggregate mixes, particularly at higher temperatures, requires a direct test to measure resistance to *shape distortion*; any indirect tests may contain hidden errors (which may be large) introduced through the assumptions required to convert the measured data to a property related to shape distortion.
- Tire-pavement contact-stress distribution plays an important role in the development of permanent deformations in the asphalt-bound layer.

¹ Some of these analyses have been included in this technical memorandum.

In order to measure, with a few specimens, permanent deformation response that is statistically meaningful, the dimensions of individual test specimens must be at least as large as the *representative volume element* (RVE).

N.B. The RVE is defined as the smallest volume large enough so that the global characteristics of the material remain constant, regardless of the location of the RVE.

For AC mixes, the RVE may not be the same in all directions; differences depend on aggregate shape and method of compaction. Results of some analyses will be presented subsequently to illustrate these points and suggest appropriate dimensions for both uniaxial/triaxial and shear test specimens.

2.1 Volume-Change versus Shape-Distortion

This section considers the relative contribution to permanent deformation by volume change and shape distortion based on available laboratory test data and analyses of the response of representative pavement sections.

2.1.1 Laboratory Test Data

AC mixes at elevated temperatures exhibit markedly different volume-change and shape-distortion deformation modes in terms of their sensitivity to temperature, rate of loading, and residual permanent deformation.

Volume-change can be defined as deformation during which the change in all three principal strains is equal. Resistance to volume change is referred to as the *bulk modulus*, K . *Shape-distortion* is a volume-preserving deformation; resistance to this form of deformation is

referred to as the *shear modulus*, G . Both forms of deformation are illustrated schematically in Figure 1.

Decomposition of deformation into these two components is useful in understanding material behavior when one of the following criteria is fulfilled:

- The material is much stiffer in one of the two deformation regimes (e.g., $K/G \gg 1$).
- The material response to change in temperature or rate of loading is significantly different in the two modes of deformation (e.g., a large discrepancy in the relaxation times).
- The amount of residual deformation after the load is removed, as a percentage of the total deformation during loading, is higher in one deformation regime.

Data obtained during the SHRP asphalt research program (2) for 15 different mixes from two types of tests, simple shear creep tests with a shear stress of 69 kPa (10 psi) and hydrostatic pressure tests with a pressure of 690 kPa (100 psi), provide some indication of the relative behavior of AC in the two deformation modes.

Both type of tests² were performed at 50°C (122°F); specimens were 150 mm (6 in.) in diameter and 50 mm (2 in.) high. In both tests the load was increased at a steady rate from 0 to the full value in 10 seconds, maintained for another 100 seconds, and reduced to 0 at a constant rate over a period of 10 seconds. Measurements continued for an additional 120 seconds after the load was removed, thus making the total test time 240 seconds.

² Neither of these tests offers a pure test in the sense of total separation of the two deformation modes. For example, the heterogeneous nature of AC mixes leads to three different principal strains when hydrostatic pressure is applied; therefore, the hydrostatic pressure test offers only an approximation of a true volume-change test. Similarly, for reasons described later, the simple shear test, is only an approximation of a pure shape-distortion test (i.e., it also includes a volume-change component). In spite of these limitations, the test data provide a good indication of the difference in AC mix behavior between the two deformation modes. In fact, because the test data do not completely separate the two deformation modes, the data underestimate the difference between the two modes. Thus, if it shows a clear difference in behavior, it is anticipated that the actual true behavior of the AC mixes shows an even greater difference between the two modes of deformations.

Figure 2 shows the average strain history for these 15 mixes in the two tests. The effective bulk modulus, K , from the hydrostatic test is roughly 25 times larger than the effective shear modulus, G , from the simple shear test. It should be noted that the hydrostatic tests were conducted at 690 kPa (100 psi), while the simple shear tests at constant height were carried out at 69 kPa (10 psi). It is also clear that the hydrostatic tests (approximating volume-change tests) exhibit significantly less creep than that observed in simple shear tests (approximating shape-distortion tests).

The same average curves are also shown in Figure 3 where each of the two curves is normalized with its value just before the load is removed. The purpose of this figure is to demonstrate that volume-change tests recover a larger percentage of the total strain present prior



Figure 1. (a) volume change

(b) shape distortion

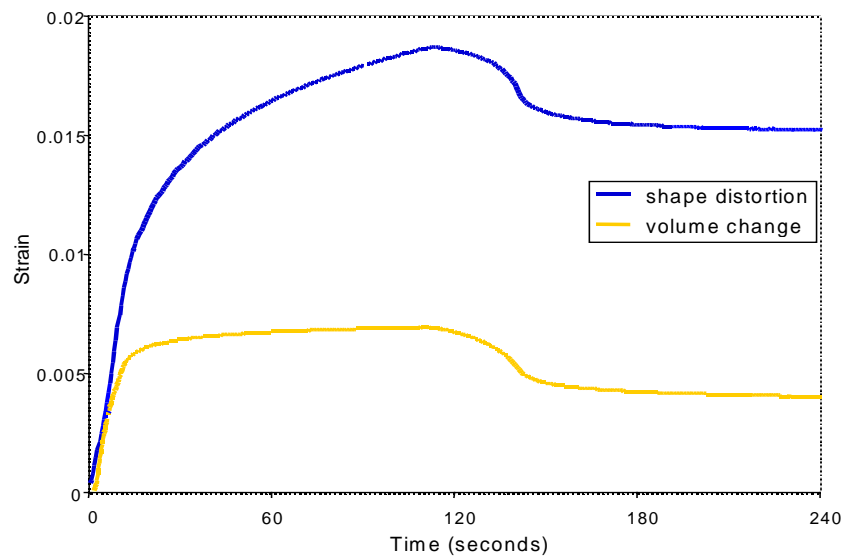


Figure 2. Average strain history for 15 different mixes (I)

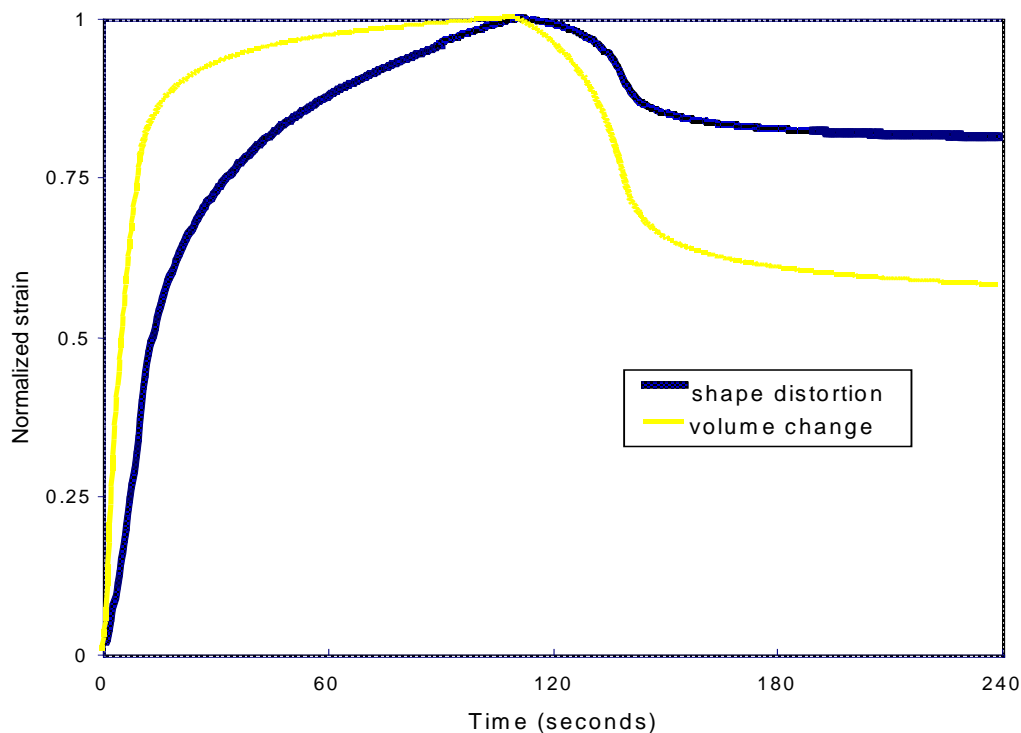


Figure 3. Normalized curves for average strain history for 15 mixes shown in Figure 2

to unloading. This specific set of data shows that, on the average, the mixes recovered only about 18 percent in the shape-distortion test, while the same mixes recovered about 42 percent in the volume-change tests.

The largest contribution to volume-loss in AC mixes is likely the reduction in the volume of air. The data shown in Figures 2 and 3 were obtained using newly fabricated specimens and thus, represent untrafficked materials. It would be expected that the percentage of strain recovery in volume-change tests would increase with additional load cycles. Therefore, in reality the difference in the percentage of recovered strain between the two deformation modes may actually be larger than that indicated by the data presented in the figures.

2.1.2 Finite Element Simulations of Pavement Response

To analyze the relative importance of the two deformation modes on the behavior of pavement systems, three-dimensional finite element simulation of three different pavement structures were examined.

The pavement sections analyzed are shown in Table 1. Pavement temperature conditions used are summarized in Table 2 and the material properties associated with each type of layer are included in Table 3. Since the study focused on the AC layer, the rest of the layers were assumed to exhibit elastic behavior for ease in computation.

2.1.2.1 AC Response. Unfortunately, no constitutive law currently available provides a good approximation of the behavior of AC mixes at elevated temperatures. Thus, for this study, a nonlinear elastic constitutive relationship was used that provided for different behavior in volume-decrease and volume-increase while allowing for temperature dependence.

This model suffers from two limitations. First, being an elastic model, it does not account for residual permanent deformations. This, however, does not restrict the main purpose of these simulations, which was to evaluate the relative importance of change in volume versus shape distortion. The elastic model can be used to represent the effective properties of the different materials during the first loading sequence. Therefore, for the first load cycle, the model can produce good indications of actual pavement behavior. Additionally, if the results during the loaded period are combined with laboratory test data, it is possible to arrive at conclusions regarding permanent deformations in the AC layer. In view of the difference in recovery during unloading (see e.g., Figure 1), the elastic simulation underestimates the relative difference between volume-change and shape-distortion.

Table 1. Geometrical layouts of cross-sections

Structure 1	
Component	Layer Thickness, mm (in.)
AC	100 (4.0)
aggregate base	200 (8.0)
Fx m recovery during unloading (see e.g., Figure 1), the elastic simulation underestimates the relative difference between volume-change and shape-distortion.subgrade	1000 ^a (40.0)

^a The subgrade layer, although semi-infinite in reality, is represented in the finite element model with a 1000 mm thick layer in all three systems considered.

Structure 2	
Component	Layer Thickness, mm (in.)
AC	212 (8.3)
aggregate base	250 (10.0)
aggregate subbase	250 (10.0)
subgrade	1000 (40.0)

Structure 3	
Component	Layer Thickness, mm (in.)
AC	125 (5.0)
Portland cement concrete	200 (8.0)
cement treated base	150 (6.0)
subgrade	1000 (40.0)

Table 2. Temperature conditions

Case Name	Temperature at Bottom	Temperature at Surface
T40	40°C (104°F)	40°C (104°F)
T60	40°C (104°F)	60°C (140°F)
T55	55°C (131°F)	55°C (131°F)

Table 3. Material properties

Materials	K (MPa)	G_{ref} (MPa) ^a	δ^b
Aggregate base	345	74	0
Aggregate subbase	230	49	0
AC	1,726	207	-8,550
Cement treated base	8,631	3,983	0
Portland cement concrete	13,152	12,008	0
Subgrade	92	20	0

^a G_{ref} is the reference shear stiffness defined in Equation 2.

^b δ is a material constant defined in Equation 2.

The second limitation of the model pertains predominantly to the AC layer, and is due to the missing rate effect in the model. However, the material constants were selected based on laboratory tests conducted at the relevant rate of loading. Therefore, this limitation did not constrain the ability to draw conclusions relative to the main questions these simulations were intended to answer.

The model selected was a nonlinear, hyperelastic, constitutive relationship. It accounts for differences in volumetric and shear responses as well as for temperature dependence:

$$W = Kf(I)_1 + 2G(T)f(I)_1J_2 \quad (1)$$

where:

W = energy function (derivative of which with respect to strain gives the stress),

K = bulk modulus,

G = shear modulus (depends on temperature),

T = temperature in degrees Kelvin,

f = scalar function (the second derivative of which, f'' , is shown in Figure 4),

$I_1 = \epsilon_{11} + \epsilon_{22} + \epsilon_{33}$

$J_2 = 0.5 \mathbf{e}:\mathbf{e}$ is the second invariant of the deviator strain \mathbf{e} .

The shear modulus G is assumed to depend on temperature as follows:

$$G(T) = G_{ref} \exp \left[\delta \frac{T - T_{ref}}{T T_{ref}} \right] \quad (2)$$

where δ is a material constant, G_{ref} is the value of G at the reference temperature, and T_{ref} is the reference temperature, 40°C (104°F) or 313°K in this instance.

2.1.2.2 Loading and Temperature Considerations. The pavement systems were loaded by a dual tire configuration. Because of symmetry between the two tires, only one-half of each pavement structure was modeled. The mesh has the form shown in Figure 5. The plan dimensions modeled are 3.5 meters from the symmetry plane in the lateral direction, x , and 7 meters in the longitudinal direction, y , (with the middle corresponding to the center of the tire in the longitudinal direction). The boundary conditions imposed were fixed at the bottom of the subgrade layer and symmetry at the plane of symmetry between the two tires. The pavement was also constrained not to move in the lateral direction at the plane located 3.5 meters away from

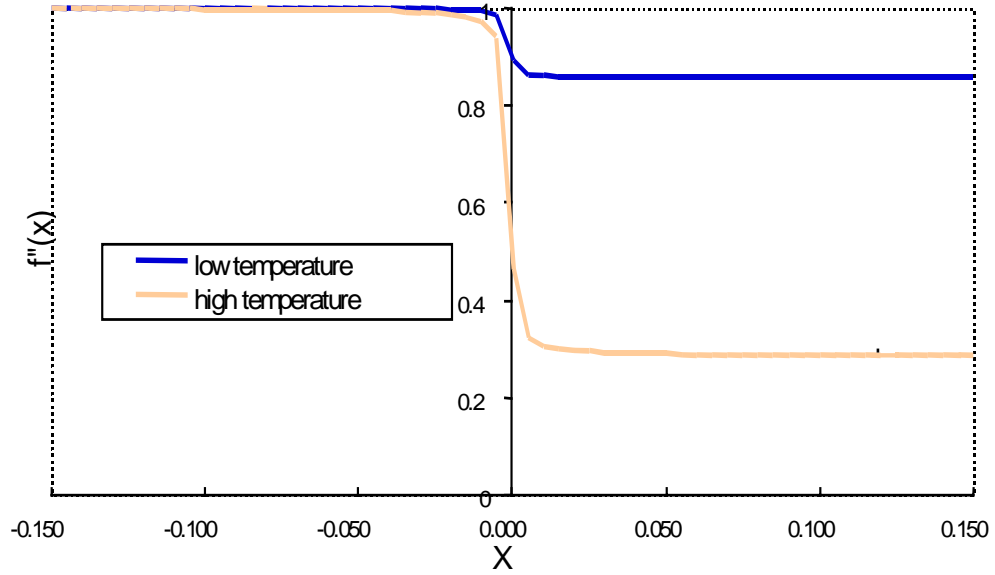


Figure 4. Variation of f'' with x , and its dependency on the temperature

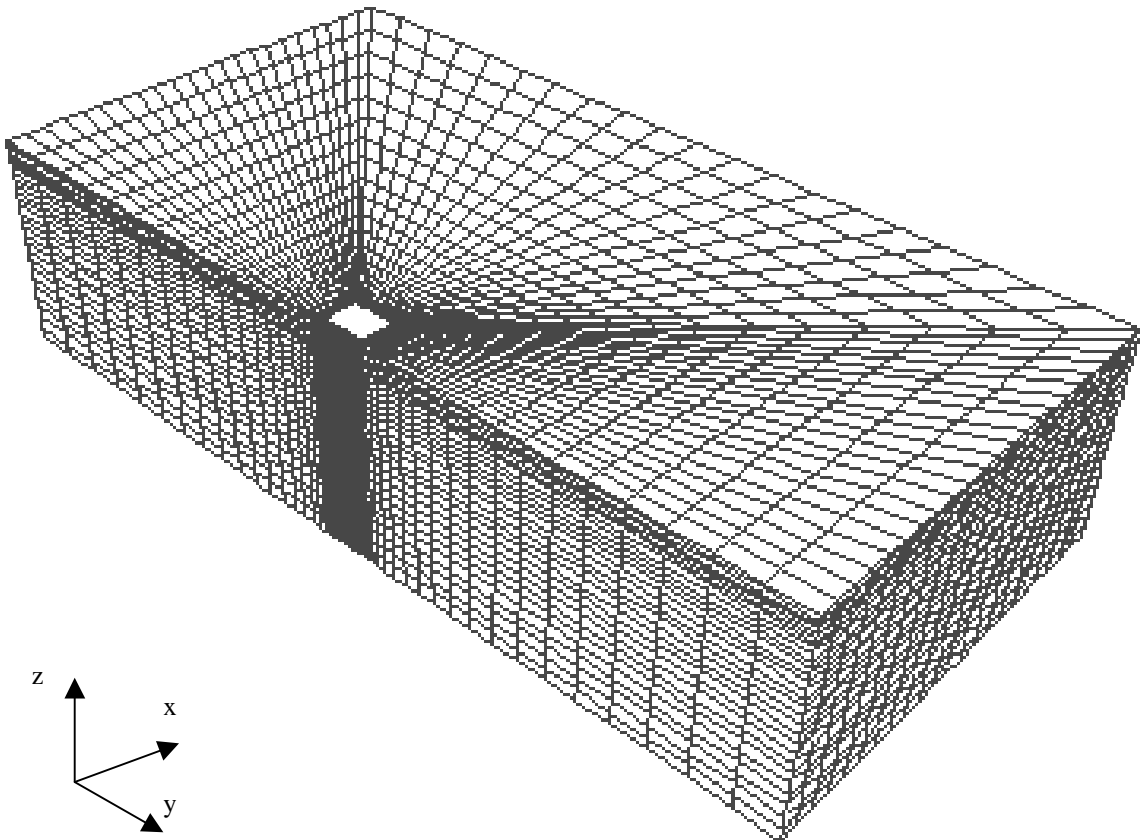


Figure 5. Perspective view of the finite element mesh used to represent AC pavement structure

the symmetry plane. Also it was constrained not to move at the front and back of the pavement sections. (N.B. The centerline of the dual tire configuration is located at the symmetry plane.)

All three pavement structures were loaded by a dual-tire configuration. The tire-pavement contact-stress distribution was that reported in Reference (3). The specific tire used was a Goodyear G159A, 11R22.5, with a load of 26 kN per tire, and a tire pressure of 690 kPa. Contour plots of the lateral, longitudinal, and vertical components of the tire-pavement contact-stress distribution are provided in Figure 6a, b, and c.³

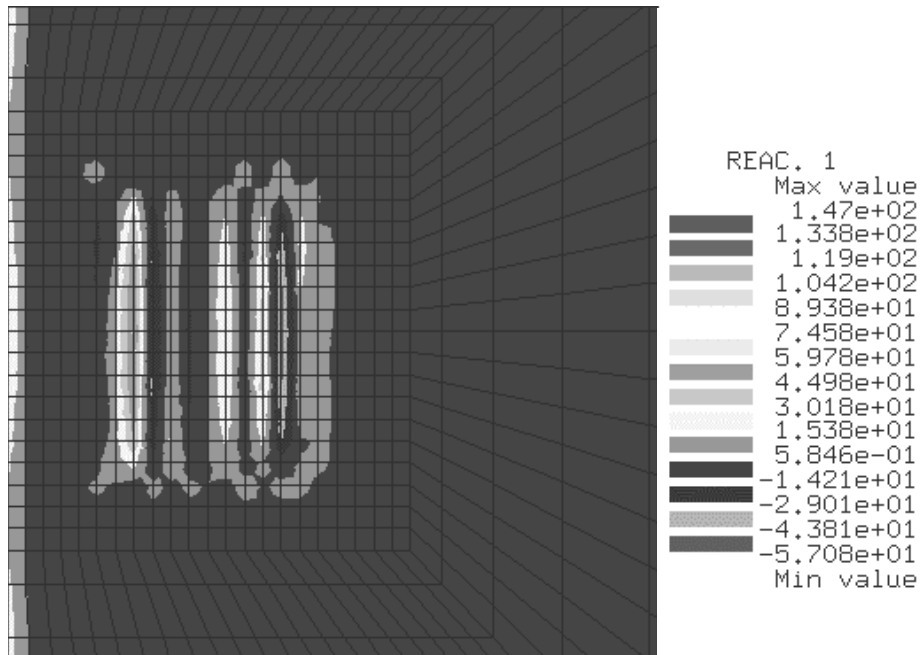
As seen in Table 2, three temperature conditions were considered. In all three cases, a temperature of 40°C (313°K) (104°F) was assumed throughout the supporting layers (i.e., all layers except for the surface AC layers). In the AC layer a linear distribution between the top surface and the bottom was assumed.

The first two temperature conditions were applied to all three structures. The objective of the third case, T55, was to evaluate the use of critical temperatures in the selection of environmental conditions for laboratory tests (4) and was applied only to Structure 2. This condition was selected so that the temperature throughout the AC layer would equal that found at 50 mm below the surface in the T60 case (one of the methods proposed to select the critical temperature for laboratory tests).

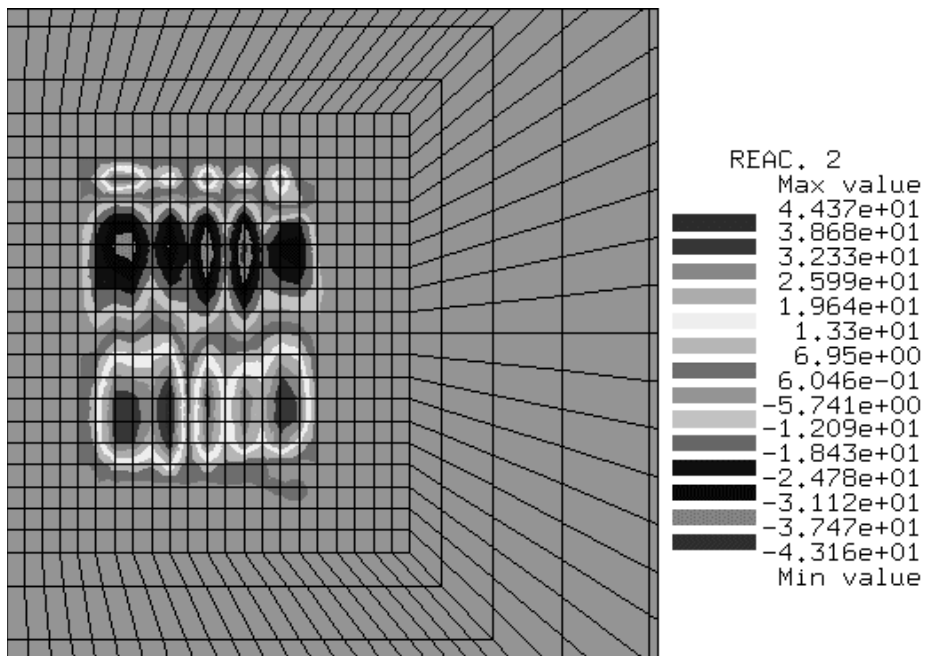
2.1.2.3 Results. From an evaluation of the results of the computations, a major pattern emerged⁴.

³ The contours in Figure 6 are actually of the reactions computed by the finite element procedure; therefore, Figure 6a, the lateral contact stress distribution, shows non-zero contours near the symmetry line (left edge).

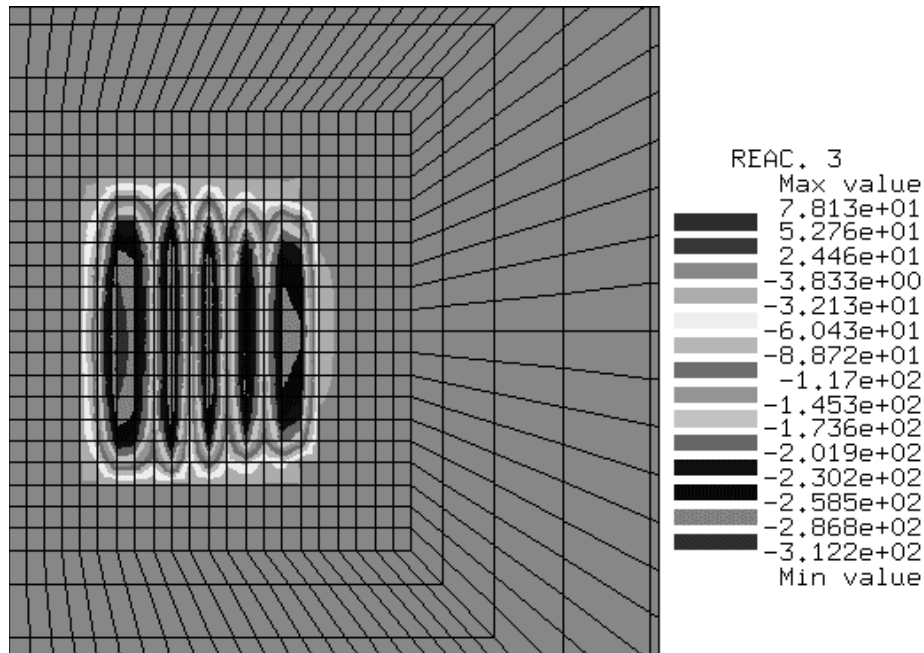
⁴ Results of the calculations are contained on a CD-ROM which show the actual output, such as deformation in a segment of the pavement in the vicinity of the tire (1).



(a) lateral (top) component



(b) longitudinal shear component



(c) normal (vertical) component

Figure 6. Tire-pavement contact stresses

There is a large concentration of all variables near the surface, under the tire. If these concentrations are combined with the assumption that the residual deformations (i.e., deformation remaining after the load has been removed) represent a certain percentage of the deformation during the load applications, then it can be concluded that the permanent deformations or ruts in the AC mix layers of all three pavement structures are predominantly confined to the top 75 mm (3.0 in.) of the pavement. This result is supported by field observations (5).

A second pattern to the importance of accurately modeling tire-pavement contact-stress distribution. A close examination of the concentrations present near the tire shows that these concentrations mirror the tire structure (i.e., treads in the tire are clearly visible even at a depth of 75 or 100 mm under the tire). Recalling the previous observation that permanent deformation in the AC layer is expected near the surface, it is possible to conclude that tire structure may play

an important role in the development of permanent deformation in the AC layer. Therefore it is important to accurately model tire-pavement, contact-stress distribution.

The computations of pseudo-energy (stress strain) for the T40 and T60 cases demonstrated that when interest is focused on rutting, attention should concentrate on the T60 case (I).

Pseudo-energy computations showed that effects are concentrated near the tire-pavement contact area (i.e., strains or stresses). In fact, at a depth of 50 or 75 mm (2 or 3 in.), the energy decayed to less than 30 percent of its maximum value and continued to decay rapidly as the distance from the loading surface increased. This result, which is supported by field measurements of residual deformations, indicates that ruts in the AC layer are predominantly a surface phenomenon. Therefore, because volume-loss in the top 50 or 75 mm (2 or 3 in.) of AC layers can account for 1 to 2 mm (0.04 to 0.08 in.) of the rut at most, and rut depths of 15 mm (0.6 in.) or more are observed, shape-distortion has to be the dominant contributor to rutting.

A comparison of the distributions of the volume-change ($I_1 = \text{volume-change}$) and shape-distortion ($\sqrt{J_2}$) the second invariant of the strain deviator tensor that can be interpreted as a measure of shear strain) also demonstrates that shape-distortion contributes much more than volume-change to the deformation of AC layers.

One of the studies involved varying G for the AC while maintaining K constant; G was first reduced by an order of magnitude, and then increased by an order of magnitude. The simulations were repeated with similar variations in K while keeping G constant. The sensitivity study was performed using only Structure 2. The resulting vertical and lateral displacements in the AC layer are shown in Figures 7 and 8. Both figures show the first 600 mm from the symmetry plane between the two tires; the tire is on the left side of the image and only the AC

layer is included. To assist in understanding this study, plots of the maximum vertical displacement and of the increase in distance between points located about 50 mm under the edges of the tire versus change in property are provided in Figure 9 and 10. As can be seen, the structural response is more sensitive to changes in the resistance of the AC layer to shape-distortion (G) than to change in its resistance to volume-change (K).

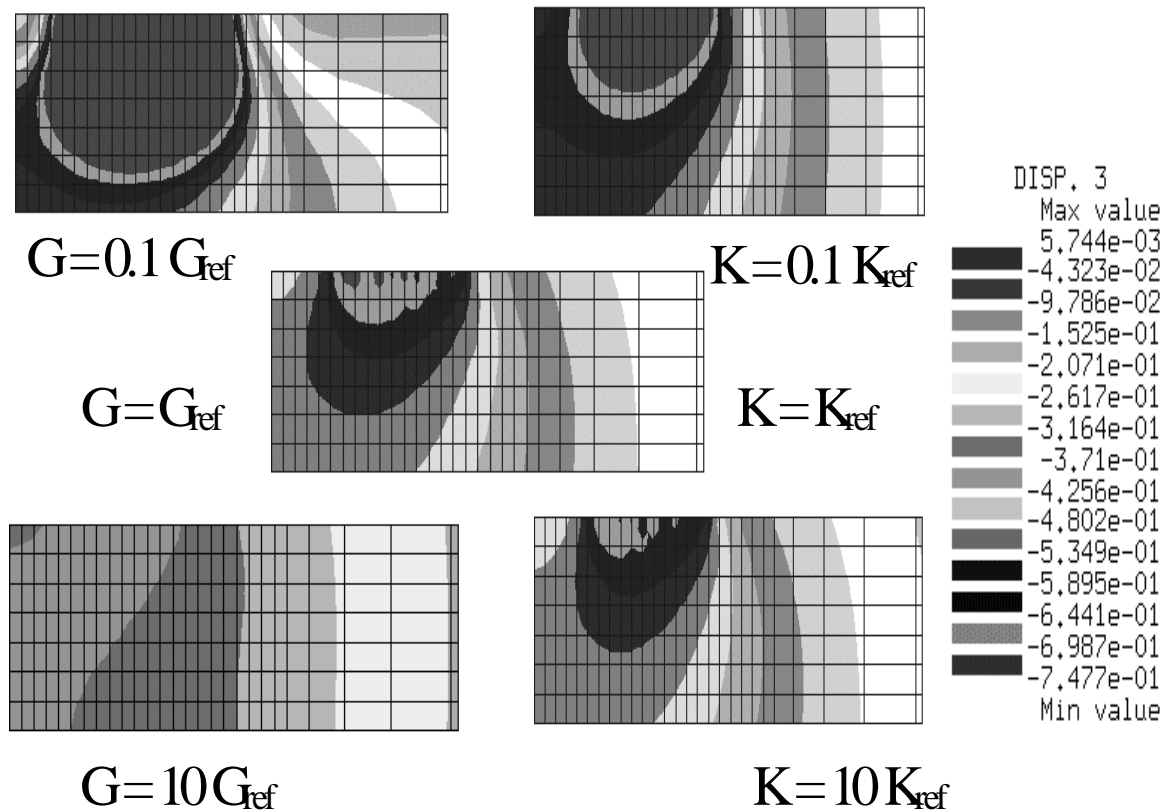


Figure 7. Vertical deformation in the AC layer first (500 mm from the symmetry plane); effect of variation in G while maintaining K constant, or vice-versa

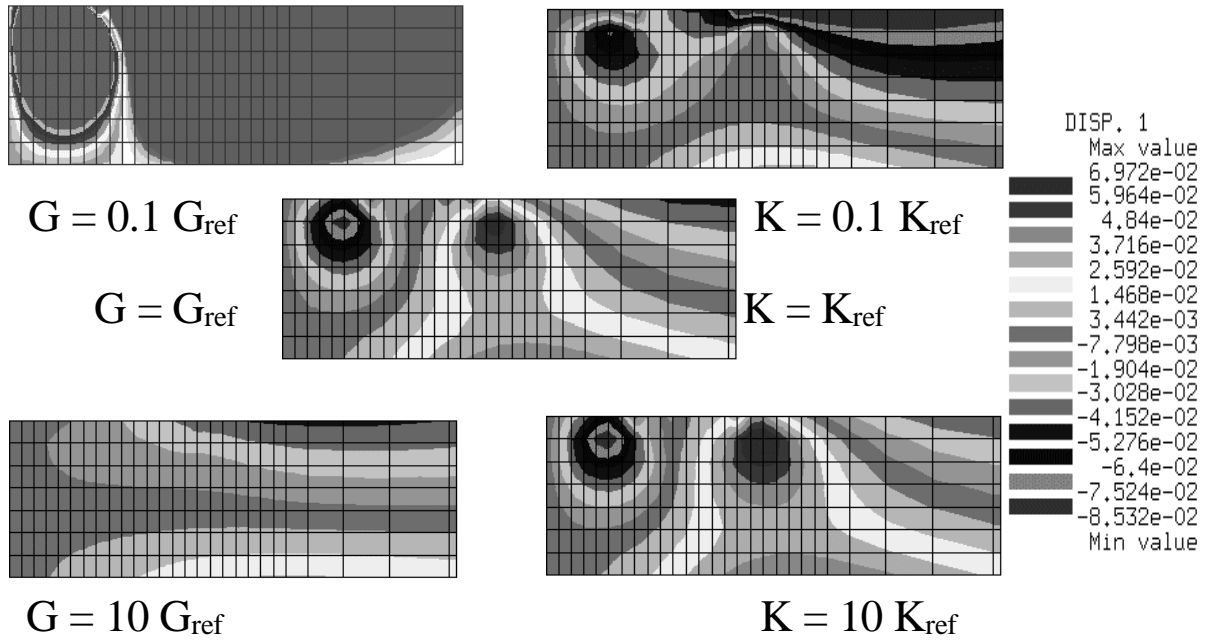


Figure 8. Lateral deformation in the AC layer (first 500 mm from the symmetry plane); effect of variation in G while maintaining K constant, or vice-versa

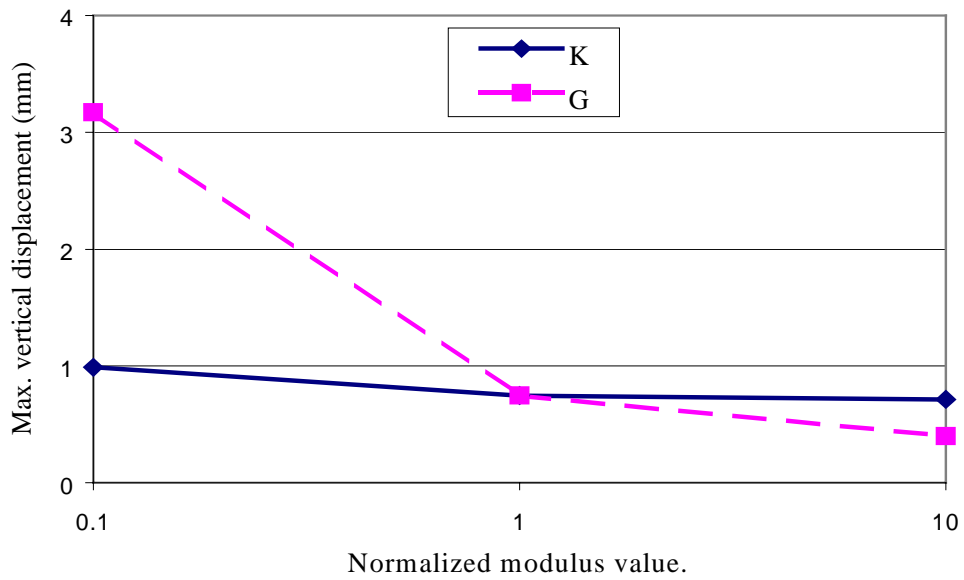


Figure 9. Variation of the maximum vertical displacement in the AC later with changes in material properties

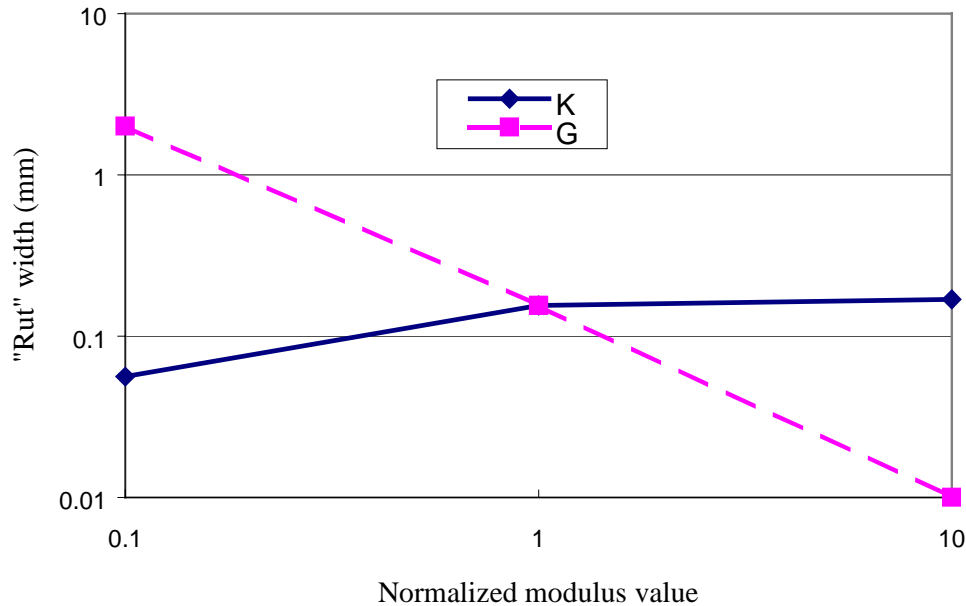


Figure 10. Variation of the distance between points located 50 mm below the tire edges (under the tire center in the longitudinal direction) as a function of the changes in material properties

2.2 Laboratory Test Considerations

Scale is an important factor to be considered in material testing. Laboratory tests are constructed around theories (e.g., continuum mechanics and constitutive relationships), and are designed to identify specific parameters associated with the models. Therefore, an important question is whether the theory stipulated is applicable to a specific test. In particular, many models in common use in the field of mechanics of materials are based on homogenization of properties across heterogeneous media. Thus, it is important to have enough material for the homogenizing process to make sense.

For some materials the question of scale between the particle size in the material and the dimensions of a practical test apparatus may not be significant, e.g. the testing of steel. For AC mixes, however, this factor becomes important since the size of the larger aggregate may not be much smaller than the specimen size. For such materials, therefore, it is important to verify at

what minimum specimen dimensions continuum mechanics, or any other theory based on homogenization, becomes applicable. This specimen dimension is referred to as the RVE and has been defined earlier. When specimens larger than the RVE are used it is likely that less variable test results will be obtained.

At times, it may not be possible to use specimens larger than the RVE; accordingly, it is important to understand the impact. A review of composite mechanics literature (6) shows that, when specimens smaller than the RVE are tested, random results are observed; some specimens may display low values of the measured property whereas others may yield high values. Consequently, the mean value of the results must be obtained from a large number of test specimens in order to arrive at a statistically meaningful property value.

Determining the property from specimens smaller than the RVE has two major disadvantages. First, as noted above, a large number of specimens may be required. Second, an averaging process ignores any bias⁵ in the test procedure, which may result in large errors. In view of these limitations, the use of specimens larger than the RVE is recommended. However, in some cases the use of specimens smaller than the RVE may be unavoidable; for example, a mix containing large aggregate. In such cases, statistically meaningful results can be obtained by testing a large number of replicates, although the above limitations should be noted.

Many current laboratory tests show large variability in test results. Differences in results of 50 and 100 percent have been found between replicate specimens even when the same computer-controlled equipment is used (7). An example of such data is presented in Figure 11 for the repetitive simple shear test at constant height (RSST-CH). The three specimens have slight differences in air void contents but these differences should not account for the large

⁵ Bias might occur, for example, because of the mix preparation method and selection of test specimens from a specific part of a compacted mix.

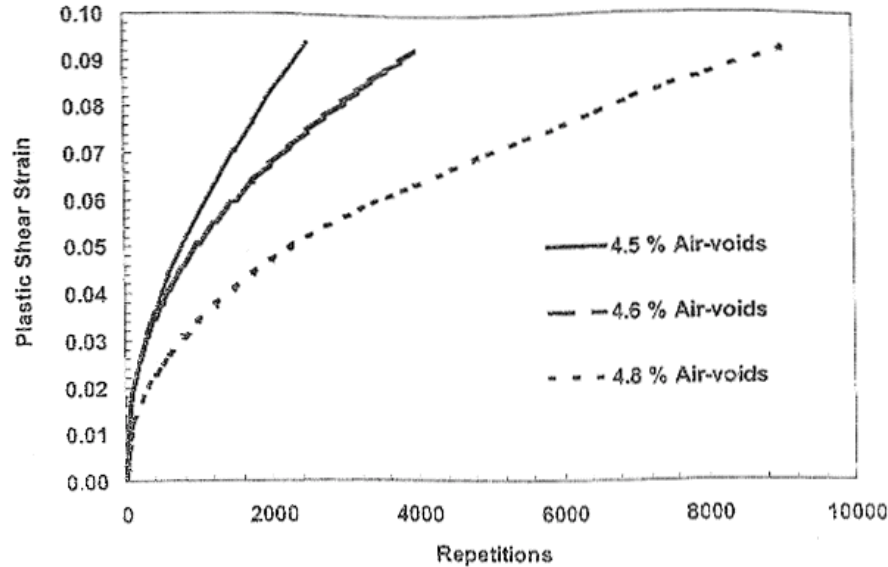


Figure 11. Test data variability for three replicate specimens: repetitive simple shear tests at constant height

differences in results. Thus, typical laboratory tests of AC mixes show the classic indications noted in the literature for specimens smaller than the RVE.

Current laboratory procedures also typically use only two to four replicates. Thus, if specimens are smaller than the RVE, there is no guarantee that the average result obtained predicts a statistically meaningful property of the material.

2.2.1 Finite Element Simulations of Test Specimens

Two-dimensional, plane strain, finite element simulations were performed to investigate the effects of the RVE on specimen response. The finite element meshes used in the analysis were obtained from actual specimens. Two mixes were used, one containing a Pleasanton aggregate (SHRP-MRL material RH) and the other containing Maryland aggregate (SHRP-MRL material RD). The nominal maximum aggregate size for both mixes was 19 mm.

Because of the resolution of the procedure by which the meshes were obtained it was not possible to represent the air voids. Small aggregates are also difficult to detect and therefore the mesh represents a two-phase material of aggregate and mastic. These shortcomings should not place any limitations on the validity of the findings because the larger-sized aggregates have a greater influence on the RVE. An example of a mesh for the Pleasanton aggregate is presented in Figure 12.

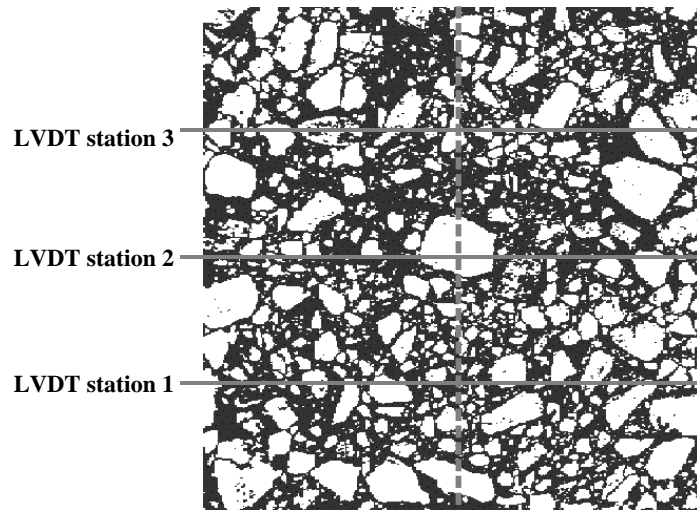


Figure 12. Example of the mesh for the Pleasanton aggregate mix, 640×640 elements, mesh dimensions are 150×150 mm.; black = mastic, white = aggregate, locations of the virtual LVDT stations for axial tests are in the horizontal direction and all LVDTs are centered about the dashed line

In the simulations, both the aggregate and mastic were assumed to be linear elastic. The stiffness of the aggregate was taken as $E = 100$ MPa (14500 psi) and Poisson's ratio was set $\nu = 0.35$. To assess the effect of temperature on the RVE, the material properties for the mastic were $E = 100, 10, \text{ and } 1$ MPa (14,500, 1,450, and 145 psi) and $\nu = 0.49$, where the value of 100 MPa (14,500 psi) was used to represent the lower temperature and the value of 1 MPa (145 psi) was to represent the higher temperature. At the elevated temperatures at which

permanent deformation occurs, the ratio of the aggregate and mastic stiffness may even be higher than the 100:1 ratio selected. It should also be noted that the rate of loading affects the stiffness of AC, and hence the varying stiffnesses used in the simulations investigate the effect of rate of loading on the RVE as well.

Anisotropic materials may have three different RVE dimensions. To investigate the anisotropy of the mix, two meshes were obtained for each mix—from the longitudinal-vertical face and from the transverse-vertical face. The direction refers to the orientation of the physical specimen during its production (specimens were produced with a rolling wheel compactor). Each two-dimensional face of the three-dimensional specimen used to obtain the meshes was 150×150 mm (6×6 in.).

Each simulation consisted of a virtual axial test. The boundary conditions had one edge fixed in the normal direction and a uniform displacement was imposed on the opposing edge in the direction of the constrained edge (i.e., axial compression). Virtual linear variable displacement transducers (LVDTs) were placed along three lines on the section, and strains were measured around the center line, as indicated in Figure 12 for an axial load applied in the horizontal direction. Results of the finite element simulations include distributions of axial deformation in the virtual specimens and effective stiffness moduli.

2.2.2 Axial Deformations

Figure 13 illustrates the distribution of axial deformations for the case where $E_{aggregate} = E_{mastic} = 100$ MPa (14,500 psi), and Figure 14 presents results for $E_{aggregate} = 100$ MPa (14,500 psi) and $E_{mastic} = 1$ MPa (145 psi), where E represents the Young's modulus of the

material. The axial deformation in Figure 13 is relatively uniform, whereas large variations are present in Figure 14 where there is a 100:1 ratio of the aggregate to mastic stiffnesses.

Figure 15 contains a plot of the axial strain in the y direction for the Pleasanton aggregate. The non uniform strain across the specimen shows that the strain at certain points in the mix, specifically in the mastic, may be considerably higher than the average imposed strain. It is therefore important to ensure that gage length is sufficiently large to measure an average strain and not the local, highly variable strain.

Figures 16 and 17 show the deformations obtained by the virtual LVDTs for the Pleasanton aggregate for the x direction. These plots indicate the variation in the axial strain measured by these LVDTs. The imposed average strain for all specimens was 1 percent. The plots indicate a band of ± 20 percent about this value. As expected, the figures associated with $E_{mastic} = 100$ MPa (14,500 psi) indicate that the RVE at low temperatures can be relatively small.

The plots of results for $E_{mastic} = 1$ MPa (145 psi) clearly show large oscillations, even for gage lengths larger than 100 mm (4.0 in.) [recall that the nominal aggregate size was 19 mm (.75 in.)]. Also, some of the results appear to show bias: the predicted strain converges from one side—either above or below. This is particularly troubling because computer simulations offer ideal frictionless test conditions. Physical tests may show considerably more bias, thus hampering the use of specimens smaller than the RVE.

The bias in the simulation is attributed to the use of specimens smaller than the RVE in which a single large aggregate may have a large local effect. The rapid convergence as the gage length increased above 125 mm (5.0 in.) may be an artifact of the simulations given that the strain at a gage length of 150 mm (6.0 in.) is imposed. Therefore, it is not clear that the measured strain converges for all simulations.

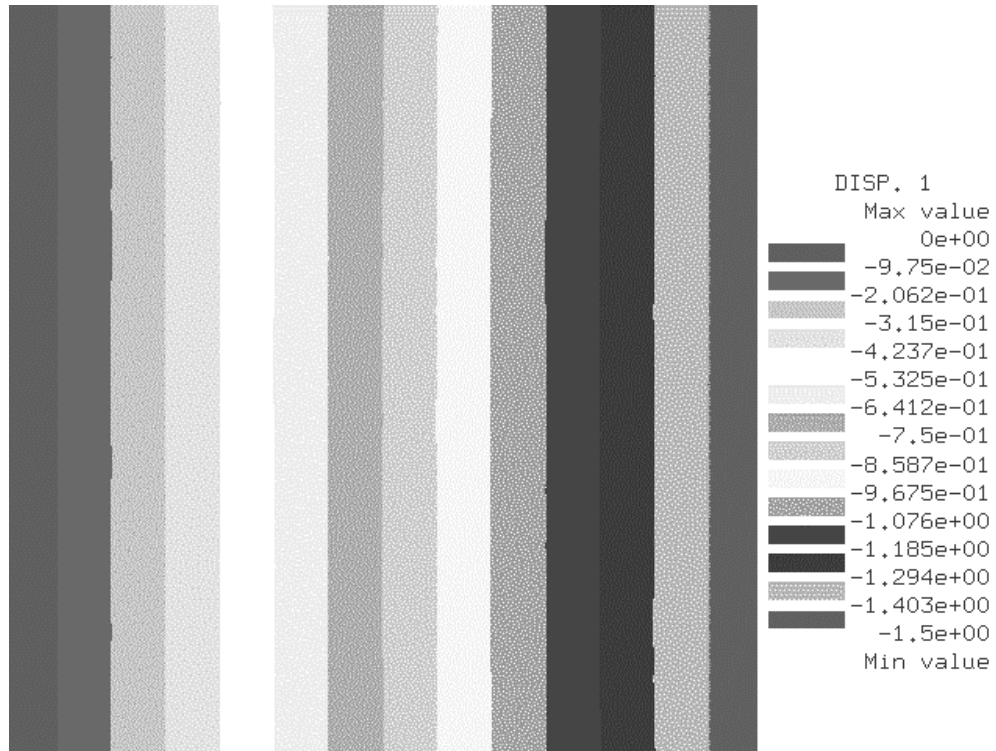


Figure 13. Contours of axial displacements (y direction): Pleasanton aggregate, $E_{aggregate} = 100$ MPa and $E_{mastic} = 100$ Mpa

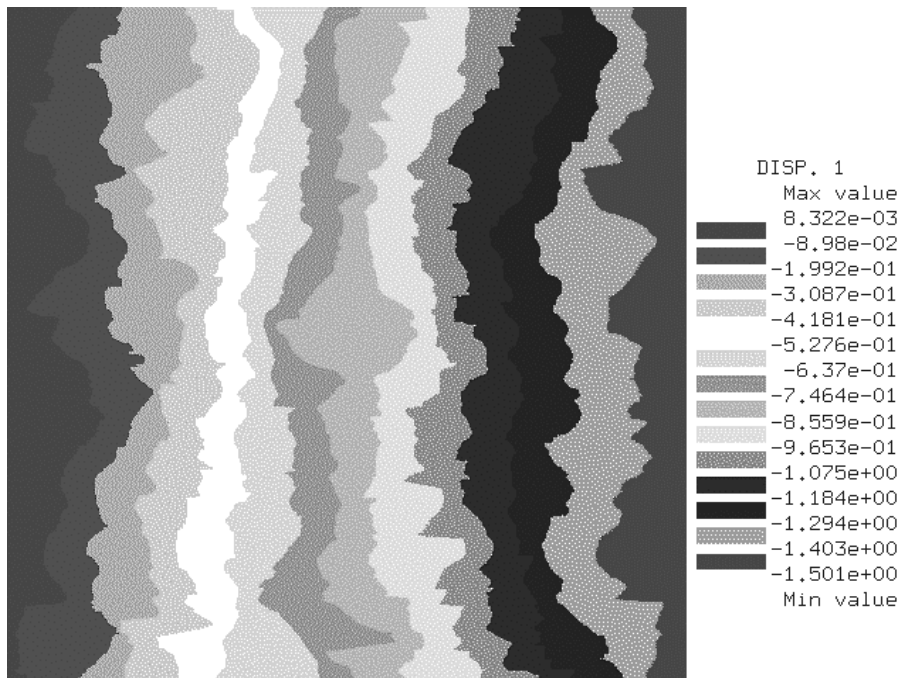


Figure 14. Contours of axial displacements (y direction): Pleasanton aggregate, $E_{aggregate} = 100$ MPa and $E_{mastic} = 1$ Mpa

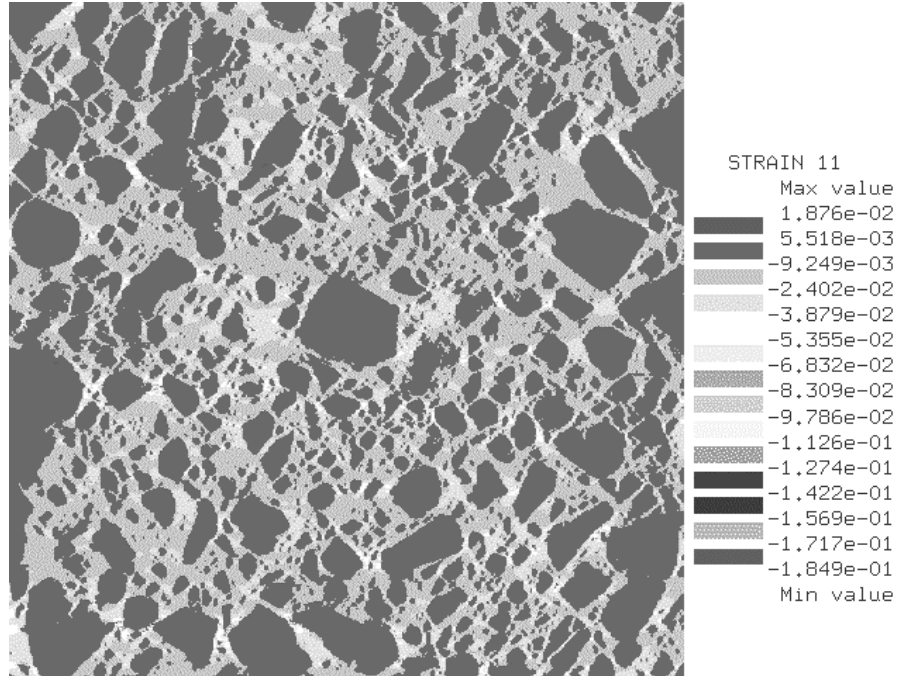


Figure 15. Contours of axial strain (y direction): Pleasanton aggregate, $E_{aggregate} = 100$ MPa and $E_{mastic} = 1$ Mpa

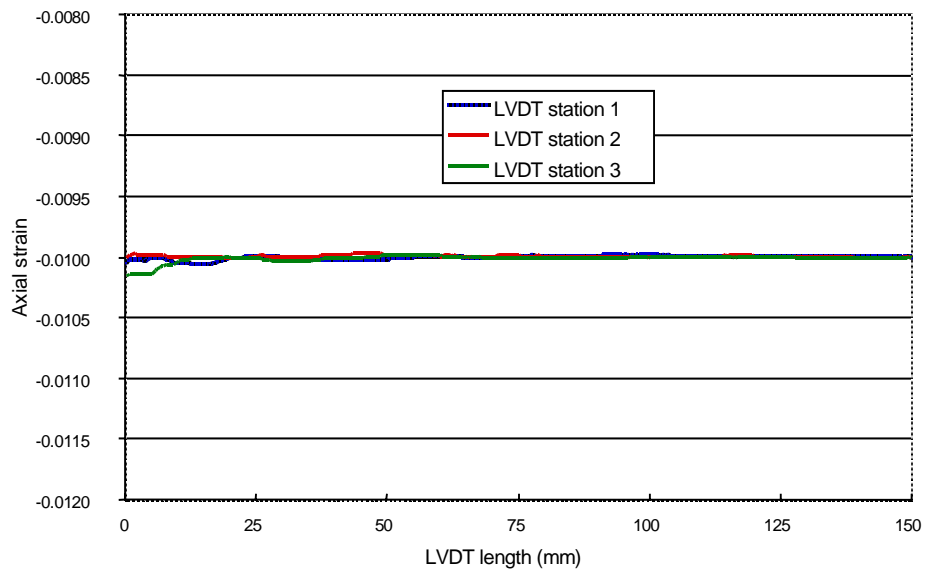


Figure 16. Effect of gage length on measured axial strain (x direction): Pleasanton aggregate, $E_{aggregate} = 100$ MPa and $E_{mastic} = 100$ MPa

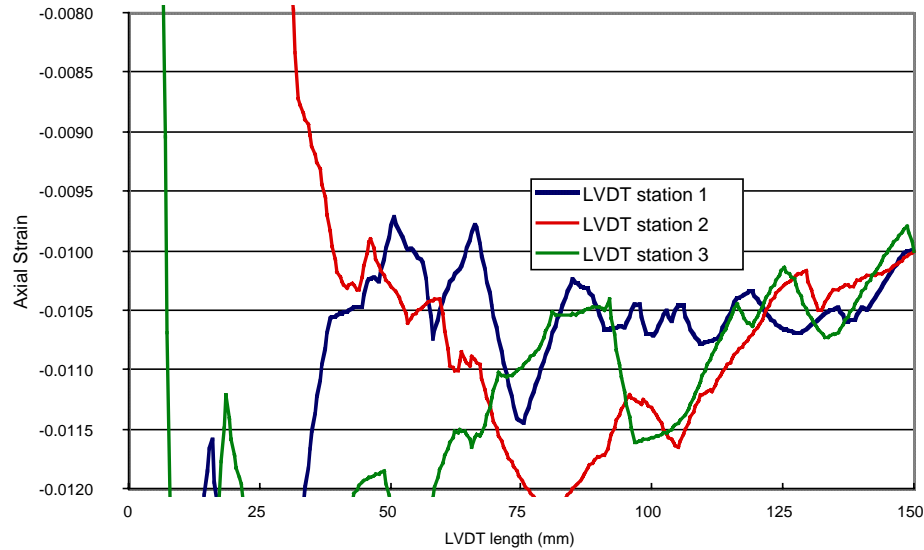


Figure 17. Effect of gage length on measured axial strain (x direction):
 $E_{aggregate} = 100 \text{ MPa}$ and $E_{mastic} = 1 \text{ MPa}$

Any set of finite-sized AC specimens will show some variability in performance. Therefore, in practice, an acceptable error level (tolerance) is set, and the RVE dimensions are selected to meet this specification. For example, consider the vertical RVE dimension for the two mixes for creep tests at elevated temperatures, and let the acceptable error level be set at 10 percent. Then, the RVE dimension in the vertical direction for the Maryland mix is about 90 mm (3.6 in.), and for the Pleasanton mix it is about 100 mm (4.0 in.). In the transverse direction, the RVE dimensions are 120 (4.8 in.) and 130 mm (5.2 in.) for the Pleasanton and Maryland aggregates respectively. These dimensions are subject to the limitations of the analysis and should be substantiated by laboratory experiments.

Important contributors to the RVE dimensions are the aggregate size, shape, and orientation. Because of this, the RVE for different mixes with different aggregates may differ from that for mixes with the same nominal-sized aggregate. (Note that the same nominal-sized aggregate does not imply that both mixes will have the same maximum aggregate size.)

Also recall that the RVE dimension depends on both temperature and rate of loading. This is due to the rate of loading and temperature dependence of the material properties of the mastic (asphalt and fine aggregate), whereas the aggregate properties are relatively insensitive to these effects. As a result, at low temperatures the properties of the two components are close, and at elevated temperatures the aggregate may be orders of magnitude stiffer than the mastic. Additionally, dynamic tests may require smaller specimens than static (creep) tests because the properties of the aggregate and mastic are closer at higher frequencies of loading. For example, smaller specimens may be used for the standard repetitive simple shear at constant height tests than are required for an equivalent creep test.

2.2.3 *Effective Stiffness Modulus*

The simulations were also used to obtain an effective stiffness modulus, E , for the mix. The results are shown in Figure 18 which indicates that, as the ratio of the aggregate stiffness and mastic stiffness is increased, the effects of the aggregate structure and orientation have more influence. The larger difference between the horizontal and vertical directions shown by the Maryland aggregate compared with the Pleasanton aggregate is attributed to the fact that the shape of the Pleasanton aggregate is more cubical.

It can be concluded that the RVE will be similarly affected by aggregate structure and orientation, and hence the RVE is unique for each mix and construction method, and the three characteristic lengths may be different.

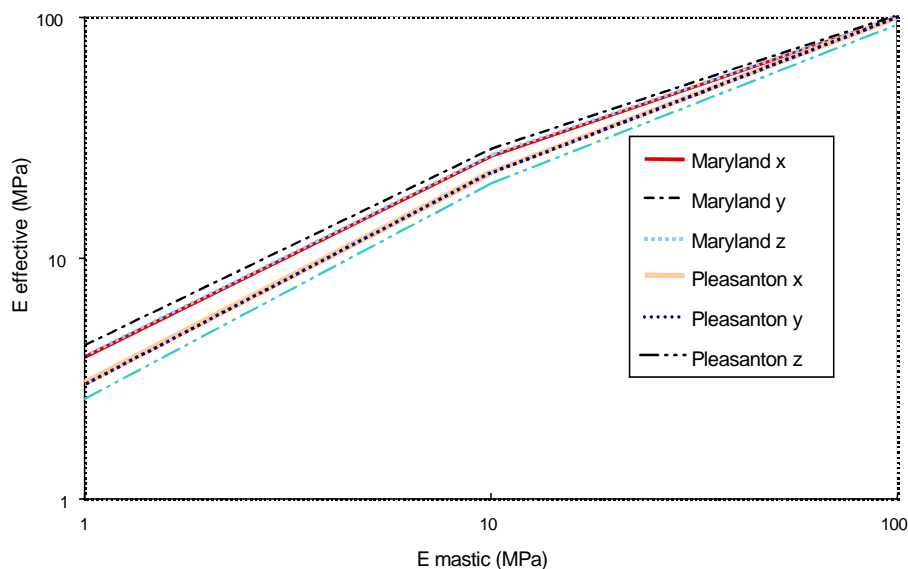


Figure 18. Variation of effective stiffness E as a function of mastic property, plotted by orientation

2.3 Non-linear Response Characteristics of Asphalt Aggregate Mixes

At higher temperatures, as noted earlier, asphalt-aggregate mixes exhibit non-linear response characteristics. Thus when making comparisons of responses determined from different tests it is important that these comparison be made at the same strain level. Evidence of this non-linearity is illustrated in this section.

The effects of frequency of loading, strain level, and temperature on shear stiffness of AC were studied using the simple shear test (8). Specimens 150 mm (6 in.) in diameter by 50 mm (2.0 in.) high were obtained from cores of a dense-graded AC being evaluated as a part of the CAL/APT program (9). Air void contents of the specimens were in the 6.0 to 7.0 percent range. Test temperatures ranged from 20°C (68°F) to 57°C (135°F); three strain levels were utilized: 0.01, 0.05, 0.10 percent⁶; and frequencies ranged from 10 to 0.01 Hz. The test method described

⁶ The AASHTO TP7-94 procedure currently calls for a shear strain of 0.005 percent for the frequency sweep tests. Our results suggest that this level is too small to measure with precision using LVDT instrumentation available in the simple shear test machines presently in.

in AASHTO TP7-94 (10) was followed except that the deformation was measured across the metal platens and not on the side of the specimen. This arrangement was used in order to provide an average measurement of specimen response across the entire specimen rather than the local response obtained when the LVDT is mounted on the side of the specimen⁷. A 37 mm (1.5 in.) gage length was used for shear strain determination since the experience at the PRC indicates that the specimen deformation is controlled by the epoxy bond in 6.5 mm (0.25 in.) of the mix adjacent to each of the platens. Details of the test procedure are described in Reference (11) and the average values for stiffness are plotted in Figure 19.

Results of the study are summarized in Table 4. The effects of strain level on complex shear modulus (G^*) versus frequency are shown for the individual specimens in Figures 20, 21, and 22 for the temperatures of 20°C, 40°C, and 57°C (68°F, 104°F, and 135°F), respectively.

In Figure 19 it will be noted that G^* increases with decreased temperature, increased frequency, and smaller shear strains. At low temperatures and high frequencies the shear stiffness, G , should be about one-third of the Young's modulus, E , at corresponding conditions. From Figure 19 it will be noted, for example, that the value of G^* at a temperature of 20°C (68°F) and a frequency of 10 Hz is about 2.2 GPa (320,000 psi). The complex modulus, E^* , determined in flexure for the same mix at the same temperature and frequency and at a strain of 0.015 percent is about 6.5 GPa (943,000 psi) suggesting that the linear elasticity assumption is reasonable for these conditions. That is, the relationship:

$$G^* = \frac{E^*}{2(1+\nu)} \quad (3)$$

⁷ This method of mounting the LVDT probably helps reduce the variability of the Superpave Gyrotory Compacted (SGC) specimens which have uncut surfaces along the sides of the cylinder.

Table 4. Average values for complex shear modulus and phase angle base on three replicate specimens

Average of Three Replicate Tests									
	0.0001 Shear Strain			0.0005 Shear Strain			0.001 Shear Strain		
	20C	40C	57C	20C	40C	57C	20C	40C	57C
Frequency	Complex Shear Modulus (kPa)			Complex Shear Modulus (kPa)			Complex Shear Modulus (kPa)		
10	2,289,697	257,980	54,129	2,240,240	199,914	27,884	955,890	178,675	23,692
5	1,918,313	175,294	42,402	1,666,067	130,792	19,150	668,267	113,083	15,857
2	1,464,797	103,062	32,642	1,172,647	74,010	12,845	508,977	64,026	10,133
1	1,171,507	69,602	27,421	891,840	48,323	10,433	396,706	41,186	7,837
0.5	921,246	48,120	24,995	693,644	36,822	8,641	314,093	26,758	6,641
0.2	629,521	31,997	22,504	479,886	22,541	7,677	223,865	15,791	5,761
0.1	445,438	24,823	20,646	354,065	16,818	6,964	167,692	11,324	5,450
0.05	283,278	20,832	21,674	232,138	13,086	6,520	118,295	8,491	5,089
0.02	176,141	17,996	21,219	147,613	10,599	6,469	76,310	6,734	4,905
0.01	108,691	16,173	17,828	100,449	9,375	6,016	63,876	5,949	4,742
	Shear Phase Angle (degrees)			Shear Phase Angle (degrees)			Shear Phase Angle (degrees)		
10	27.2	54.8	54.8	20.3	60.5	60.3	14.2	60.3	62.1
5	29.3	56.8	48.2	22.4	60.7	54.4	16.3	62.5	57.0
2	32.0	56.9	41.1	27.1	61.9	46.4	21.8	63.6	47.6
1	34.8	55.2	38.2	30.9	61.1	41.6	27.2	63.3	41.0
0.5	38.3	51.3	35.4	35.2	56.2	36.8	31.4	61.5	33.6
0.2	43.5	45.6	32.4	40.9	51.2	30.9	36.4	56.5	28.1
0.1	46.5	38.8	31.0	44.5	46.8	28.1	40.1	51.1	26.7
0.05	38.4	36.2	27.1	47.1	40.4	24.9	42.9	44.0	23.1
0.02	45.0	36.7	31.1	51.2	35.4	26.3	47.1	36.1	22.0
0.01	45.6	35.8	30.4	53.8	31.7	25.5	49.1	30.5	21.0

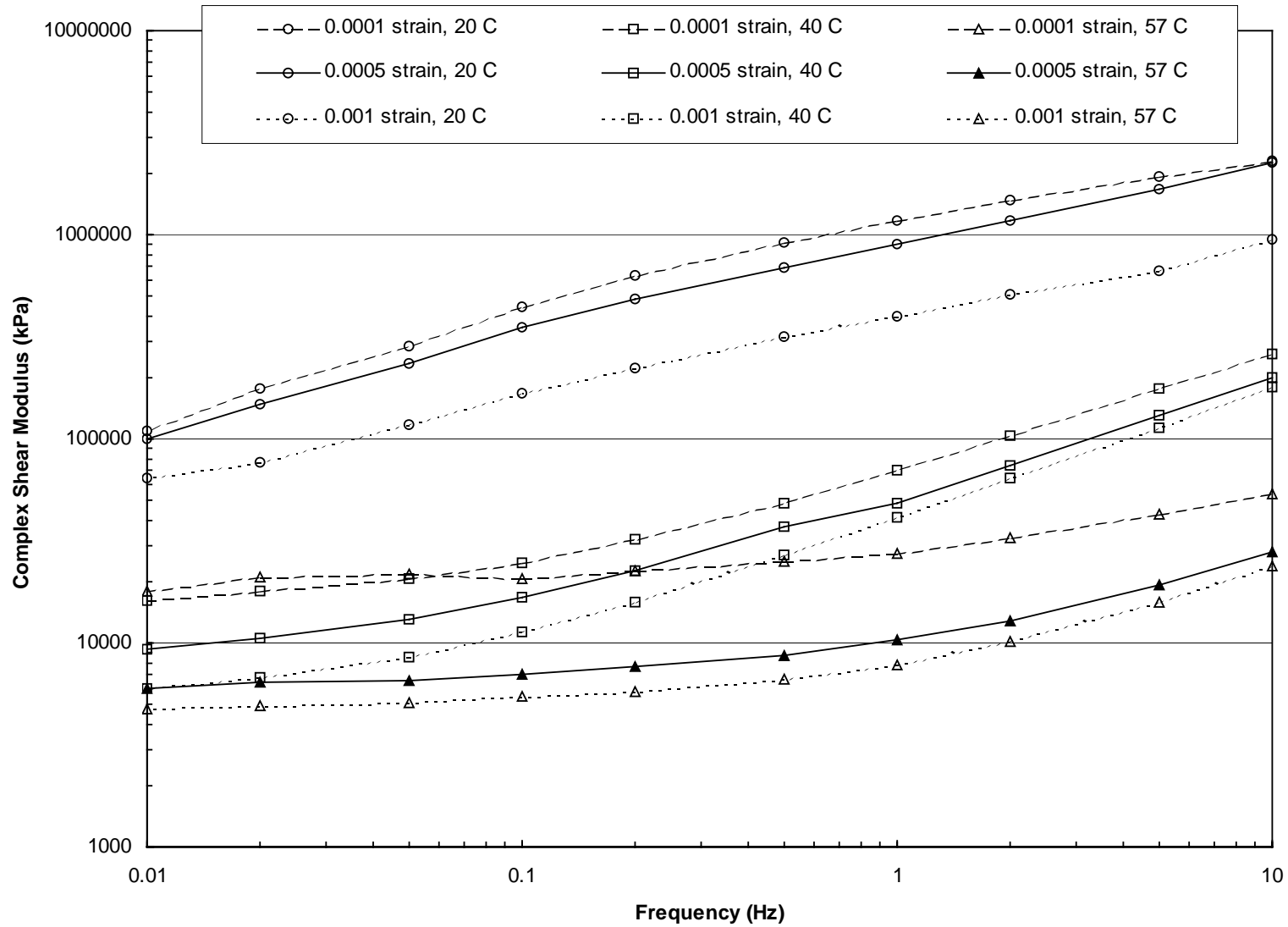


Figure 19. Averaged results of the three replicate specimens for each strain and temperature

where:

ν = Poisson's ratio.

can be used. However, as the temperature and strain amplitude increase, this assumption becomes less valid. For example, even at 20°C (68°F), G^* at a strain of 0.1 percent is only about one-third of its value at 0.01 percent.

Figures 20, 21, and 22 as well as Figure 19 illustrate the non-linear behavior of shear stiffness, G^* as a function of temperature (and strain level). While the data at a particular strain level can be used to construct master curves of G^* versus frequency using the concept of interchangeability of time and temperature⁸, it must be emphasized that such relationships cannot be used to directly determine the correct values of the complex Young's modulus, E^* , since the material exhibits non-linear response. This of course also applies in reverse. That is, if the complex Young's modulus is measured, determination of a correct shear modulus to define the shape distortion characteristics is questionable.

That the dependency of shear stiffness is non-linear on both frequency and temperature is also illustrated in Table 5. In this table, ratios of G^* measured at 0.05 percent and 0.10 percent to that measured at 0.01 percent strain are shown. In general, it will be noted that as the strain and temperature increase and the frequency decreases, the modulus ratio decreases. Another example of the limitations of indirect tests (that is, tests that do not directly measure a desired property) is contained in Reference (12). This study reports the results of tests

⁸ Strictly speaking, time-temperature superposition is only valid for linear viscoelastic materials. Generally these materials are considered to be thermorheologically simple, a requisite for time-temperature superposition to be applicable.

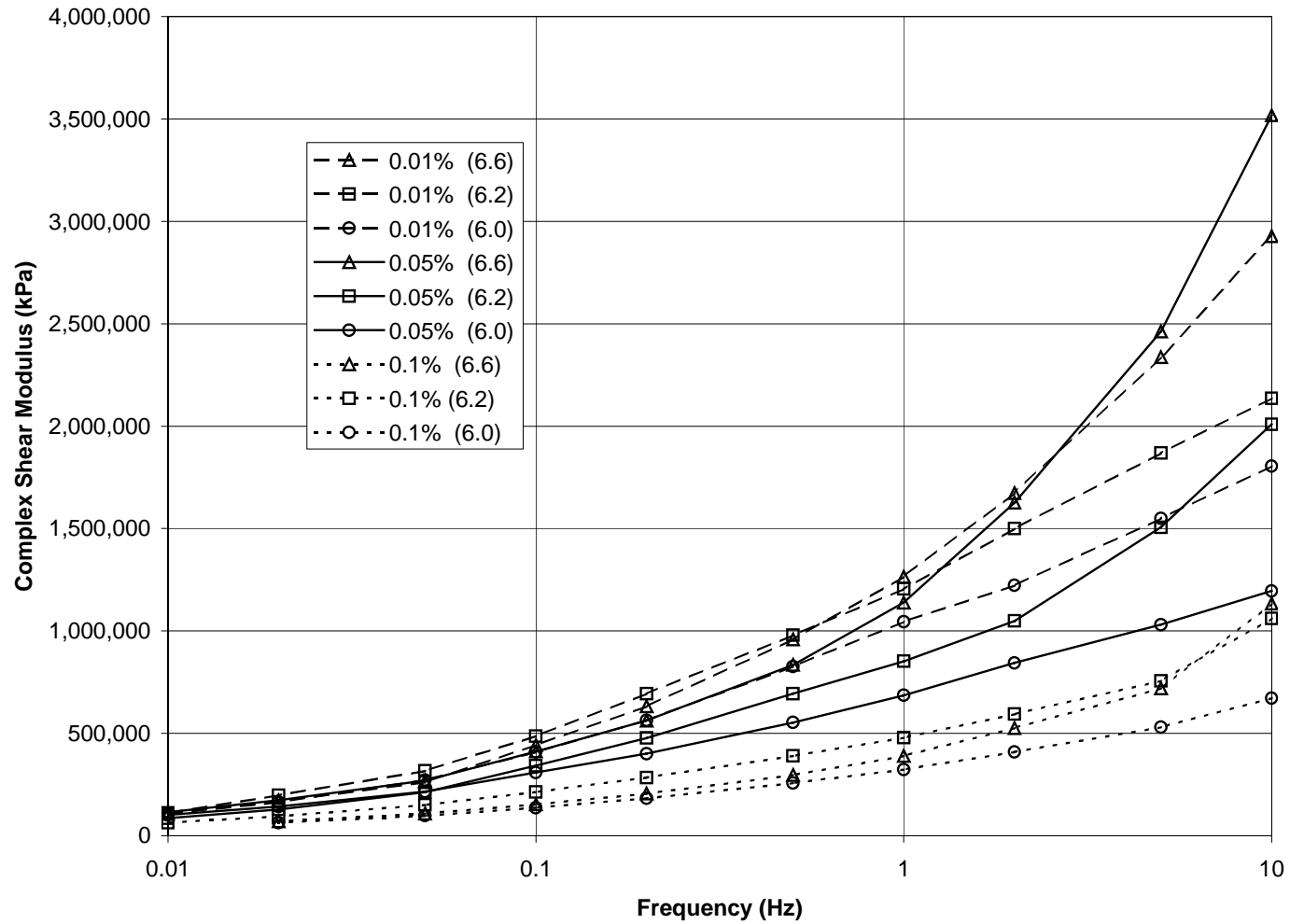


Figure 20. Complex shear modulus versus frequency at 20°C

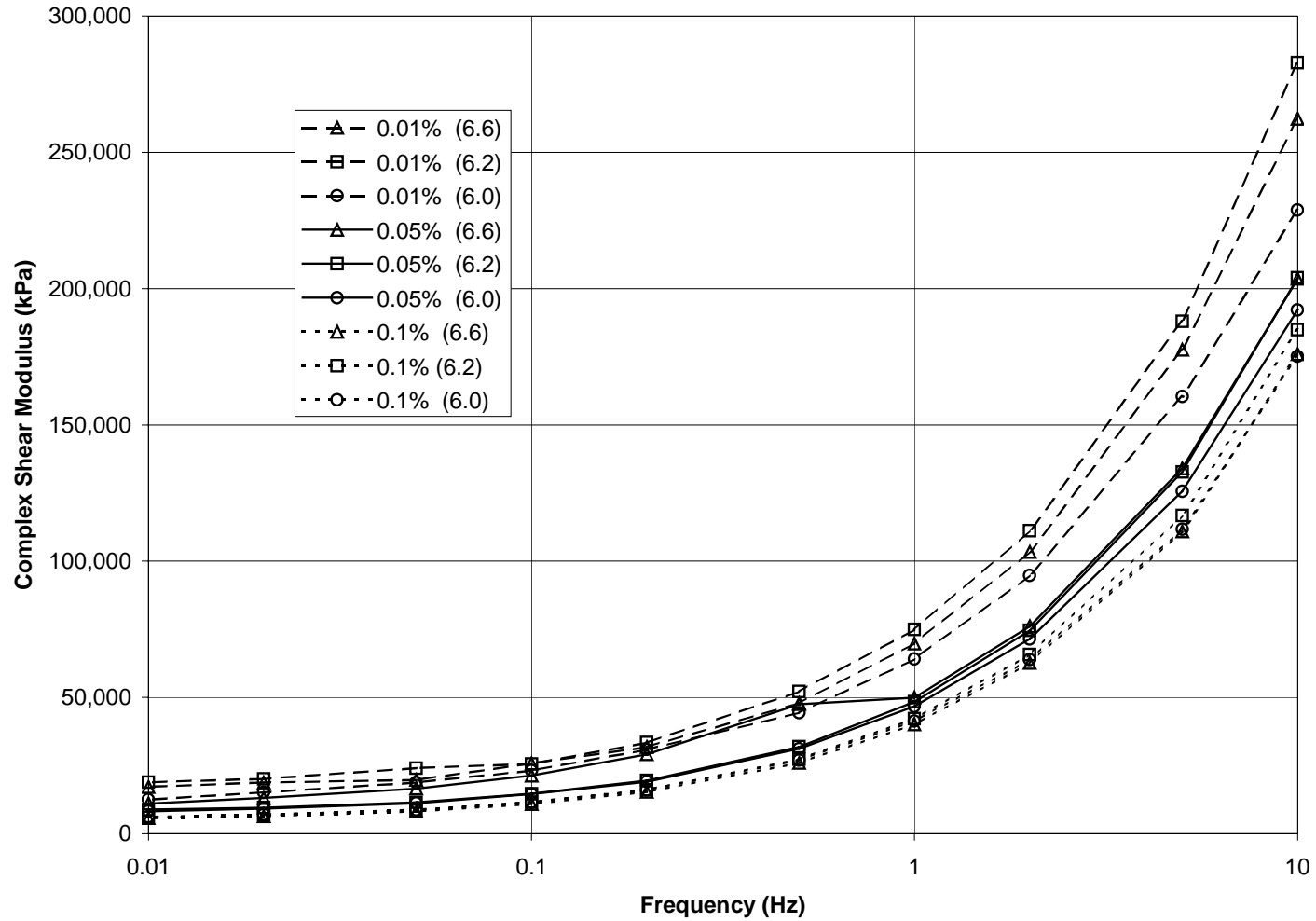


Figure 21. Complex shear modulus versus frequency at 40°C

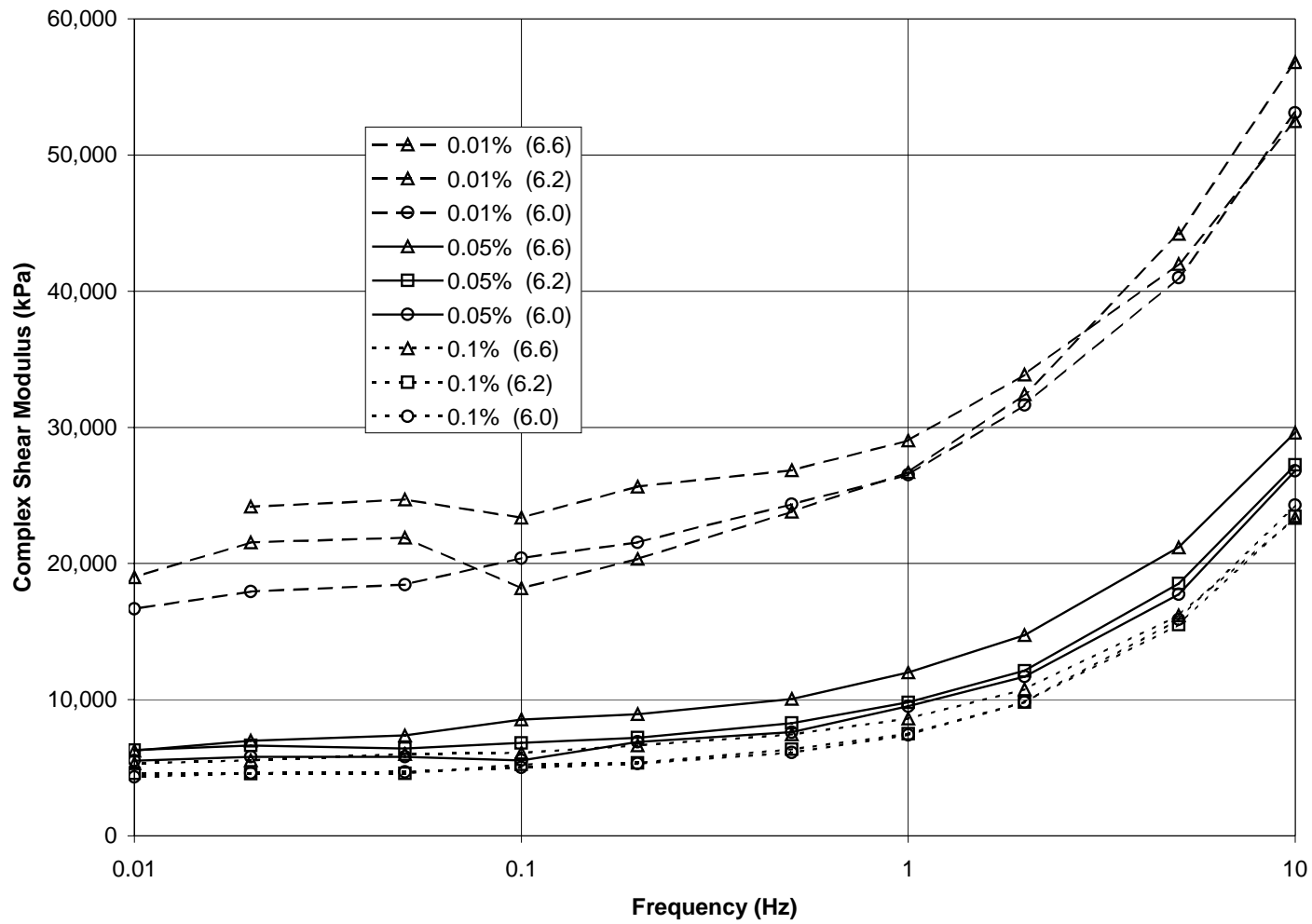


Figure 22. Complex shear modulus versus frequency at 57°C

Table 5. Ratios of G^* at 0.05 and 0.1 percent strain to that measured at 0.01 percent strain

Frequency (Hz)	Complex Shear Modulus Ratio					
	$\frac{G^* \text{ at } 0.05\% \text{ strain}}{G^* \text{ at } 0.01\% \text{ strain}}$			$\frac{G^* \text{ at } 0.1\% \text{ strain}}{G^* \text{ at } 0.01\% \text{ strain}}$		
	20°C	40°C	57°C	20°C	40°C	57°C
10	0.98	0.77	0.51	0.42	0.69	0.44
5	0.87	0.75	0.45	0.35	0.64	0.37
2	0.80	0.72	0.39	0.35	0.62	0.31
1	0.76	0.69	0.38	0.34	0.59	0.29
0.5	0.75	0.76	0.35	0.34	0.56	0.27
0.2	0.76	0.70	0.34	0.35	0.49	0.26
0.1	0.79	0.68	0.34	0.38	0.46	0.26
0.05	0.82	0.63	0.30	0.42	0.41	0.23
0.02	0.84	0.59	0.30	0.43	0.37	0.23
0.01	0.92	0.58	0.34	0.58	0.37	0.27

on AC mixes configured as hollow cylinders. Loading conditions included axial, torsion, and a combination of the two.

Poisson's ratios were predicted using Equation 3 from values of G^* and E^* both of which had been measured directly. With this approach dynamic Poisson's ratio values as high as about 5.5 were calculated as seen in Figure 23.

Direct measurements of Poisson's ratio were also made using strain gages bonded to the external and internal walls of the cylinder. Figures 24 and 25 show the plots of dynamic Poisson's ratio versus frequency, defined by the ratio of peak lateral strain to peak axial strain. The magnitude of Poisson's ratio varied between 0.15 and 0.4 in these experiments. The results are only reported for the high stress level measurements. At low stress level, the resulting lateral strains were generally below the 1 micro strain level, which was the lower detection limit of the strain gages.

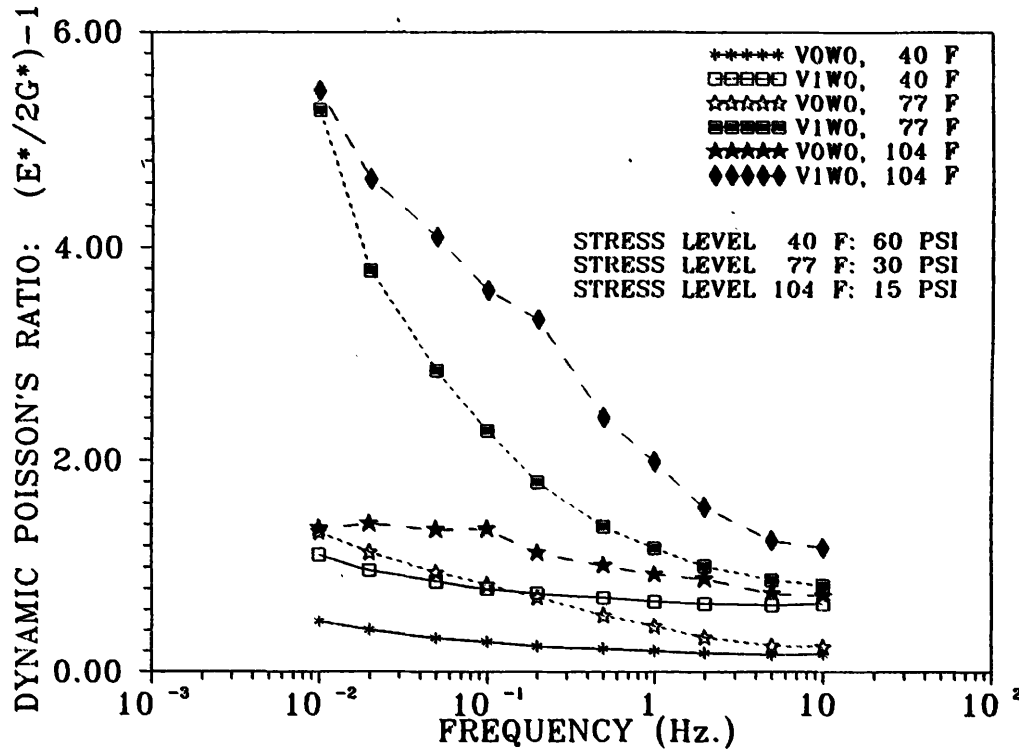


Figure 23. Apparent Poisson's ratio versus frequency, low air void content mixes

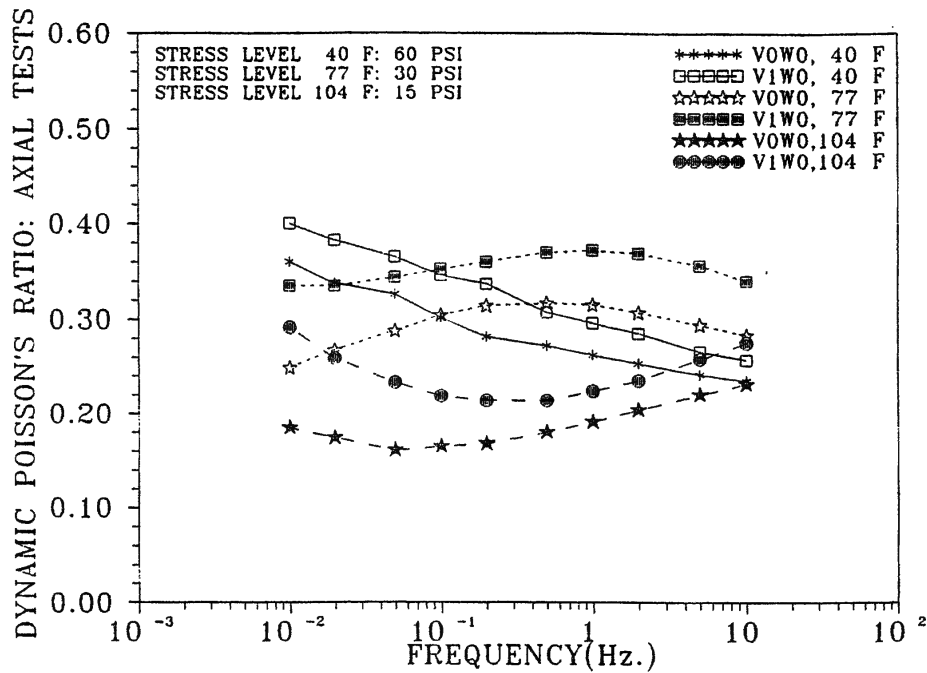


Figure 24. Poisson's ratio versus frequency, low air void content mixes

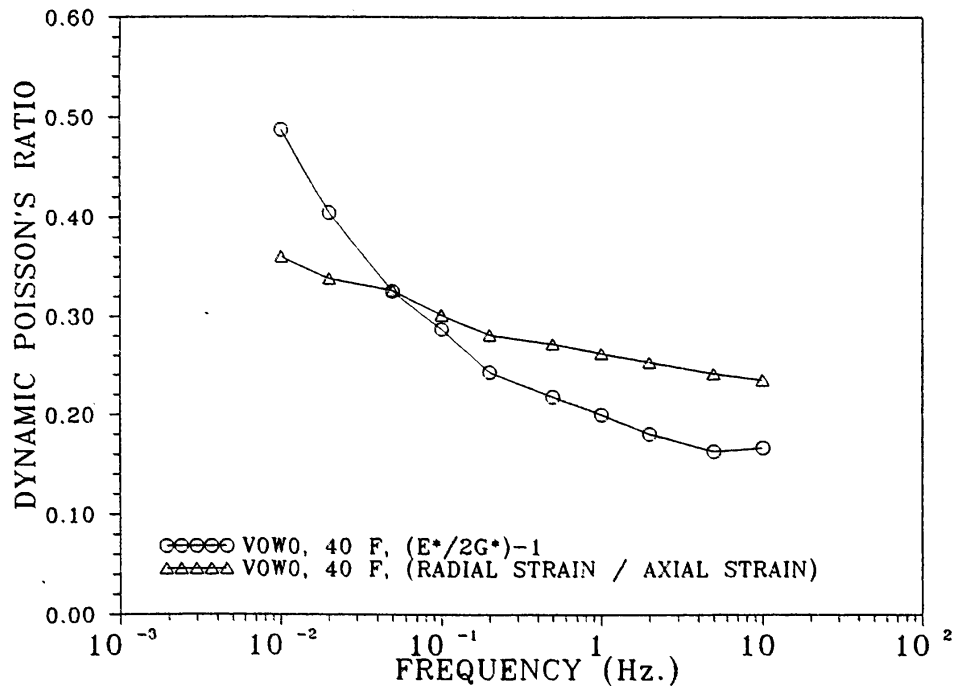


Figure 25. Poisson's ratio versus frequency, high air void content mixes

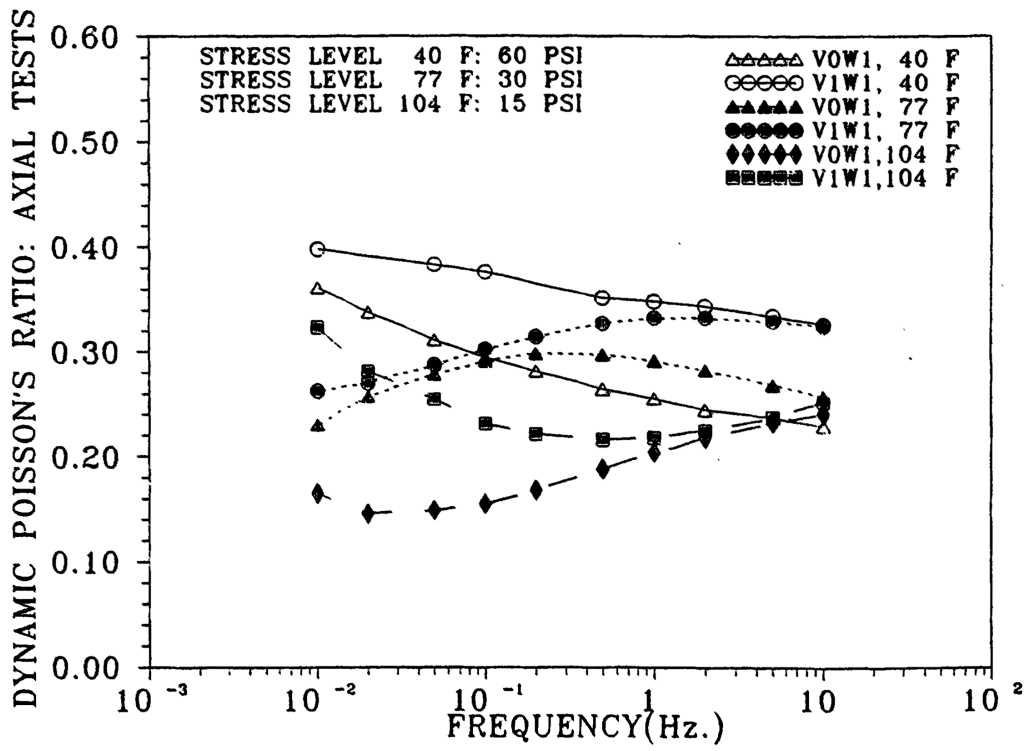


Figure 26. Comparison of direct Poisson's ratio values and apparent Poisson's ratio values, mix VOW0

Both Figures 24 and 25 show that the dynamic Poisson's ratio is both frequency and temperature dependent. At low temperature, 4°C (40°F), Poisson's ratio increases with decreasing frequency. At the other two temperatures, 25°C (77°F) and 40°C (104°F), Poisson's ratio passes through a transitional stage in the frequency domain.

A comparison of Poisson's ratio computed by Equation 3 with that measured directly is shown in Figure 26. For this case, at the low temperature of 4°C (40°F), the values of directly measured and computed values were closer to each other than for the other conditions. As the temperature increases, as seen by comparing the results in Figure 23 with those in Figure 24, the computed and measured values differ significantly. Thus one must conclude that the use of Equation 3 to deduce G^* from E^* or vice versa is reasonable only at low temperatures and high frequencies.

3.0 LABORATORY TESTS

While a number of tests to characterize the permanent deformation response of asphalt-aggregate mixes are being evaluated, only the triaxial and simple shear tests will be discussed. Specimens required for each type of test are discussed with respect to the RVE and specific test imperfections.

3.1 Triaxial Test

The triaxial test utilizes a cylindrical specimen which is subjected to a confining or lateral pressure (compression) and is loaded axially in tension or compression. For the tests currently under investigation for asphalt-aggregate mixes in which a confining pressure is used, the lateral pressure is uniform in all directions.⁹

Typically, axial compression has been used to determine the complex modulus, E^* (13,14) and an axial resilient modulus designated as E (or M_R), e.g. Reference (15). The test has also been used to define mix response is creep loading and repeated axial loading (16,17).

In compression, imperfections may result from friction between the end platens, even though care is taken to obtain “frictionless” end conditions. Friction will introduce a localized state of stress near the ends which is different than that intended. Because of friction the test actually measures:

$$E_{measured} = E + \alpha K \quad (4)$$

where:

E = Young’s modulus,

K = bulk modulus (i.e., the resistance to volume change), and

⁹ The test can also be performed in the unconfined state, which is often the procedure followed. Also special equipment can be designed so that the confining pressure is applied only to the vertical faces of the cylinder (18).

α = a geometric constant that depends on the specimen shape and friction between the specimen and the end platens.

If the specimen's aspect ratio of height to diameter is greater than 1, and the end platens are well lubricated, then at low temperatures α is small (<1 percent), and even at high temperatures it may not be greater than 1 percent (the reason for the difference is that the coefficient of friction depends on temperature). However, although K and E have roughly similar values at low temperatures, K may be as much as three orders of magnitude larger than E at high temperatures. Thus at low temperatures the error in $E_{measured}$ is relatively small, whereas at elevated temperatures the term αK may be much larger than E and therefore this test may not accurately measure E .

In the case of axial tension the end platens would necessarily be glued to the specimen; in this case α assumes a larger value. Thus to achieve the same accuracy as in the compression test, a larger height to diameter ratio is required.

Earlier it had been emphasized that for permanent deformation, the deviatoric component of strain is of primary concern. To measure the deviatoric component of strain with an axial test, a tensile stress in the axial direction and a compressive stress in the radial direction are required for cylindrical specimens. Since AC is, strictly speaking, a non-linear material, strains rather than stresses should be applied, as shown in Figure 27, with $\epsilon_1 = -\epsilon_3$.¹⁰

The test configuration shown in Figure 27 typically requires a specimen with a height/diameter ratio of 2 to 1. (Data presented earlier suggest that the length should be increased due to the RVE.) To achieve such a length with gyratory compacted specimens, one

¹⁰ The state of stress shown in Figure 27 will only result when equal but opposite stresses are applied if the material is an elastic isotropic material.

possibility would be to take two gyratory-compacted specimens, place a deformation gage or gages on one, saw the other in half and bind the two halves to the other specimen, as shown in Figure 28. As noted in Figure 27, the specimen should be subjected to tension in the axial direction and a confining pressure applied in the radial direction.¹¹ It would seem likely that the results of such a test would be questionable (the effects of gluing would be difficult to quantify and may vary from specimen to specimen) and certainly the test equipment would not be inexpensive.

If a tension test were performed on a cylinder consisting of an elastic material and both the axial force and change in radius were measured, the relationship between the ratio of G measured to the actual G (G_m/G) and the ratio of the length of the specimen to its diameter (L/D) is shown in Figure 29 (19)¹². For an elastic material the error in G for a value of L/D equal to 1 is value of G_m is less than G . Thus for the axial test, a higher modulus (i.e., unconservative) is obtained, while in the shear test a lower (conservative) value results.

This concept is for a purely elastic material. Unfortunately, with AC there is the added complexity of converting the measured data to a property related to shape distortion. This problem results from the non-linear nature of AC at elevated temperatures. At the moment, there are no good constitutive relationships for modeling AC under these conditions. Thus it is very difficult to estimate the difference between measured and predicted response when using indirect tests.

Relative to measuring radial strains an added confounding factor is that AC is at the least orthotropic, if not anisotropic, and the reduction to determine the radial strain does not account

¹¹ It would be difficult to apply a fixed strain in the radial direction with available equipment.

¹² Results shown in this figure are based on a finite element simulation using an applied axial strain of 0.1 percent (displacement control) with the specimen glued top and bottom to the loading platens.

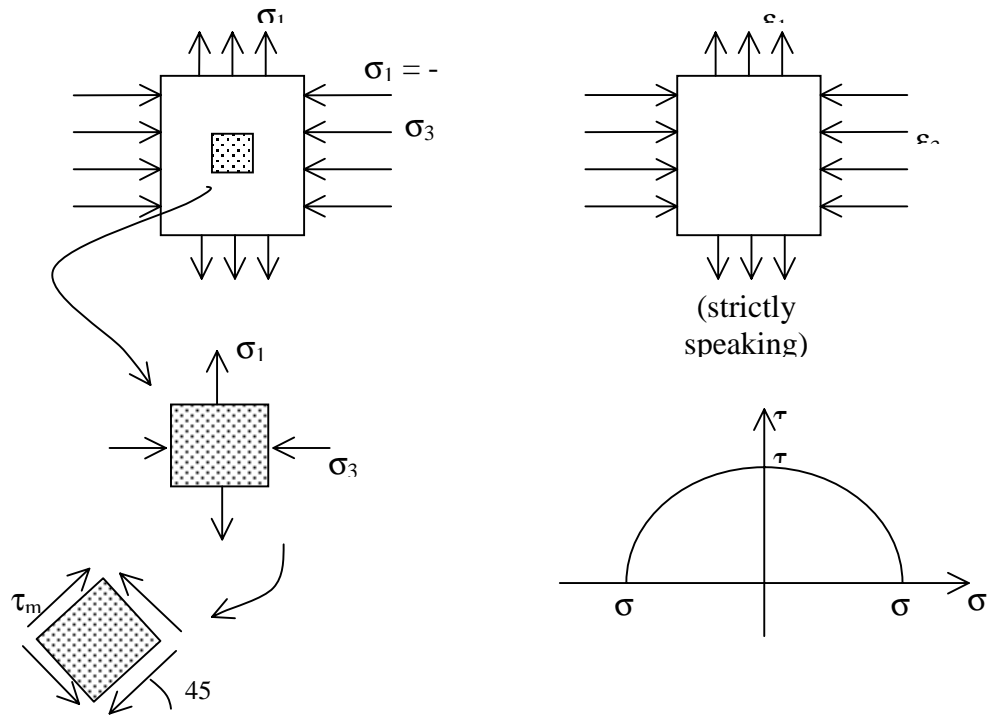


Figure 27. Axial loading to measure deviatoric distortion

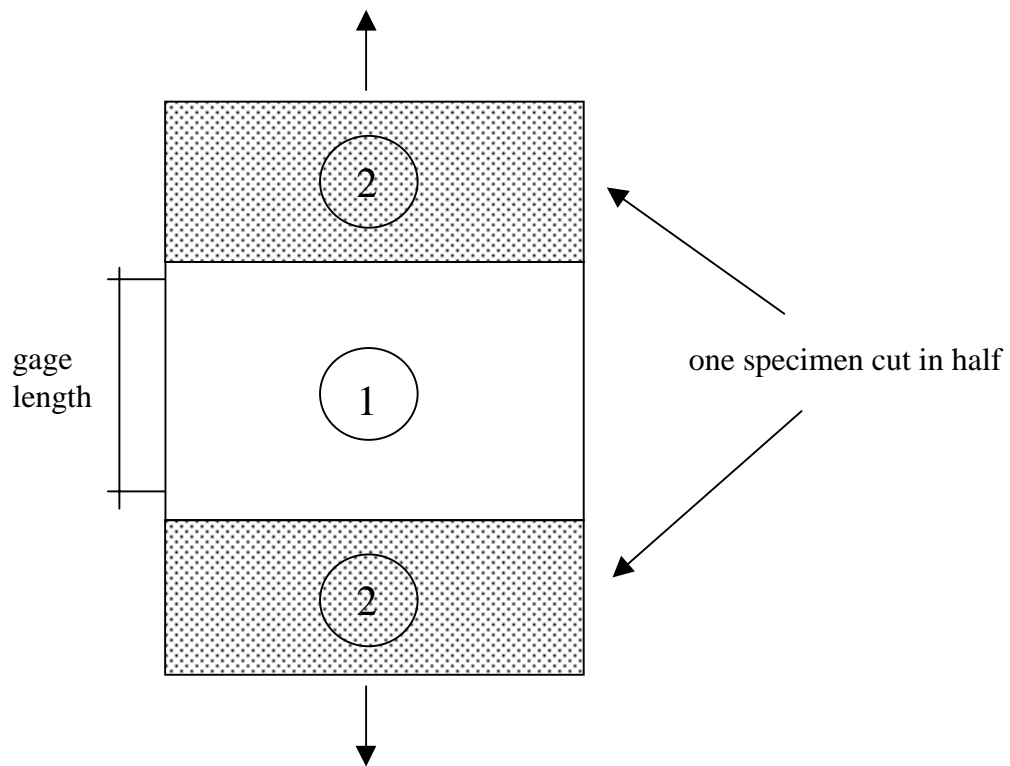


Figure 28. Proposed test configuration using two gyratory-compacted specimens

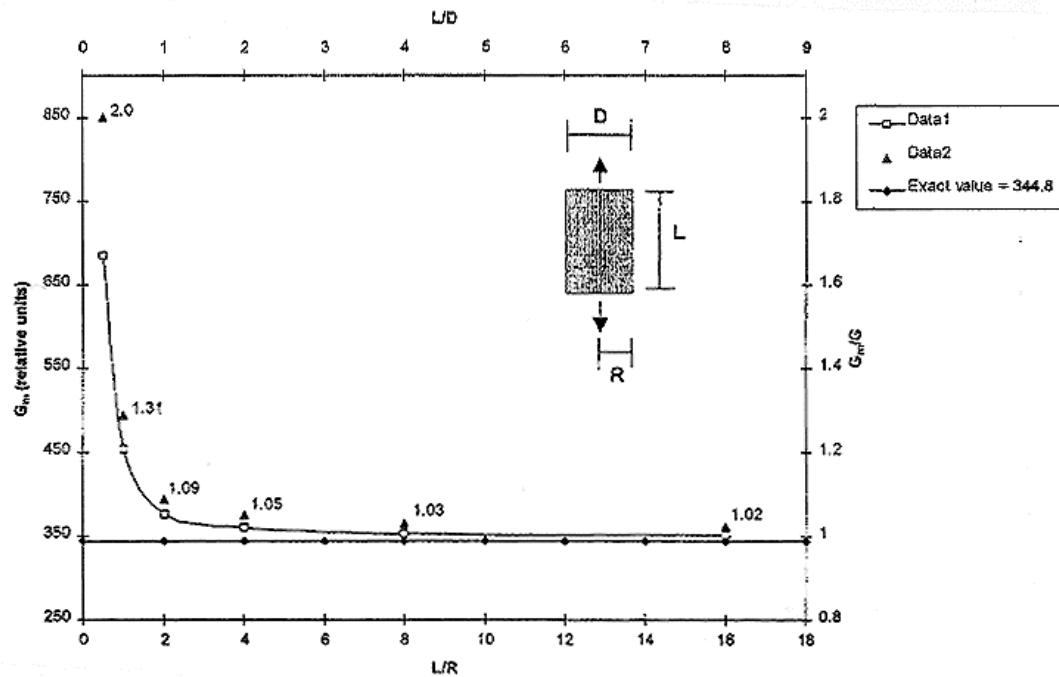


Figure 29. Ratio of measured G to actual G as a function of L/R or L/D (19)

for this material property. Because the material is not isotropic, under the action of hydrostatic pressure the two horizontal (planar) strains are most likely not equal; this will affect determination of the radial strain. There is also the question of accuracy of radial strain measurements with current “inexpensive” equipment.

Relative to *specimen dimensions* for the triaxial test the above discussion suggests the following. The specimen diameter should be greater than the larger of the two in-plane (horizontal) RVE dimensions, and its height should be at least twice the diameter plus the RVE in the vertical direction. Twice the diameter is required to eliminate end effects and thus diminish the importance of the αK component of Equation 4.

However, the RVE is still important in the sense that an RVE within the specimen length should be maintained free of end effects, which necessitates the addition of the two-diameter requirement and an RVE length in the vertical direction. As a result of this requirement,

specimen dimensions for a 19-mm nominal aggregate, the type studied here, may have to be about 125 mm (5.0 in.) in diameter and as much as 350 mm (14.0 in.) tall. Such a large specimen poses severe problems for testing field cores because the AC layer of many pavements is less than 200 mm thick. It must be emphasized that these dimensions are subject to the limitations of the analysis and should be validated by laboratory testing.

An underlying assumption about the triaxial test is that the specimen is in an axisymmetric state. Therefore, if radial strain measurements are made, the radius of the specimen should equal the RVE dimension in that direction (i.e., the diameter should be twice the RVE dimension).

3.2 Constant Height Simple Shear Test

The objective of this test is to measure properties associated with the shear response of AC mixes. This test can directly measure shear properties that the triaxial test cannot measure with a single specimen of reasonable size. On the other hand, the shear test does not measure the deviatoric component of normal strains that can be measured in the triaxial test. Therefore, to fully characterize shape distortion properties of a mix, both the triaxial test and the simple shear test at a constant height should, strictly speaking, be performed. For the shear test, in current practice the majority of testing is done with cylindrical specimens with a diameter of 150 mm (6.0 in.) and a height of 50 mm (2.0 in.).

The major imperfection in this test comes from missing tractions on the leading and trailing edges of the specimen, as indicated in Figure 30. This introduces boundary layers near these edges that may effect the solution. Fortunately, the width of this boundary layer is

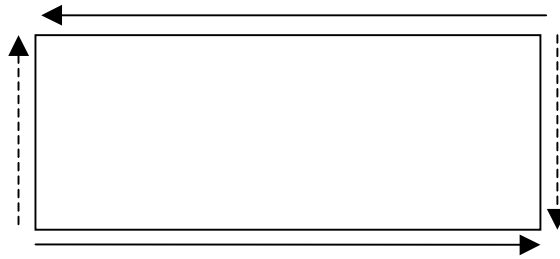


Figure 30. Simple shear test; traction represented by dotted arrows in not applied

independent of the specimen length and instead depends on the specimen height. Therefore, the relative contribution of these boundary layers can be diminished if the length-to-height ratio of the specimen is increased.

To demonstrate the effect of the length-to-height ratio, a series of three-dimensional finite element simulations were conducted (1). In these simulations, a 50 mm (2.0 in.) high and 100 mm (4.0 in.) wide specimen, with length that varied between 25 and 500 mm (1.0 and 20.0 in.), was used. A nonlinear elastic material model was used; and the results are shown in Figure 31.

Figure 31 highlights two important findings. First, 10 percent error, or less, in the predicted shear modulus (G) can be expected for specimens with a length-to-height ratio greater than 3. Second, $G_{measured}$ converges to G monotonically from below. As noted earlier, this provides a conservative value for G . In general these results indicate that the level of error can be reduced by increasing the length-to-height ratio. Thus, assuming the specimen height is prescribed by the RVE requirements, it is possible to select a specimen length that would result in an error level smaller than a specified value.

The second finding may lead to the establishment of correction factors that could be used to remove systematic errors due to test imperfections and reduce the effect of test bias. It is important to recall that the values presented in Figure 31 are accurate only for the specific model used—true mixes may lead to different curves. However, the general shape and rate of

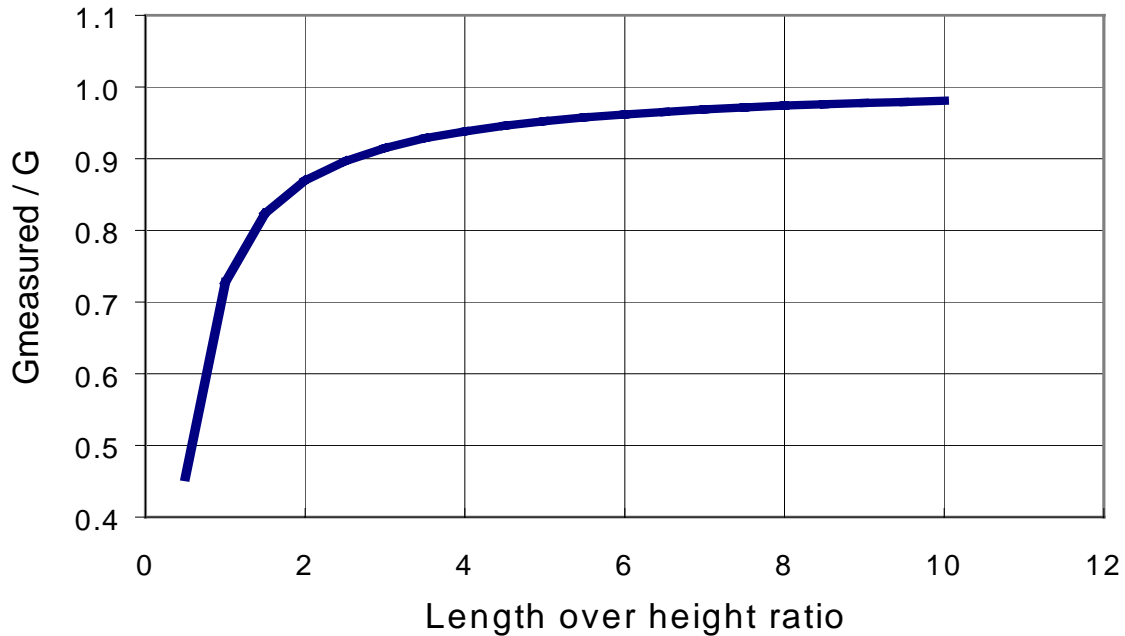


Figure 31. Convergence of the measured of G with increased ratio of length-to-height

convergence are expected to be the same. Laboratory tests are required to demonstrate this point.

Additional plane-strain finite element simulations were carried out to further study the boundary layers forming near the leading and trailing edges (I). In these simulations, the technique used to generate meshes for the RVE study was again used. Four different meshes, all based on the Pleasanton mix, were evaluated. The meshes were 75 mm (3 in.) high¹³ and 75, 150, 225, and 300 mm (3.0, 5.0, 9.0, and 12.0 in.) long. Linear elasticity was used to model both aggregate and mastic. The properties for aggregate were $E = 100$ MPa (14,500 psi) and $\nu = 0.35$ and the properties for the mastic were $E = 10$ MPa (1,450 psi) and $\nu = 0.49$. The boundary conditions applied were free leading and trailing edges, the bottom edge fixed in both horizontal and vertical directions, and a uniform horizontal displacement of 0.75 mm (0.03 in.) prescribed for the top edge (an average engineering shear strain of 1 percent) and fixed in the vertical

¹³ The 75 mm. height was selected for these simulations based on the RVE study described earlier, e.g., Figure 17.

direction. The distribution of the engineering shear strain is presented in Figure 32 and the distribution of the vertical displacements is presented in Figure 33. Both figures clearly indicate the boundary layers.

The variation in the effective $G_{measured}$ versus the length-to-height ratio is presented in Figure 34. The behavior is the same as that indicated in Figure 31. The only significant difference is that $G_{effective}$ is slightly smaller for the case of a length-to-height ratio of 4 than for the case of a length-to-height ratio of 3. A possible explanation for this effect is that the RVE dimension in the vertical direction is probably greater than 75 mm (3.0 in.). As a result, some oscillations are introduced into the convergence.

The cylindrical specimens currently used for simple shear tests at constant height have a varying length-to-height ratio across the specimen. This ratio is small (<1) near the sides of the specimen, but it is acceptable near the center, where it is 3. Thus, in view of the previous discussion, the contribution from the sides of the specimen actually reduces the overall reliability of tests with these specimens. This suggests that rectangular parallelepiped rather than cylindrical specimens should be used.

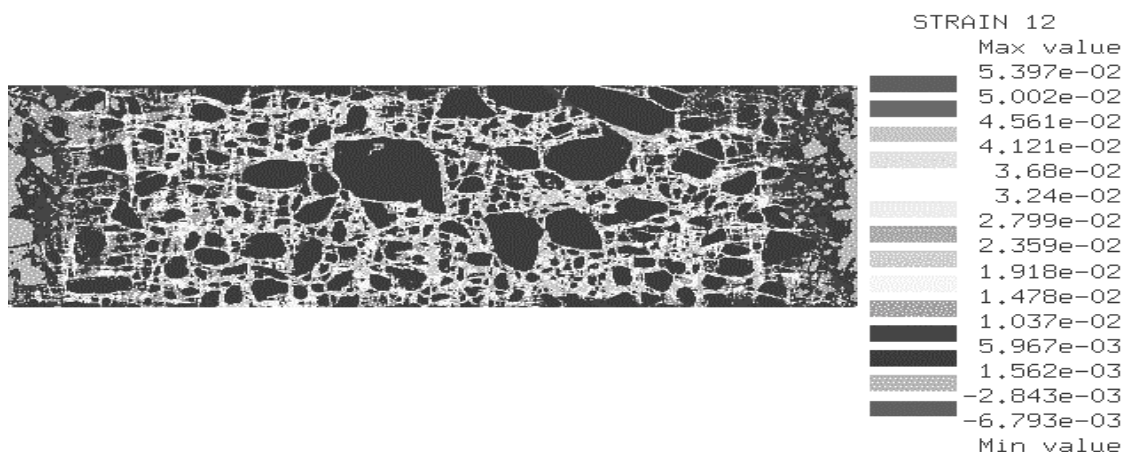


Figure 32. Engineering shear strain distribution for plane-strain simulation of a simple shear at constant height test: height = 75 mm, length = 225 mm

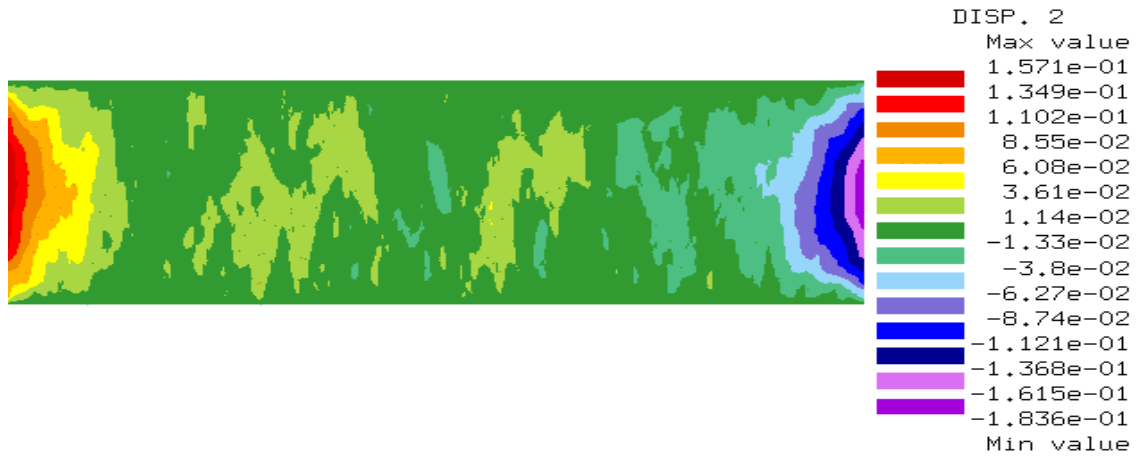


Figure 33. Vertical displacement distribution for plane-strain simulation of a simple shear at constant height test: height = 75 mm, length = 225 mm

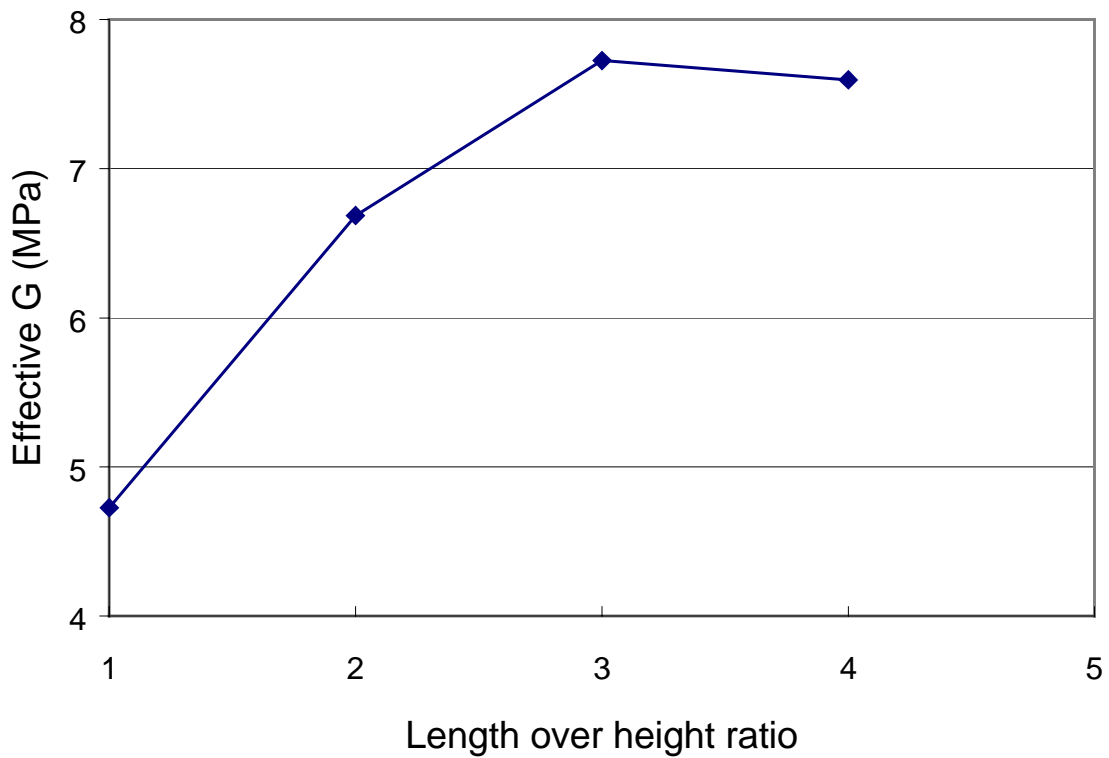


Figure 34. Plane-strain simulations of a simple shear at constant height test: variation of measured effective G as a function of length-to-height ratio

4.0 CREEP VERSUS REPEATED LOADING

With both the triaxial compression and shear tests, creep and repeated loading have been used to define permanent deformation response characteristics. A few examples will be cited to illustrate.

In the Shell pavement design procedure (20) provision has been made to compare the permanent deformation characteristics of different mixes as measured in creep and to select a mix or mixes in which the estimated rutting for specific traffic loading and environmental conditions would not exceed some predetermined value.

The rut depth at the pavement surface due only to permanent deformations in the asphalt-bound layer is determined from the following expression:

$$\Delta h_1 = C_M \cdot h_1 \cdot \frac{\sigma_{av}}{S_{mix}}, mm \quad (5)$$

where:

C_M = correction factor for the so-called “dynamic effect” which takes account of differences between static (creep) and dynamic (rutting) behavior. This factor is dependent on the type of mix and has been found empirically to be in the range 1-2,

h_1 = design thickness of asphalt layer, mm.

σ_{av} = the average stress in the pavement under the moving wheel, N/m^2

$$\sigma_{av} = Z \cdot \sigma_o, N/m^2$$

Z is a parameter dependent on the stiffness of the pavement layers; σ_o is the contact stress between tire and pavement,

S_{mix} = the value of the stiffness of the mix at $S_{bit} = S_{bit, visc}$.

The value of S_{mix} is determined from a plot of S_{mix} versus S_{bit} , S_{mix} having been obtained from creep loading over a range in times of loading. The procedure to select the value S_{bit} which in turn permits determination of S_{mix} , is described in Reference (20).

While this approach, that is the use of the creep test to define S_{mix} , has worked satisfactorily for mixes containing conventional asphalt cements, Valkering, et. al. (21) reported that when the procedure was used for mixes containing non-conventional binders “a correction is required to take account of the different relationship between rutting and binder viscosity. The dynamic creep test has shown potential for a more universal applicability, extending to include those asphalts based on a *modified* binder...The greater suitability of the dynamic test for rating the effect of the binder modification is ascribed to the recovery effects of the test.”

In another publication (22), the work of the Shell investigators suggest that the use of creep test data may overpredict rutting for mixes containing some modified binders.

The research of Tanco (23) on the pavement deformation response of conventional and modified asphalt-aggregate mixes under simple and compound loading conditions supports the work of the Shell investigators. He found that repetitive load tests were more responsive to the presence of modified binders in AC mixes than static constant load (creep) tests. Similar research had been reported earlier by Tayebali (17).

Both Tayebali and Tanco also presented convincing evidence that a conventional test like the Hveem Stabilometer¹⁴, while adequate for mix design with conventional asphalt binders, is not suitable for mixes containing modified binders.

This point is also illustrated by data obtained from tests on mixes containing a conventional AR-8000 asphalt and a PBA-6A binder (24). Table 6 contains a summary of

¹⁴ The Hveem Stabilometer test utilizes a slow, controlled rate of deformation (0.05 in. per min.) to load cylindrical specimens prepared by kneading compaction; temperature of test is 60°C (140°F).

Table 6. Stabilometer “S” values for mixes containing AR-8000 and PBA-6A binders (24)

Mix	Stabilometer “S” Values			
	Asphalt Content – percent by weight of aggregate			
	4.2	4.7	5.2	5.7
AR-8000	36	39	40	34
PBA-6A	—	26	35	26

Hveem Stabilometer test results obtained for both mixes. These results suggest that mixes containing the AR-8000 binder should have greater permanent deformation resistance than those containing the PBA-6A binder. Test results using the RSST-CH, however, indicate that the mix with the PBA-6A will sustain more traffic to a fixed rut depth [~ 13 mm. (0.5 in.)] than the mix with the AR-8000 asphalt as seen in Figure 35. These results are similar to those described above by the Shell researchers and by Tanco and Tayebali and stress the importance of using a “dynamic” rather than a static test to measure permanent deformation response.

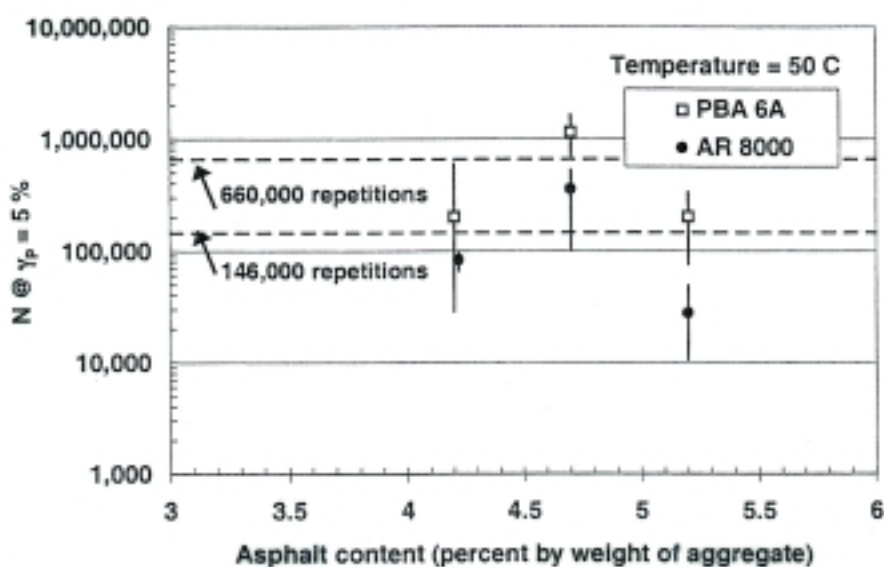


Figure 35. Repetitions to a permanent shear strain of 5 percent versus binder content; tests performed at 50°C (122°F)

5.0 TEST SPECIMEN PREPARATION

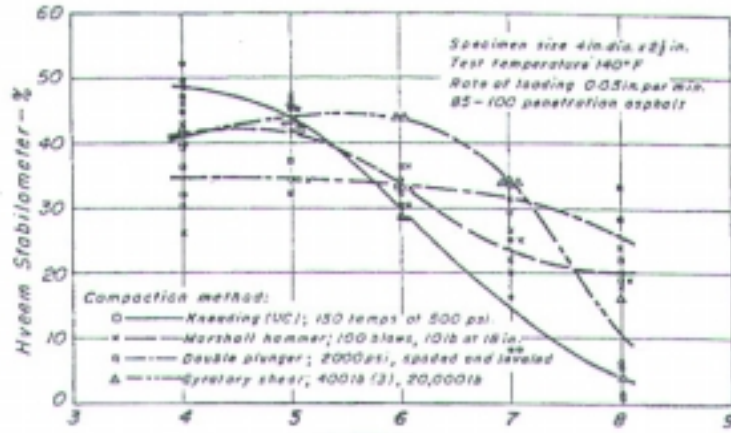
When preparing specimens for permanent deformation evaluation in laboratory tests, it is important that the aggregate structure of the laboratory-compacted mix be about the same as that of the mix compacted in situ by existing compaction equipment (i.e., steel wheel static, and vibrating rollers and pressurematic tire compaction).

Hveem was one of the first asphalt researchers to recognize this and the Triaxial Institute Kneading compactor (25) resulted from his understanding of mix performance. Other investigators, e.g., References (26 and 27), presented data comparing mix properties prepared by different methods of compaction using the Hveem Stabilometer and triaxial compression tests. Examples of these comparisons are shown in Figure 36 and 37 illustrating the influence of laboratory compaction procedure.

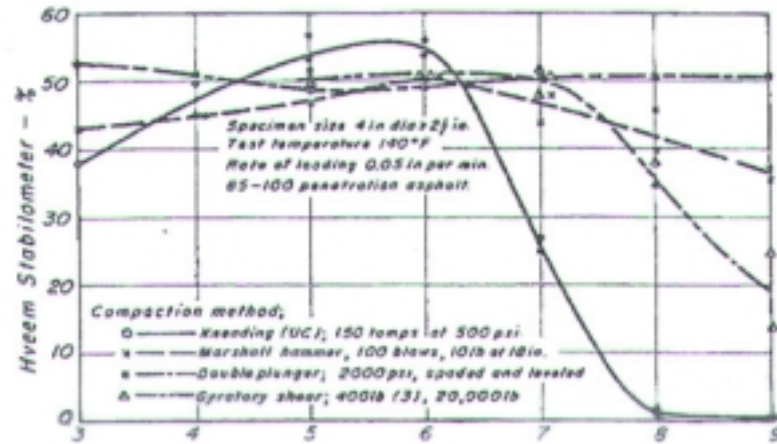
Data presented in Figure 36 compare results of tests on specimens prepared by static, impact, gyratory, and kneading compaction. The impact compaction method was the 50 blow procedure used by the U. S. Army Corps of Engineers (28), while gyratory compaction was the hand operated procedure used by the Texas DOT at the time (29).

The change in stability as measured by the Hveem Stabilometer with asphalt content is reflected by the effects of aggregate structure as produced by the four different compaction procedures. A similar result is shown in Figure 37 where stability (measured by the stress corresponding to 2 percent strain in a triaxial compression test) versus asphalt content is shown; in this case the specimens consisted of cylinders 100 mm (4.0 in.) in diameter and 200 mm (8.0 in.) high (27).

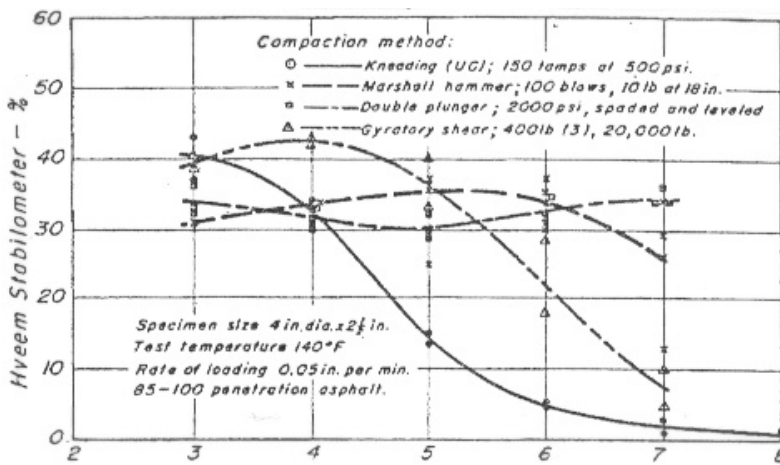
The Laboratoire Central Ponts et Chaussees (LCPC) conducted a study of specimens prepared by a number of different compaction procedures soon after the introduction of their



(a) crushed granite



(b) crushed quartzite



(c) crushed gravel

Figure 36. Effect of compaction procedure stabilometer "S" value (26)

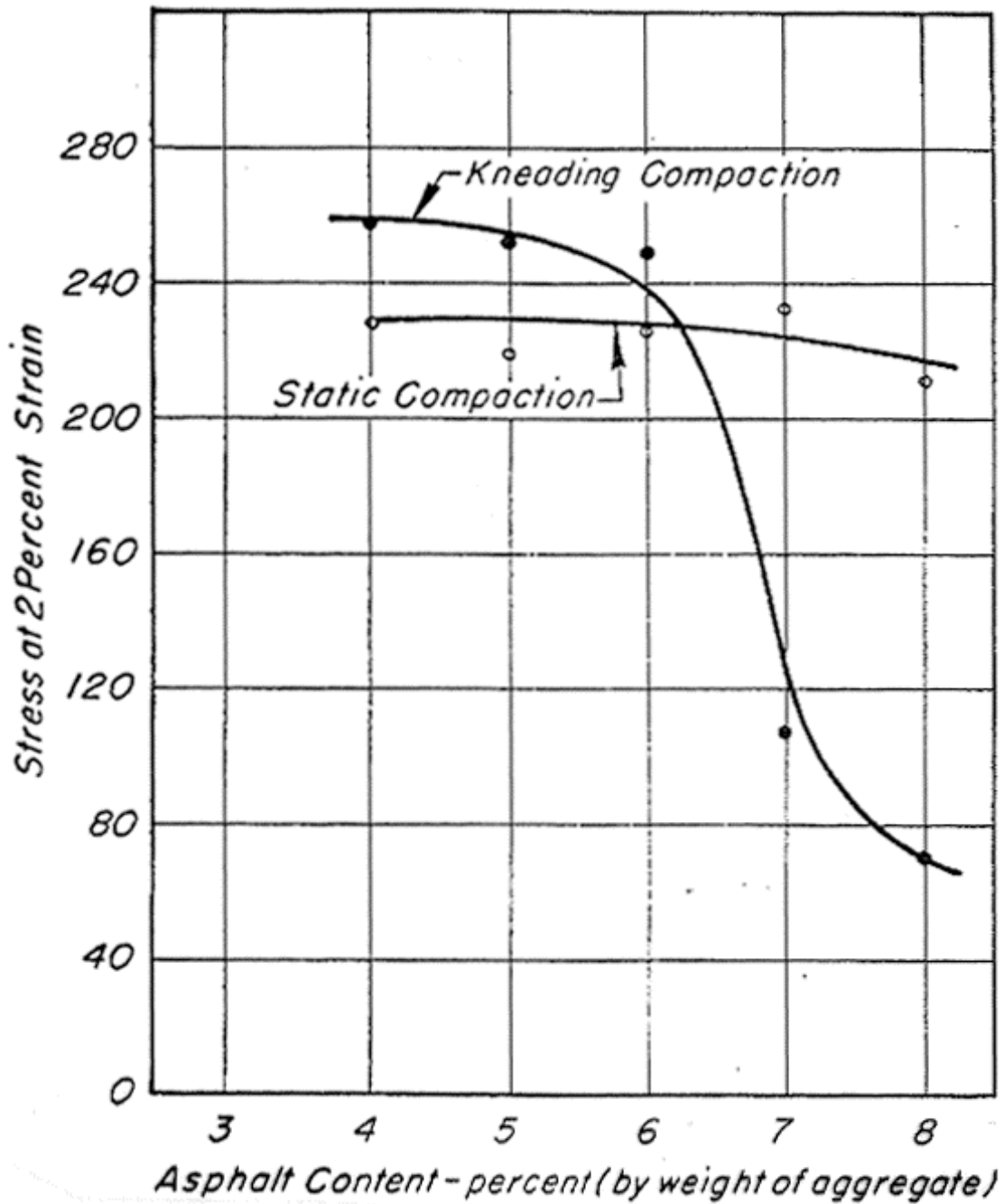


Figure 37. Comparison of stress at 2 percent strain for specimens prepared by static and kneading compaction; constant rate of strain triaxial compression tests at 60°C (27)

gyratory compactor developed to evaluate the compactability of mixes. The results of their study are shown in Figure 38. In this figure it will be observed that the rolling wheel compactor developed by the LCPC produced specimens that best reflected performance on comparable specimens compacted in situ (30).

It should also be noted that LCPC investigators have produced data on gyratory-compacted specimens which exhibit substantial density gradients both radially and vertically. The mix in the outer periphery of the cylinder is less dense than the interior; similarly, the top and bottom of the mix is less dense than the material near mid height. Both because of the density gradients and the differences shown in Figure 38, the LCPC does not use gyratory-compacted specimens for permanent deformation evaluation; rather they use a form of rolling wheel compaction (31).

During the Strategic Highway Research Program an extensive study was conducted of the influence of compaction method on the permanent deformation response of mixes. The compaction procedures included a mechanized version of the Texas Gyratory Compactor [150 mm (6 in.) diameter mold], the Triaxial Institute Kneading Compactor and a form of rolling wheel compaction (32). Results of the study supported the work of the LCPC suggesting that some form of rolling wheel compaction was most suitable for laboratory specimen preparation.

Recently, through the CAL/APT program it was possible to compare the permanent deformation characteristics of mixes compacted by laboratory rolling wheel compaction (33) and the Superpave (Pine) Gyratory Compactor, with cores obtained from two overlay pavements constructed according to Caltrans procedures. The pavements have been used for accelerated pavement testing at the Pavement Research Center, University of California, Berkeley (9). One of the overlays consisted of a mix containing a conventional dense-graded aggregate with an

AR-4000 asphalt cement while the other utilized a gap-graded material (same aggregate as the dense-graded material), and a crumb rubber modified (CRM) binder.

The laboratory compacted specimens were prepared from samples of the field mixes obtained at the time of construction of the pavements. Both the conventional dense-graded mix and the gap-graded aggregate CRM mix were placed on existing AC pavements which exhibited fatigue cracking from earlier Heavy Vehicle Simulator (HVS) loading. These overlays were compacted using a steel wheel vibratory roller.

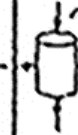
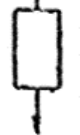
Simple shear tests (RSST-CH) were performed at 40°, 50°, and 60°C (104°, 122°, and 140°F) using a shear stress of 69 kPa (10 psi), a time of loading of 0.1 sec. and a time interval between loading of 0.6 sec. Results of these tests are summarized in Figures 39 and 40.

Figure 39 contains the test data obtained at the three temperatures for the conventional dense-graded AC, and Figure 40 the same information the asphalt rubber mix.

In these figures it will be noted that the specimens prepared by the SHRP gyratory compactor exhibit greater resistance to permanent deformation than the field cores. Also the data suggest that the specimens prepared by rolling wheel compaction are similar in response to the field cores. Table 7 has been prepared using the mean values for the tests for the three different methods of compaction. Generally the differences are largest at 40°C and decrease somewhat as the temperature is increased. Nevertheless, the data suggest that there is a difference in mix response when specimens are prepared by the SHRP gyratory compaction as compared to field compaction and laboratory rolling wheel compaction. This difference is due, in a large part (8), to the difference in aggregate structure created by the SHRP gyratory compactor as compared to rolling wheel compaction.

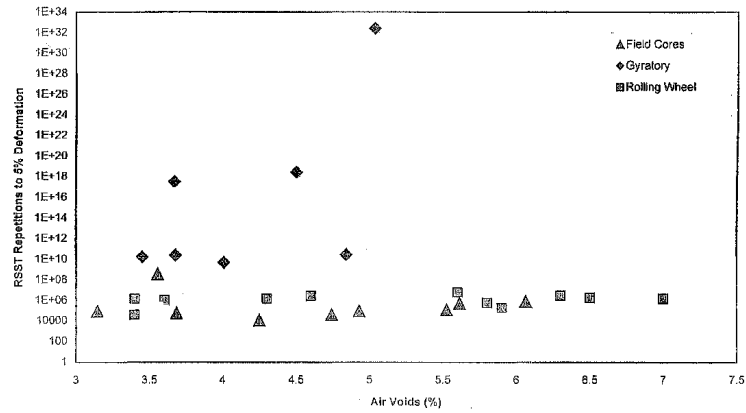
Table 7. Comparison of permanent deformation response measured in RSST-CH for specimens compacted by gyratory, laboratory rolling wheel, and field vibratory compactors

Specimen Preparation	Temperature – °C					
	40		50		60	
	V_{air} percent	RSST-CH: N at $\gamma = 5\%$ strain	V_{air} percent	RSST-CH: N at $\gamma = 5\%$ strain	V_{air} percent	RSST-CH: N at $\gamma = 5\%$ strain
Field	5.0-5.5	1.46×10^8	5.1-5.4	1.37×10^3	5.3-5.7	1.31×10^3
Rolling Wheel	4.7-5.4	1.04×10^8	5.6-5.8	3.21×10^4	5.0-5.4	2.58×10^3
Superpave Gyratory	5.3-5.8	1.70×10^{17}	5.5-5.8	7.95×10^7	5.8-6.1	2.24×10^5
Field	6.1-6.4	1.48×10^5	6.3-6.6	1.30×10^3	6.3-6.6	3.13×10^3
Rolling Wheel	6.1-6.4	3.08×10^9	6.5	1.61×10^4	6.3-6.5	1.22×10^3
Superpave Gyratory	6.3-6.8	7.76×10^{32}	6.6-6.8	1.01×10^7	6.4-6.7	2.79×10^4

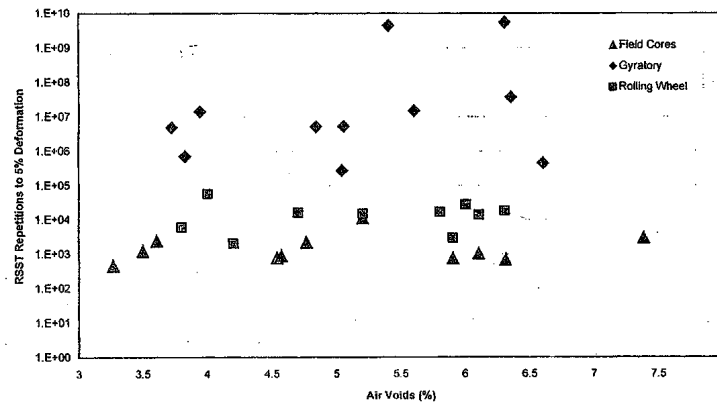
ESSAIS COMPACTAGE LABO	FLUAGE				R_c	E	E	E^*	F
				ORNIERAGE L.P.C				\sim	\sim
MARSHALL	-					O			
COMPRESSION	-				+	-	+	=	=
P.C.G.	-				=	-	+		
PNEU LPC	(=)			+	=	=	=		
ROUE METALLIQUE	=		=						
VIBROCOMPRESSION	-				=		+		

- : Laboratory < field; + : Laboratory > field; = : Laboratory = field; O : Direction of variation cannot be determined

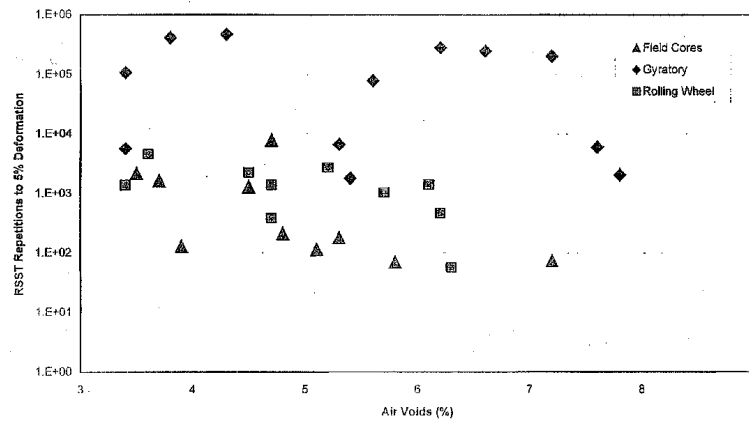
Figure 38. Comparison of mechanical performance [LCPC (30)]



(a) 40°C

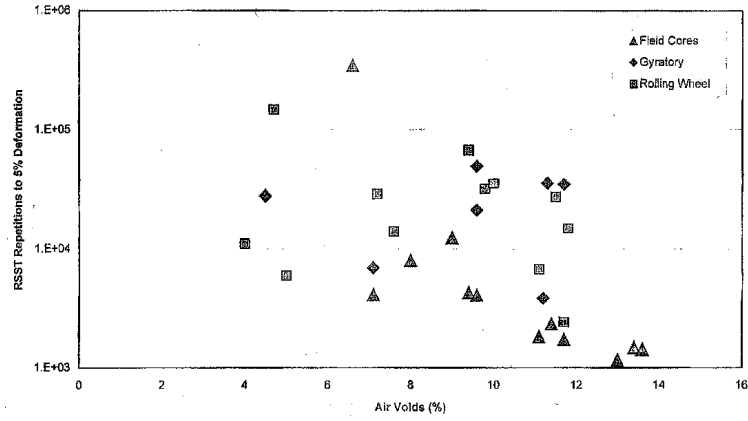


(b) 50°C

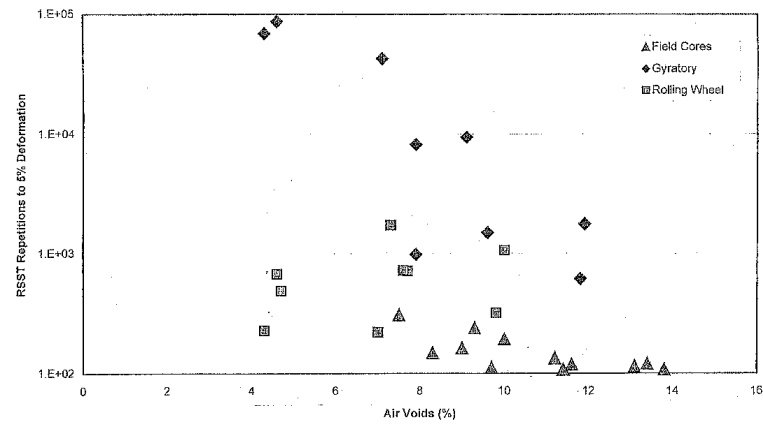


(c) 60°C

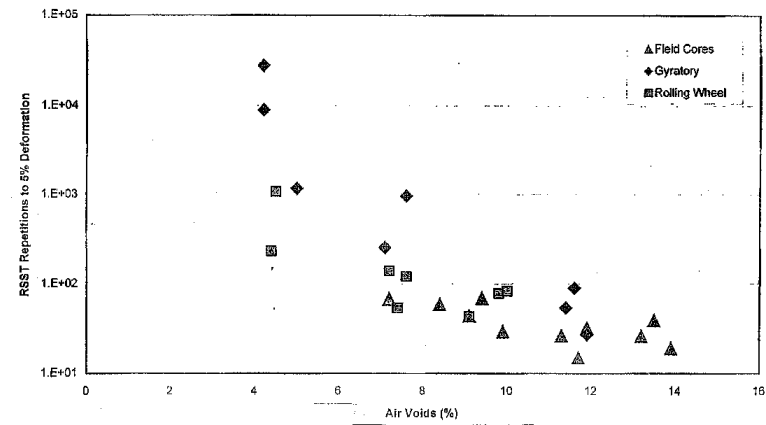
Figure 39. Influence of compaction method on behavior of mixes in the RSST-CH at 40°C, 50°C, and 60°C; conventional dense-graded AC (33)



(a) 40°C



(b) 50°C



(c) 60°C

Figure 40. Influence of compaction method on behavior of mixes in the RSST-CH at 40°C, 50°C, and 60°C; gap-graded asphalt-rubber hot mix

6.0 MIX DESIGN, ANALYSIS, AND PERFORMANCE EVALUATION

Some experience in mix design (24), performance evaluation (35), and pavement analysis (36) has been developed using the RSST-CH. Results from these investigations are summarized in this section. While the use of stiffness (modulus) for AC mix design purposed has been suggested, some data are included suggesting that this parameter should be used with caution.

6.1 Mix Design

The RSST-CH has been used, in a number of cases for mix design purposes; that is, to select the binder quantity. The basic approach is described in Reference (2). The framework, illustrated in Figure 41, is briefly summarized as follows.

Tests are conducted over a range in binder contents using the RSST-CH. These tests are performed using an applied shear stress of 69 kPa (10 psi) with a time of loading of 0.1 sec. and a time interval between load applications of 0.6 sec. Normally the test is conducted for 5,000 stress repetitions, or a permanent shear strain of 5 percent if this occurs at less than 5,000 repetitions.¹⁵ Figure 42 illustrates a relationship between permanent shear, γ_p , and stress repetitions, N , for a mix containing a PBA-6A binder tested at 50°C. Results of tests for this mix over a range in binder contents are plotted as shown in Figure 35. Also shown on the figure are results for a mix containing the same aggregate and grading with an AR-8000 asphalt cement. Normally the tests are done with specimens prepared by rolling wheel compaction to an air void

¹⁵ In some instances loading may be continued to as much as 20,000 repetitions to assist in the extrapolation of the data to 5 percent permanent strain, a value associated with rut depths of 12-13 mm (~0.5 in.) in thicker sections of AC.

content in the sample of 3 to 3.5 percent. The test is performed at a temperature termed the critical temperature, 50°C for the data shown in Figure 35.

As seen in Figure 41 the results of the laboratory tests termed N_{supply} (the repetitions corresponding to 5 percent shear strain) must satisfy the following:

$$M_{supply} \geq M \cdot N_{demand} \quad (6)$$

In this expression, N_{demand} is determined from the estimate of the design *ESALs*, a temperature conversion factor (*TCF*) which converts the traffic applied year round to an equivalent number applied at the critical temperature, and a shift factor (*SF*) which converts the repetitions applied in the field to an equivalent number in the laboratory; that is:

$$N_{demand} = Design \text{ ESALs} \cdot TCF \cdot SF \quad (7)$$

For the example shown in Figure 35 the design *ESALs* were estimated to be 30×10^6 , the $TCF=0.11$, the $SF=0.04$ (2), and $N_{demand} = 660,000$ repetitions.

The term M in Equation 6 represents a reliability multiplier which reflects the test variance and the estimated variance in the $\ln(ESALs)$ for a specified level of reliability. In the example, M was determined to be equal to 5.0. In Figure 35 it will be seen that the mix with the PBA-6A asphalt will satisfy the design requirements at a binder content of 4.7 percent (by weight aggregate).

It should be noted that the response of the PBA-6A mix at 4.2 percent binder content is less than the 660,000 repetitions. However, the air void content of this mix was at about 6 percent. Had it been in the range 3 to 3.5 percent it would have exhibited at least the same behavior as the mix at 4.7 percent binder content. This point is illustrated in Figure 43 that contains data for a asphalt rubber gap-graded mix (ARHMGG) for which the design binder content is 7.3 percent at a level of reliability of 95 percent.

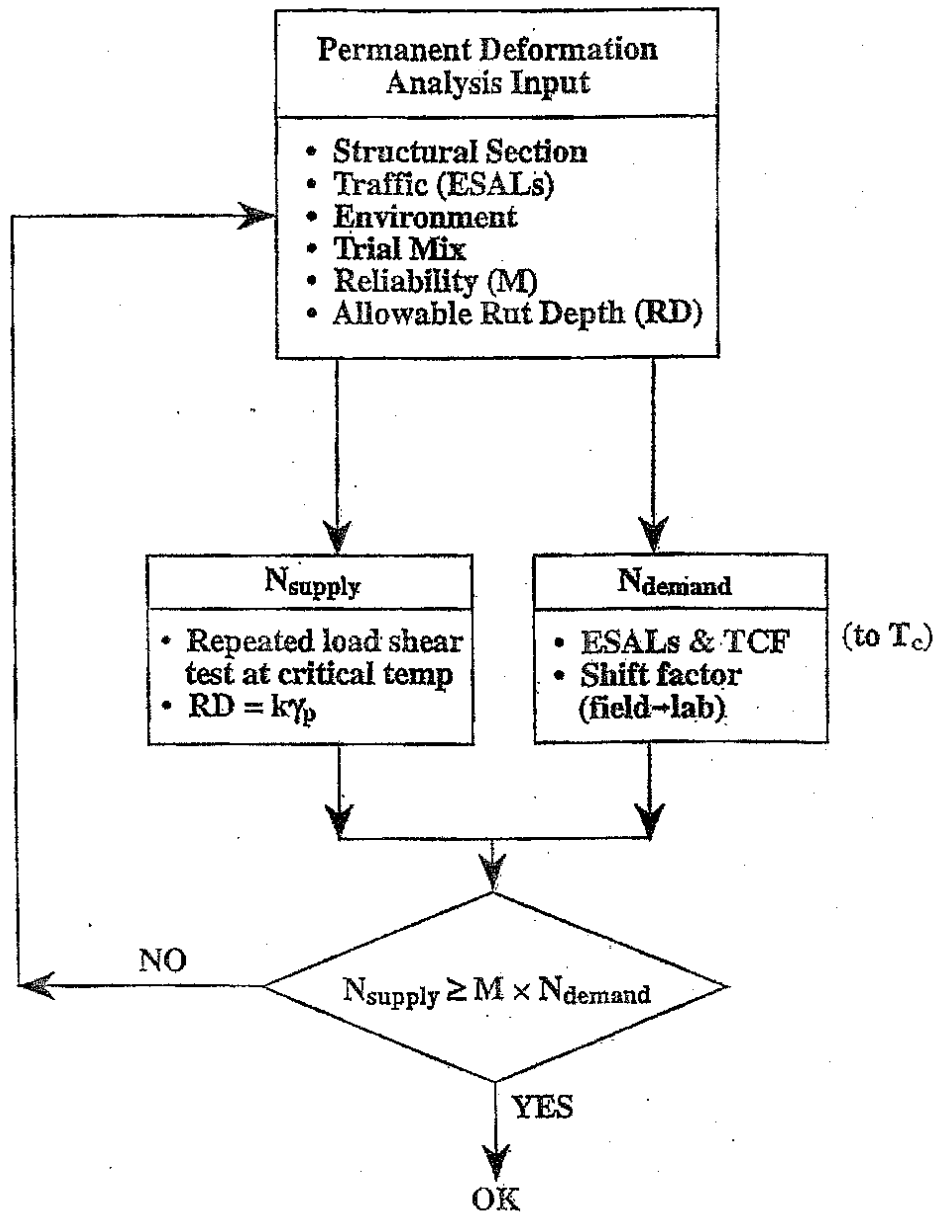


Figure 41. Permanent deformation system

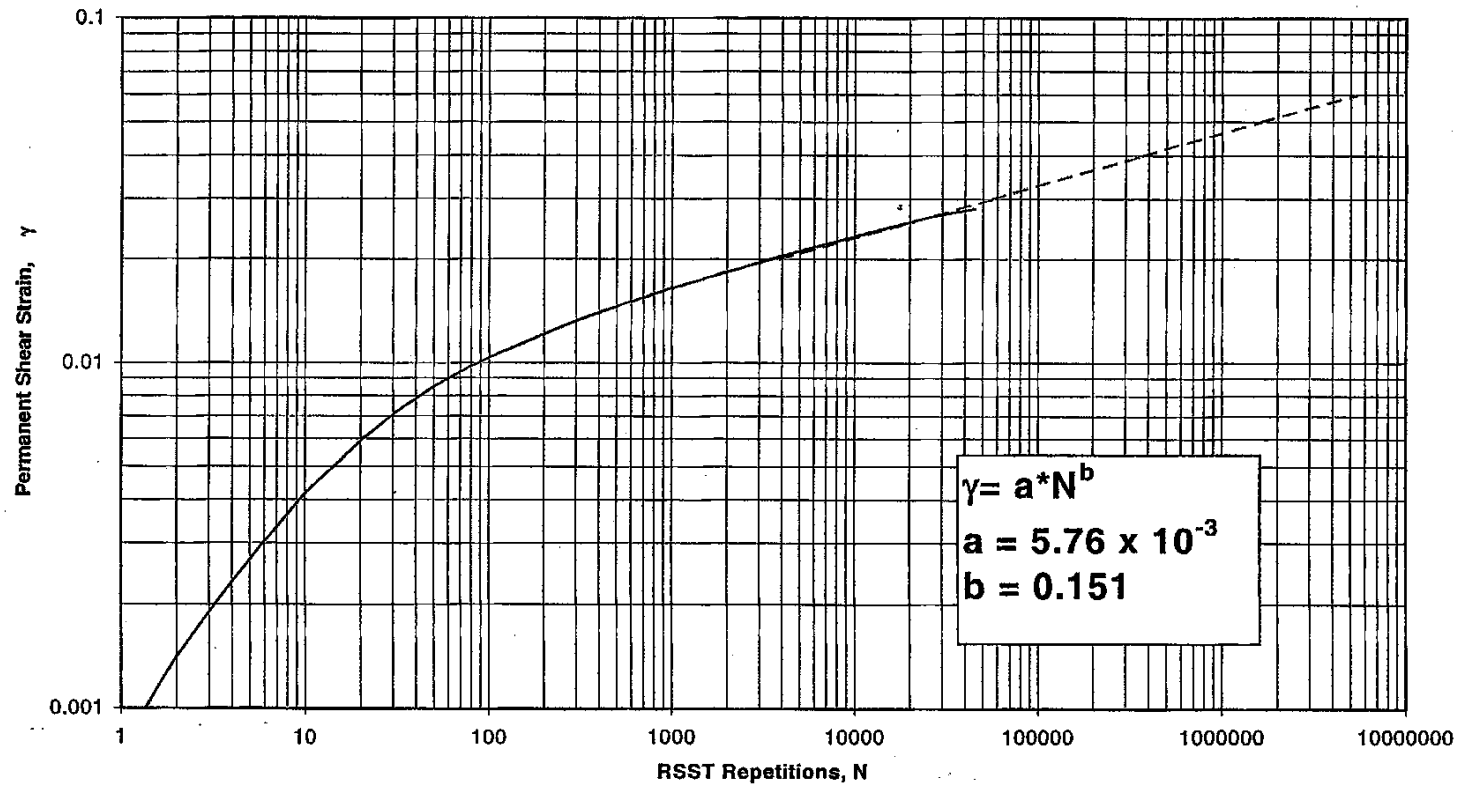


Figure 42. Permanent shear strain versus stress repetitions in RSST-CH at 50°C; PBA-6A mix, 4.7 percent binder control

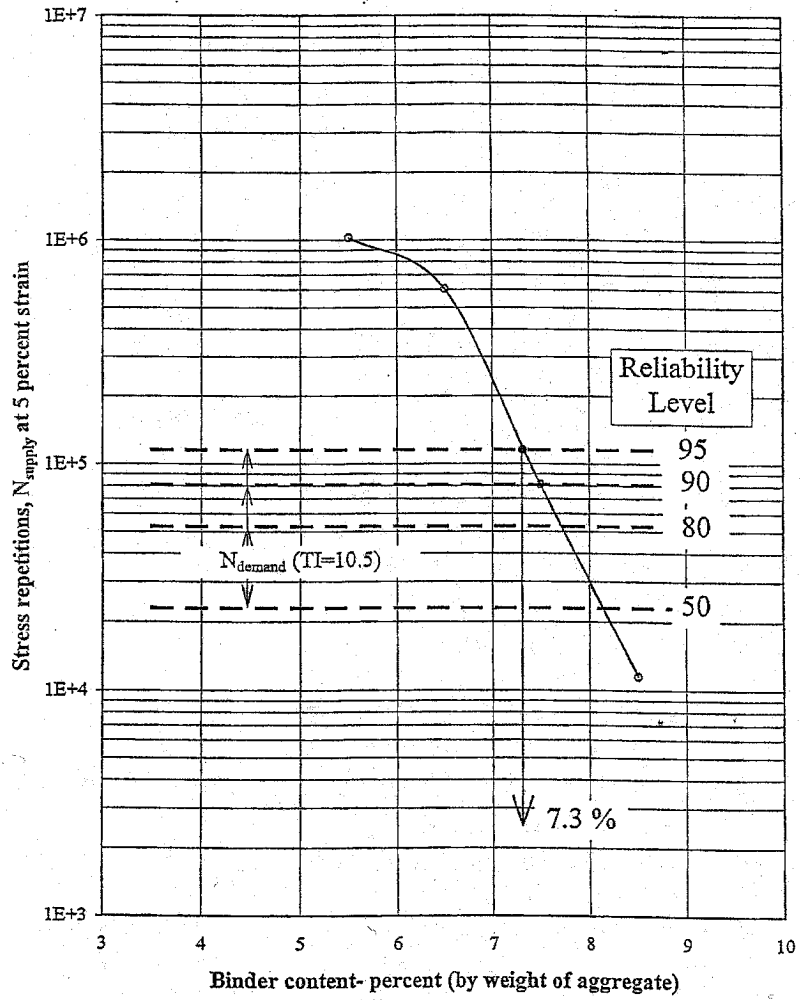


Figure 43. Mix design example, gap-graded with crumb rubber modified binder

6.2 Performance Analysis/Evaluation

6.2.1 San Francisco International Airport

A study of mix performance on taxiways at the San Francisco International Airport (SFIA) provided the opportunity to develop performance criteria for the use of the RSST-CH in mix design for this type of pavement (35).

In the summer of 1996 when air temperatures were about 35°C (95°F), excessive permanent deformations were observed in a taxiway subjected to turning movements of the B747-400. Soon after this distress occurred, rutting (dimpling) was also observed in the taxiways leading to the departure runways utilized by the B747-400's operating in a stop-and-go mode. It should be noted that up to this time (prior to the introduction of the B747-400) the AC, designed according to FAA standards, had performed in a satisfactory manner.

These conditions provided an excellent opportunity to study the resistance of these mixes to permanent deformation in the RSST-CH. In addition, soon after rutting was observed, a mix termed a *high stability mix* was introduced to minimize the effects of rutting. While the earlier mixes exhibiting rutting had contained AR-4000 or AR-8000 asphalt cements with crushed aggregate and some natural sand, the high stability mix was composed of an AR-16000 asphalt with all-crushed aggregate. A comparison of the grading containing the AR-4000 and AR-8000 binders with that used for the high stability mix is shown in Figure 44.

Shear tests performed on cores of the high stability mix and those which exhibited rutting are shown in Figures 45 and 46 respectively. In these figures a reference curve has been drawn which provides a separation between the mixes exhibiting rutting and the high stability mix. The location of this curve was based initially on "engineering judgement". Subsequently a statistical

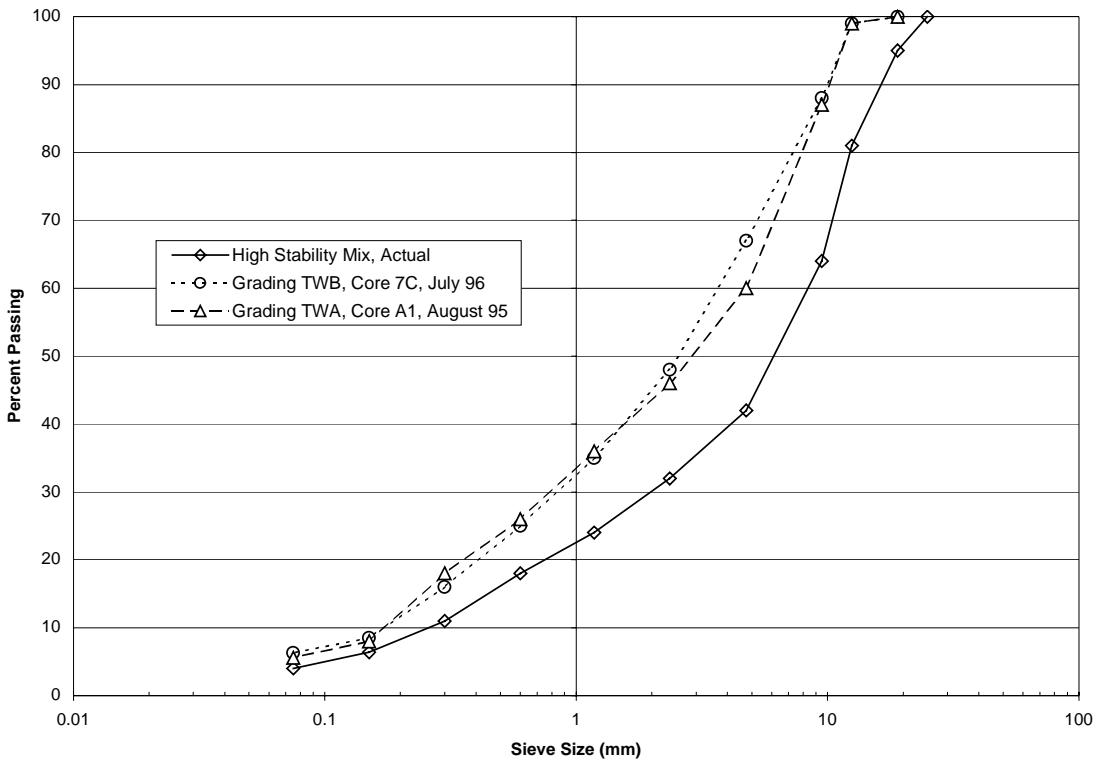


Figure 44. Aggregate gradations

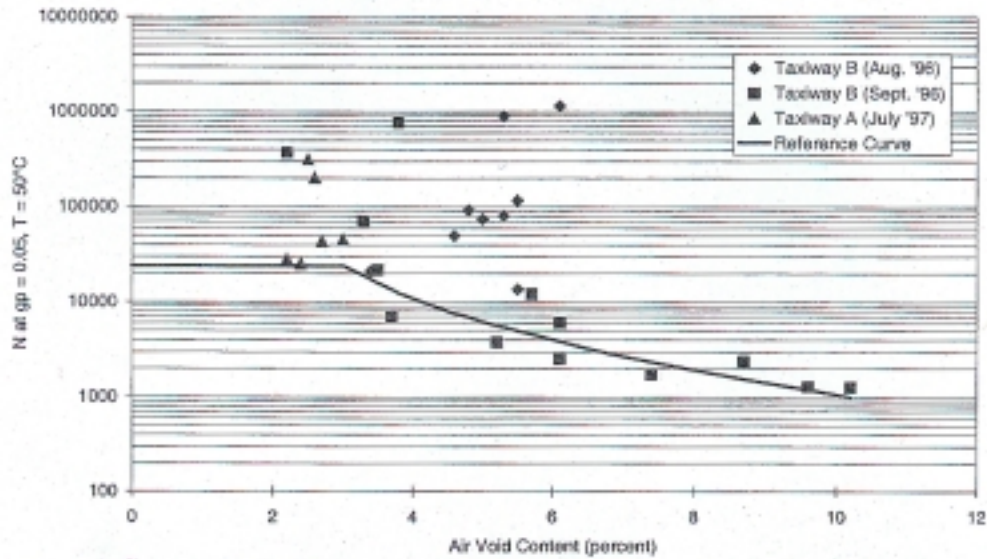


Figure 45. Shear stress repetitions to 5 percent shear strain versus air-void content at 50°C-High Stability mixes

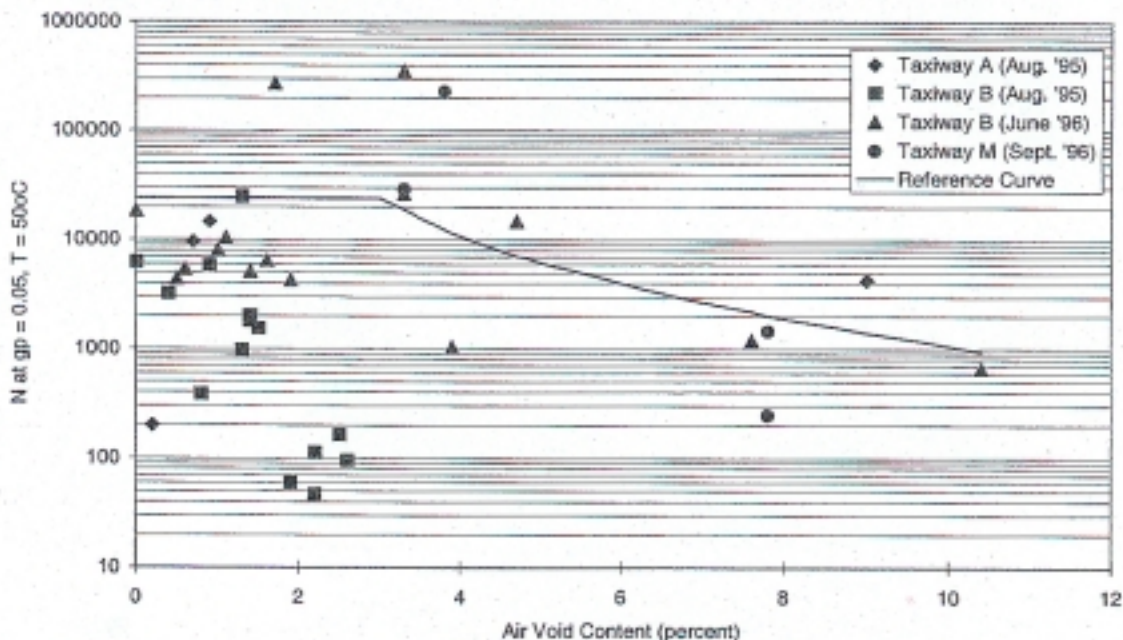


Figure 46. Shear stress repetitions to 5 percent shear strain versus air-void content at 50°C—mixes containing AR-4000 asphalt content

analysis was conducted and a regression equation defining the probability of failure (rutting) was established. The results of this analysis are shown in Figure 47 and the equation representing the different curves of probability of failure is:

$$Probability\ of\ Failure = \frac{1}{1 + \exp(-11.8119 + 0.6001 \cdot AV + 0.9995 \cdot \ln N)} \quad (8)$$

where:

AV = percent air-void content, and

$\ln N$ = natural log of the repetitions to 5 percent shear strain.

The reference curve shown in Figures 45 and 46 corresponds to a probability of failure of 50 percent. Thus, based on Figure 47, tentative criteria for mix design using the shear test (RSST-CH) can be established for different probabilities of rutting failure. Allowable repetitions

to failure in the RSST-CH at 50°C (122°F) for the conditions of loading described herein for probabilities of failure of 20 to 50 percent, at an air-void content of 3 percent are as follows:

Probability of Failure	N_p at $\gamma_p = 5$ percent
50	25,000
40	35,000
20	100,000

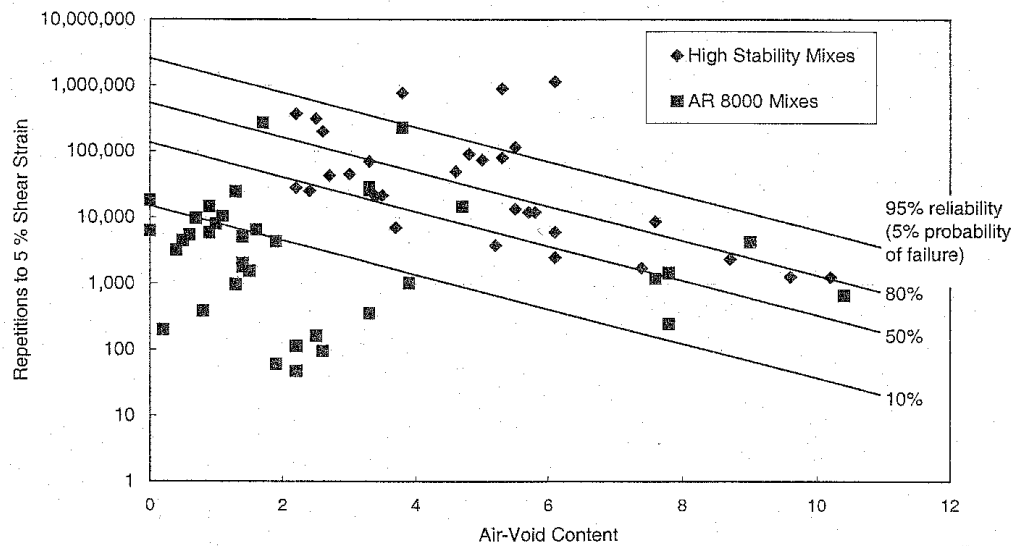


Figure 47. Shear stress repetitions to 5 percent shear strain versus air-void content at 50°C—all mixes

6.2.2 WesTrack

The WesTrack experiment (36) also provided an opportunity to assess the applicability of the RSST-CH test to evaluate rutting performance of asphalt-concrete mixes subjected to up to 5.0×10^6 ESALs.

Three general mix types were utilized termed *coarse*, *fine*, and *fine plus*; the gradation designations are related to the location of curves relative to the 0.45 grading line on the FHWA

0.45 power grading chart. The *coarse* grading lies below the 0.45 power line while the *fine* and *fine plus* are above, Figure 48. For the initial tests a total of 26 sections were placed in which the asphalt content and air void content were varied. The various mixes are summarized in Table 8.

In addition to the original sections, 8 sections were replaced and new mixes were constructed; these are referred to as *replacement* sections. The replacement sections consisted of mixes containing only the coarse grading but a different aggregate than the original 26 sections. Table 8 also contains a summary of the characteristics of these mixes as well, while Table 9 briefly summarizes the characteristics of the aggregates and binders used in both the original and replacement sections.

To arrive at the stress repetitions in the laboratory RSST-CH tests at which to select the strains for comparative purposes, Equation 7 was used. For the original sections, in order to use all of the results, the comparisons are based on rutting data obtained at about 1.5×10^6 ESALs. Use of Equation 7¹⁶ provided a value of $N = 7000$ repetitions. For the replacement sections, the comparisons are made at about 0.6×10^6 ESALs for the same reason; use of Equation 7 provided a value of $N = 2700$ repetitions.

Results of these analyses are presented in Figures 49, 50, and 51 for the original *coarse*, *fine*, and *fine plus* sections respectively and in Figure 52 for the *replacement* mixes. These figures contain plots of downward measured rut depth versus the plastic strain corresponding to either 7000 or 2700 repetitions in the RSST-CH. The shear test results were obtained from tests at 50°C (122°F) and a shear stress of 69 KPa (10 psi). For the original mixes, each data point represents the average of two tests on cores obtained prior to trafficking (referred to as $t = 0$).

¹⁶ In Equation 7 a *TCF* of 0.116 and a *SF* of 0.04 were used.

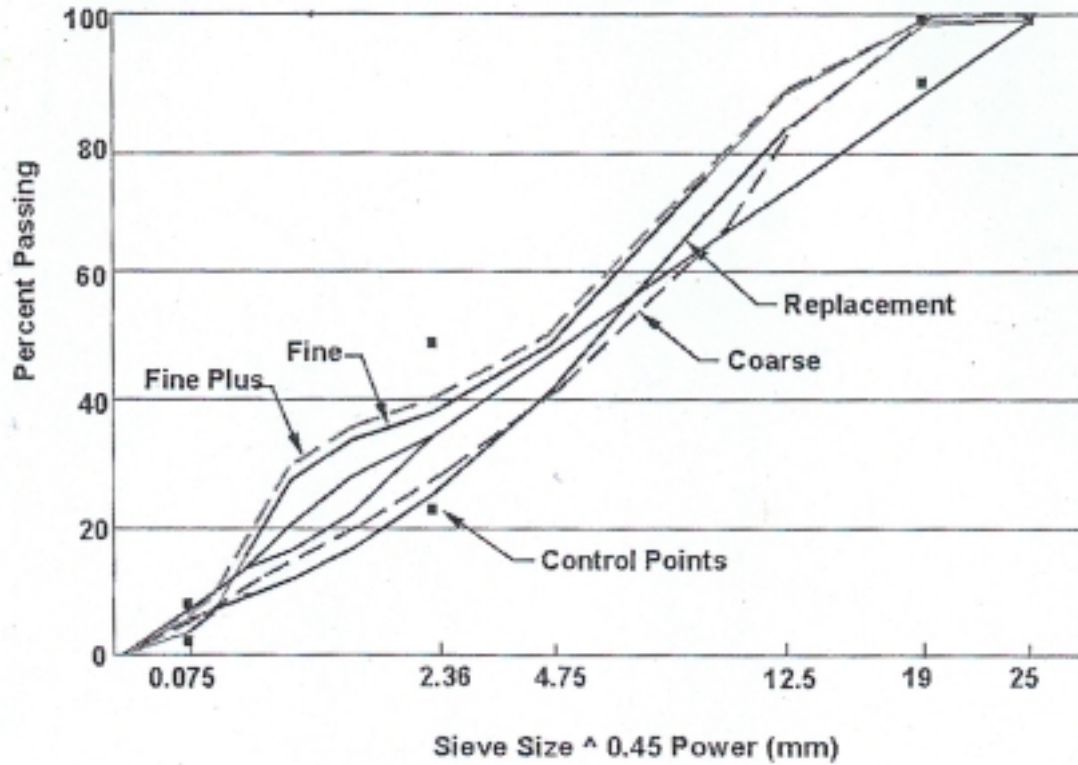


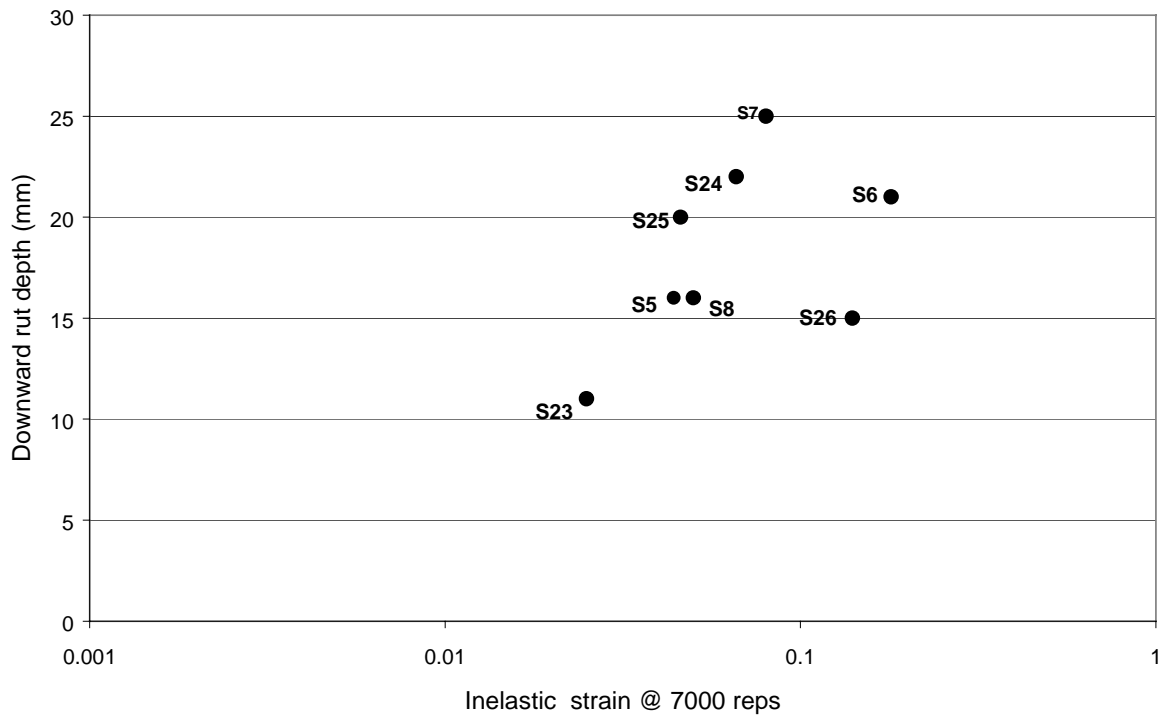
Figure 48. Mix target gradations

Table 8. Experiment designs WesTrack sections

Design Air Void Content	Aggregate Gradation Designation								
	Fine			Fine Plus			Coarse		
	Design Asphalt Contents								
	Low	Opt.	High	Low	Opt.	High	Low	Opt.	High
Low	X	04	18	X	12	19/21	X	23 (39)	25 (55)
Medium	02	01/15	14	22	11/19	13	08 (38)	05/24 (35,54)	07 (37)
High	03/16	17	X	10	20	X	26 (56)	06 (36)	X

Table 9. Aggregate and binders used in WesTrack test sections

	Original Test Sections	Replacement Test Sections
binder grade and source	PG 64-22 West Coast	PG 64-22 Idaho
Aggregate source and gradations	Quarry near Dayton, Nevada (partially crushed fluvial deposit) Sand from Wadsworth, Nevada coarse, fine and fine-plus gradings	Quarry near Lockwood, Nevada (crushed andesite) Sand from Wadsworth, Nevada Coarse gradings only

**Figure 49. Downward rut depth versus γ_p at $N=7000$ repetitions in RSST-CH at 50°C ; coarse mixes, original test sections**

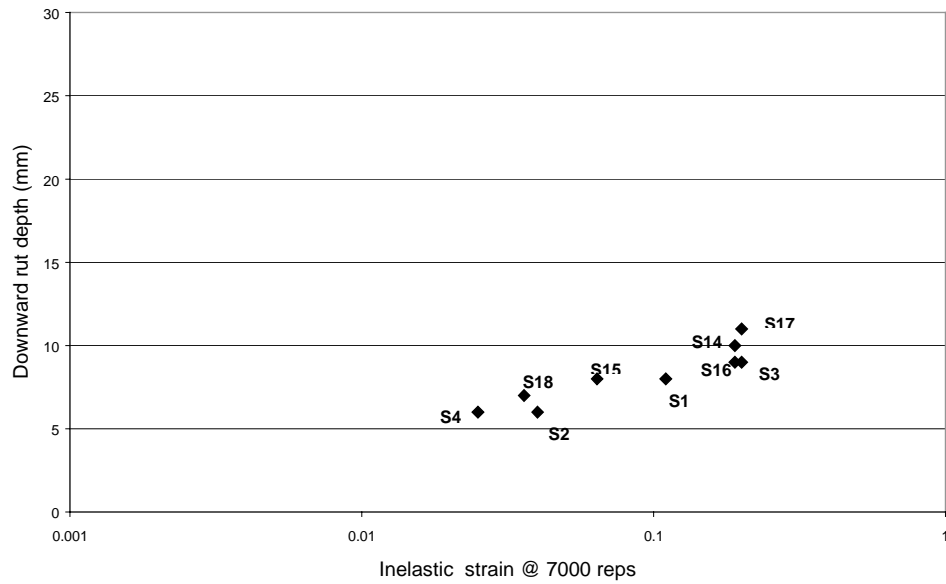


Figure 50. Downward rut depth versus γ_p at $N=7000$ repetitions in RSST-CH at 50°C ; fine mixes, original test sections

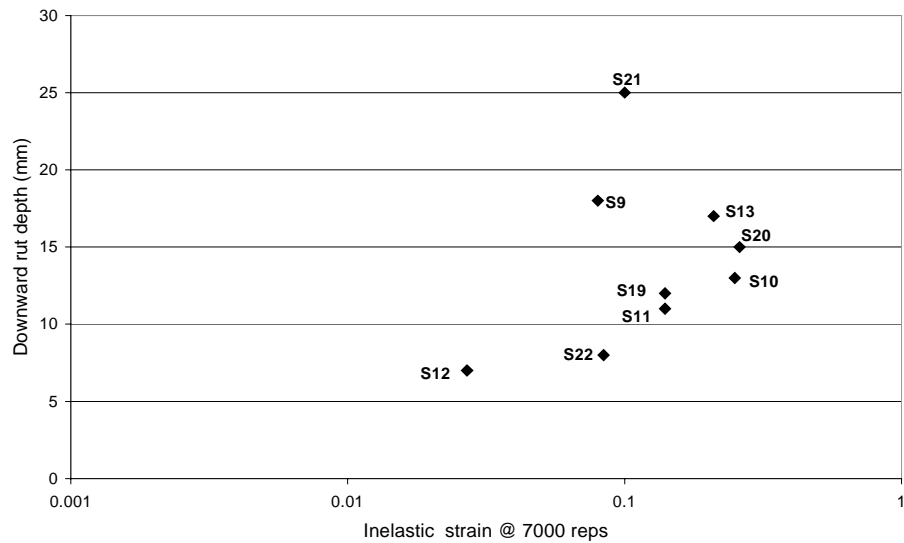


Figure 51. Downward rut depth versus γ_p at $N=7000$ repetitions in RSST-CH at 50°C ; fine plus mixes, original test sections

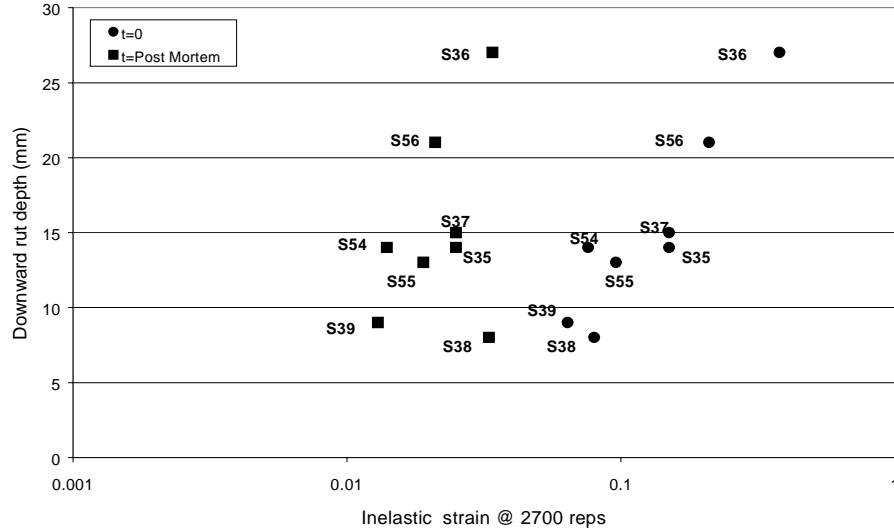


Figure 52. Downward rut depth versus γ_p at $N=2700$ repetitions in RSST-CH at 50°C ; coarse mixes, replacement sections. (Note: test data from both $t=0$ cores and from cores obtained at the conclusion of traffic $t = \text{post mortem}$ are included.)

For the replacement sections, in addition to the $t = 0$ test data, results of tests on cores after the trafficking was complete (post mortem) are also shown.

In general, for each set of mixes there is a reasonable relationship between rut depth and plastic strain as measured in the RSST-CH test at 50°C .

6.3 Mix Stiffness Considerations

Some consideration has been given to the use of mix stiffness as a potential mix characteristic for defining permanent deformation resistance. Stiffness data associated with mix performance information presented herein suggest that *caution is required when considering this parameter as a criterion for mix performance.*

Data presented in Figure 53 illustrate this point dramatically. Shear stiffness values determined at 50°C from the RSST-CH tests on the mixes described in the previous section are shown. The following relation was used for this determination:

$$G = \frac{\tau}{\gamma_{recov.}} = \frac{\text{shear stress [69 KPa (10 psi)]}}{\text{recoverable shear strain at } N = 100} \quad (9)$$

From the shear stiffness values shown, it would be difficult to differentiate between the mixes containing the AR-4000 asphalt cement which rutted under the B747-400 loading and the *high stability mix* which has performed in a satisfactory manner to date.

The data presented for the mix evaluations for the Interstate 710 project illustrate this point. Table 10 contains a summary of stiffness measurements performed on both the PBA-6A and AR-8000 mixes in both flexure and shear. For the range in temperatures considered, the AR-8000 mix is stiffer than the PBA-6A mix. As seen in Figure 53, however, the response of the PBA-6A mix to repeated shear deformations is significantly better than the AR-8000 mix, both of which contained the same aggregate and gradation and were tested at the same binder contents (expressed by weight of aggregate).

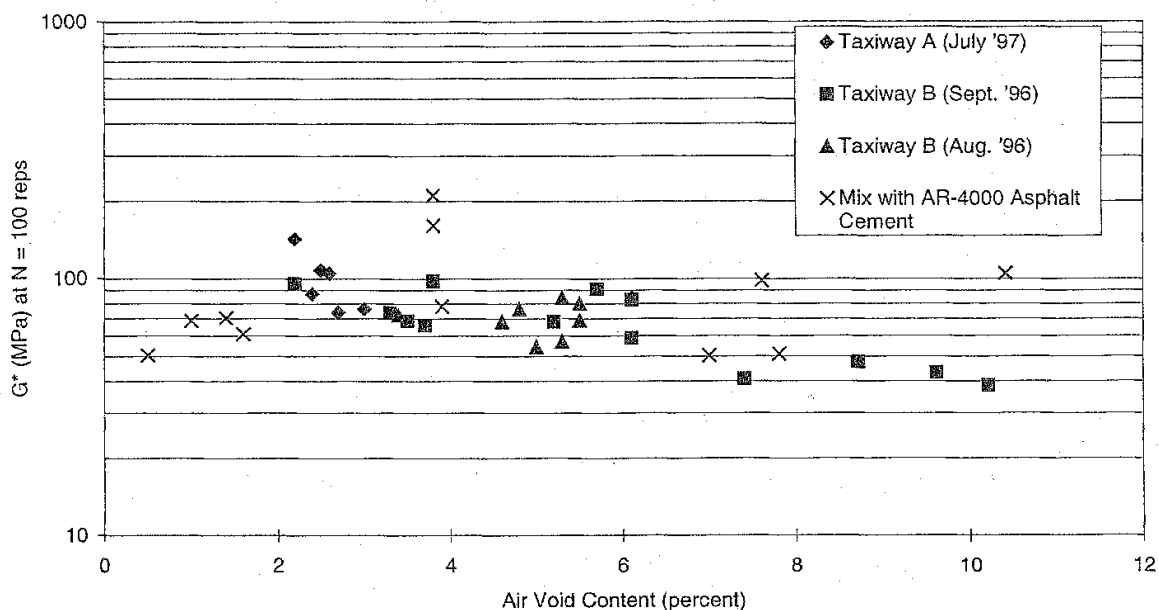


Figure 53. Mix stiffness measured in shear versus air-void content

Table 10. Mix stiffness for mixes considered for Interstate 710 project

Mix		V _{air} Percent	Temperature °C (°F)	Flexural Stiffness MPa (psi) (10Hz)	Shear Stiffness MPa (psi)
Binder Type	Binder Content (-percent by weight of aggregate)				
AR-8000	4.7	5.6	20 (68)	6375 (0.93×10 ⁶)	
	5.2	3.2	20 (68)	6900 (1.00×10 ⁶)	
	4.7	3.6	50 (122)		82.0 (11,900)
	4.7	4.2	60 (140)		42.3 (6,100)
PBA-6A	4.7	5.2	20 (68)	1010 (1.5×10 ⁵)	
	5.2	3.3	20 (68)	920 (1.4×10 ⁵)	
	4.7	5.8	10 (52)	3000 (4.35×10 ⁵)	
	4.7	5.9	25 (77)	520 (75,400)	
	4.7	5.8	30 (86)	310 (45,000)	
	4.7	3.8	50 (122)		3.21 (4700)
	4.7	2.9	60 (140)		24.4 (3550)

7.0 SUMMARY AND CONCLUSIONS

The information presented herein indicates that shear deformations contribute a significantly greater proportion to total permanent deformation (rutting) than volume change as seen from the results of the laboratory, and the results of a representative pavement section. These results are supported by observed rutting in in-service pavements as well. Moreover, the shear deformations leading to rutting are limited to the upper portion of the AC layer. This suggests that a laboratory test which measures primarily shear deformations appears to be the most effective way to define the propensity of a mix for rutting. Moreover, to make this evaluation, a specimen representative of the upper 75-100 mm (3-4 in) appears most appropriate; this suggests, in turn, a specimen which reflects the mix in this part of the pavement, both in terms of aggregate structure and degree of compaction.

For the triaxial test, if shear deformation response is the primary contributor to specimen performance, then a test with the form of loading shown in Figure 27 should be utilized. If this is the case, to satisfy RVE requirements for a mix containing 19 mm maximum size aggregate, a specimen 125 mm (5 in.) in diameter by at least 350 mm (10 in.) high should be used, since it will be necessary to glue the loading plates to the ends of the specimens. Similarly in shear, it is likely that a specimen 100 mm high by 300 mm long should be used based on the information contained herein. When it is not possible to use specimens of these dimensions the implications described herein should be noted.

It has been shown that asphalt mixes are non-linear in terms of applied stress, particularly at higher temperatures and comparatively slow rates of loading. This non-linearity negates the possibility of deducing shear response from an axial test unless a configuration for both

specimen size and loading of the type noted above are used. Similarly it would be difficult to deduce axial response from a test which measures primarily shear response, for the same reason.

It should also be noted that if perfectly smooth ends are not used for relatively short ($H/D \sim 1$) specimens, the effects of the bulk modulus, K , on the laboratory determined $E_{modulus}$ becomes more significant especially at elevated temperatures since the bulk modulus is significantly larger than the $E_{modulus}$ under these conditions.

In addition to the above items pertaining to specimen size and shape to define the propensity of mixes to rutting, information has also been presented on the effects of mode of loading (creep versus dynamic/repeated) and aggregate structure are as influenced by method of compaction. For mixes containing modified binders, available data indicate that it is important to use dynamic (repeated) loading rather than creep loading. In addition, available data suggest that to simulate aggregate structure resulting from field compaction, a form of rolling wheel compaction is necessary.

Finally, data are presented which illustrate the efficacy of the SHRP-developed simple shear test, performed in the repeated load, constant height mode, for mix design and performance evaluation. Moreover, the data suggest that this type of test better evaluates the permanent deformation response of mixes containing modified binders as compared to conventional tests such as the Hveem Stabilometer.

8.0 REFERENCES

1. Weissman, S. L. *The Mechanics of Permanent Deformation in Asphalt-Aggregate Mixtures: A Guide to Laboratory Test Selection*. Symplectic Engineering Corp., Dec. 1997.
2. Sousa, J. B., et al. *Permanent Deformation Response of Asphalt Aggregate Mixes*. Report SHRP-A-415, Strategic Highway Research Program, National Research Council, Washington, D.C., 1994, 437 pp.
3. de Beer, M., and C. Fisher. *Contact Stresses of Pneumatic Tires Measured with the Vehicle-Road Surface Pressure Transducer Array (VRSPTA) System for the University of California at Berkeley (UCB) and the Nevada Automotive Test Center (NATC)*. Transportek, CSIR, South Africa, Vols. 1 and 2, June 1997.
4. Deacon, J., J. Coplantz, A. Tayebali, and C. Monismith. "Temperature Considerations in Asphalt-Aggregate Mixture Analysis and Design," *Transportation Research Record 1454*. Transportation Research Board, 1994, pp. 97-112.
5. Brown, E. R., and S. A. Cross. "A Study of In-Place Rutting of Asphalt Pavements," *Asphalt Paving Technology*. Associations of Asphalt Paving Technologists, Vol. 58, 1989, pp.1-39.
6. Hashin, Z. "Analysis of Composite Materials—A Survey." *Journal of Applied Mechanics*. Vol. 50, 1983, pp. 481-505.
7. Weissman, S. L., J. T. Harvey, J. L. Sackman, and F. Long. "Selection of Laboratory Test Specimen Dimension for Permanent Deformation of Asphalt Concrete Pavements," *Transportation Research Record 1681*. Transportation Research Board, Washington, D.C., 1999, pp.113-120.
8. Harvey, J. T., I. Guada, and F. Long. *Effect of Material Properties, Specimen Geometry, and Specimen Preparation Variables on Asphalt Concrete Tests for Rutting*. Report to Office of Technology, Applications, FHWA, Pavement Research Center, University of California, Berkeley, March 1999, 83 pp.
9. Harvey, J. T., T. Hoover, N. F. Coetzee, W. A. Nokes, and F. C. Rust. "Caltrans Accelerated Pavement Test (CAL/APT) Program—Results from Tests on Asphalt Pavements 1994-1998," *Seventh Conference on Asphalt Pavements for Southern Africa (CAPSA)*. Victoria Falls, Zimbabwe, August/September 1999, 27 pp.
10. American Association of State Highway and Transportation Officials (AASHTO). "Test Method for Determining the Permanent Deformation and Fatigue Cracking Characteristics of Hot Mix Asphalt (HMA) Using the Simple Shear Test (SST) Device, AASHTO TP7-94," *AASHTO Provisional Standards*. March 1995, pp. 164-186.

11. Pavement Research Center (PRC), University of California, Berkeley. "Revision to AASHTO TP7 (TP7-99)." submitted to AASHTO for consideration. 1999. (N.B. Procedure is available from PRC.)
12. Alavi, S. *Viscoelastic and Permanent Deformation Characteristics of Asphalt-Aggregate Mixes Tested as Hollow Cylinders and Subjected to Dynamic Axial and Shear Loads*. Ph.D. thesis, University of California at Berkeley, 1992.
13. Kallas, B. F. and J. C. Riley. "Mechanical Properties of Asphalt Pavement Materials." *Proceedings*. Second International Conference on the Structural Design of Asphalt Pavements. University of Michigan, Ann Arbor, Michigan, 1967. pp. 931-937.
14. Kallas, B. F. "Dynamic Modulus of Asphalt Concrete in Tension and Tension-Compression." *Proceedings*. Association of Asphalt Paving Technologists. Vol. 39. 1969. pp.1-23
15. Tayebali, A. A., et al. *Stiffness of Asphalt-Aggregate Mixes*. Report SHRP-A-388, Strategic Highway Research Program, National Research Council, Washington, D.C, 1994, 101 pp.
16. Bolk, H. J. N. A. *The Creep Test*. Study Centre for Road Construction, The Netherlands, 1981 (SCW Record 5), 96 pp.
17. Tayebali, A. A. *Influence of Rheological Properties of Modified Asphalt Binders on the Load-Deformation Characteristics of the Binder-Aggregate Mixtures*. Ph. D. thesis, University of California, Berkeley, 1990, 420 pp.
18. McLean, D. B. *Permanent Deformation Characteristics of Asphalt Concrete*. Ph. D. thesis, University of California, Berkeley, 1974.
19. Letter to John Bukowski, FHWA, from C. L. Monismith, dated April 1, 1998 (finite element analysis done by Dr. S. W. Weissman).
20. *Shell Pavement Design Manual*. Shell International Petroleum Company, Limited, London, 1978; and, *Addendum to the Shell Pavement Design Manual*. Shell International Petroleum Company, Limited, London, 1985.
21. Valkering, C. P., D. J. L. Lancon, E. de Hiltster, and D. A. Stoker. "Rutting Resistance of Asphalt Mixes Containing Non-Conventional and Polymer-Modified Binders," *Journal*. Association of Asphalt Paving Technologists, Vol. 59, 1990, pp. 590-609.
22. Lizenga, J. "On the Prediction of Pavement Rutting in the Shell Pavement Design Method," *2nd European Symposium on Performance of Bituminous Materials*. Leeds, UK, April 1997.

23. Tanco, A. J. *Permanent Deformation Response of Conventional and Modified Asphalt-Aggregate Mixes under Simple and Compound Shear Loading Conditions*. Ph. D. thesis, University of California, Berkeley, 1992, 273 pp.
24. Pavement Research Center, University of California, Berkeley. *Mix Design and Analysis and Structural Section Design for Full Depth Pavement for Interstate Route 710*. TM-UCB-PRC-99-2, June 1999.
25. Vallerga, B. A. "Recent Laboratory Compaction Studies of Bituminous Paving Mixtures," *Proceedings*. Association of Asphalt Paving Technologists, Vol. 20, 1951, pp.117-153.
26. Endersby, V. A., and B. A. Vallerga. "Laboratory Compaction Methods and their Effects on Mechanical Stability Tests for Asphaltic Pavements," *Proceedings*. Association of Asphalt Paving Technologists, Vol. 21, 1952, pp. 298-348.
27. Monismith, C. L. and B. A. Vallerga. "Relationship Between Density and Stability of Asphaltic Paving Mixtures," *Proceedings*. Association of Asphalt Paving Technologists, Vol. 25, 1956, pp. 88-108.
28. *Investigation of the Design and Control of Asphalt Paving Mixtures*. TM 3-254, Vol. 1, 2, 3, Corps of Engineers, Department of the Army, May 1948.
29. Philippi, O. A. *A Resume of the Investigations Conducted by the Texas Highway Department in Developing a Method and Device for Molding Specimens of Bituminous Concrete Paving Mixtures*. (Gyratory shear method.) Unpublished report.
30. van Grevenynghe, M. P. "Influence des modes de préparation et du prélèvement des éprouvettes sur les caractéristiques structurelles et mécaniques des enrobés." Internal RILEM Report, 1986.
31. Bonnot, J. "Asphalt Aggregate Mixtures," *Transportation Research Record 1096*. Transportation Research Board, Washington, D.C., 1986, pp. 42-51.
32. Sousa, J. B., J. A. Deacon, and C. L. Monismith. "Effect of Laboratory Compaction Method on the Permanent Deformation Characteristics of Asphalt-Aggregate Mixes." *Journal*. Association of the Asphalt Paving Technologists, Vol. 60, 1991, pp. 533-585.
33. Harvey, J. T. *Rutting of Caltrans Asphalt Concrete and Asphalt-Rubber Hot Mix under Different Wheels, Tires, and Temperatures—Accelerated Pavement Testing*. University of California, Berkeley.
34. Harvey, J. T. *Asphalt Concrete Specimen Preparation Protocol*, TCM-UCB-A-003AA-91-2. University of California, Berkeley, August 1991, 77 pp.

35. Monismith, C. L., et al. *Asphalt Mix Studies, San Francisco International Airport*. Pavement Research Center, University of California, Berkeley, July 1999, 40 pp. (plus appendices).
36. Monismith, C. L., J. A. Deacon, and J. T. Harvey. *WesTrack: Performance Models for Permanent Deformations and Fatigue*. Pavement Research Center, University of California, Berkeley, December 1999.